OPTICAL SPANNERS AND IMPROVED OPTICAL TWEEZERS

Neil B. Simpson

A Thesis Submitted for the Degree of PhD
at the
University of St Andrews

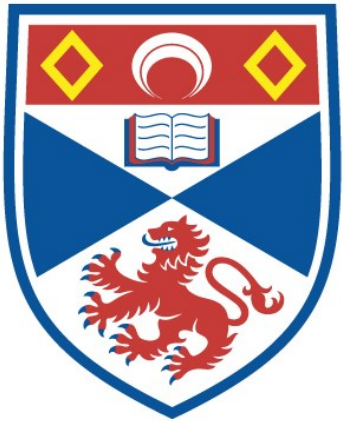

1998

The University of St. Andrews

Optical Spanners and Improved Optical Tweezers

Neil B. Simpson B.Sc. M.Sc.

Thesis submitted in partial fulfilment of the requirements for the degree of Doctor of Philosophy

September 1997

ProQuest LLC.
789 East Eisenhower Parkway
P.O. Box 1346
Ann Arbor, MI 48106 – 1346

Declarations

I, Neil Benjamin Simpson, hereby certify that this thesis, which is approximately 35,700 words in length, has been written by me, that it is the record of work carried out by me and that it has not been submitted in any previous application for a higher degree.

date 2-3-98 signature of candidate .....

I was admitted as a research student in September 1994 and as a candidate for the degree of Doctor of Philosophy in September 1994; the higher study for which this is a record was carried out in the University of St. Andrews between 1994 and 1997.

date 2-3-98 signature of candidate .....

I hereby certify that the candidate has fulfilled the conditions of the Resolution and Regulations appropriate for the degree of Doctor of Philosophy in the University of St. Andrews and that the candidate is qualified to submit this thesis in application for that degree.

date 2-3-98 signature of supervisor .....

In submitting this thesis to the University of St. Andrews I understand that I am giving permission for it to be made available for use in accordance with the regulations of the University Library for the time being in force, subject to any copyright vested in the work not being affected thereby. I also understand that the title and abstract will be published, and that a copy of the work may be made and supplied to any bona fide library or research worker.

date 2-3-98 signature of candidate .....

When things go wrong as they sometimes do,
When the road you're trudging seems all uphill,
When funds are low and debts are high,
And you want to smile, but have to sigh,
When care is pressing you down a bit,
Rest, if you must but don't you quit,
Life is queer with its twists and turns,
As everyone of us sometimes learns,
And many a failure turns about,
When he might have won if he'd stuck it out,
Don't give up though the pace seems slow
You may succeed with another blow,
Success is failure turned inside out,
The silver tints of the clouds of doubt,
And you never can tell how close you are,
It may be near, when it seems so far,
So stick to the fight when you're hardest hit,
It's when things seem worst that you
Must Not Quit.

Acknowledgements

I would firstly like to thank my supervisor, Dr Miles Padgett, for all of his guidance and encouragement throughout my PhD. His enthusiasm and interest in the work has been much appreciated. Also, I wish to thank Les Allen, the co-proposer of this work on Optical Spanners, for his invaluable discussions and advice throughout the course of the experimental work. Also, I acknowledge the financial support for this work from the Engineering and Physical Sciences Research Council.

I would like to thank those colleagues and Departmental staff who have contributed in some way to my work over the last three years, in particular to Kishan Dholakia for his expert experimental advice. Many thanks to the ever-increasing number of Padgett People who have made the office a most enjoyable and amusing place: Darren "chocolate biscuit" Steers, Johannes "no music in the office" Courtial, Brett "Macintosh" Patterson, Graham "OPO" Gibson, Paul "yah" Lesso, Tracy "air freshener" McKechnie and Jochen "sax-man" Arlt.

There are various people I would also like to thank, without whom my time in St. Andrews would just not have been the same. In particular, to Mark Holden, for experiencing life in St. Andrews with me, through all the highs and lows for three years - the tales we could tell! Also, to Mary Wilson, for her support and some very happy and memorable times. Finally, many thanks to all the inmates, both past and present, of Flat 63 for all of those very enjoyable times: Gus, Aaron, Dave, Rob and Steve.

Lastly and by no means least, I would like to thank my family for their continued love and support throughout my time here. Thank you for everything and I dedicate this thesis to you.

Abstract

This thesis describes the experimental and theoretical work that investigated the transfer of orbital angular momentum from light to matter. This was achieved by combining two established areas of laser physics which were "optical tweezers" and Laguerre-Gaussian laser modes.

The optical tweezers are essentially a tightly focussed laser beam from a high numerical aperture microscope objective lens, which traps particles in three dimensions just below the beam focus. By incorporating a Laguerre-Gaussian laser mode into the tweezers system, the trapping efficiency was doubled. These improved optical tweezers have been successfully demonstrated both theoretically and experimentally.

In addition to the spin angular momentum which is associated with the polarisation state, the Laguerre-Gaussian laser modes also possess orbital angular momentum. The "optical spanners" utilised this property by transferring orbital angular momentum from the laser beam to the trapped particle, causing it to rotate whilst being held in the optical trap. This effect was theoretically modelled and experimentally observed.

Using the optical spanners, the spin angular momentum of the laser was used to directly cancel the orbital angular momentum in the beam, which was observed as a cessation in rotation of the trapped particle. This demonstrated the mechanical equivalence of the spin and orbital components of angular momentum in a light beam, and gave experimental evidence for the well defined nature of the orbital angular momentum present in Laguerre-Gaussian laser modes.

Cartoon taken from article "Microscopic tools of the trade" in the *Financial Times - Weekend*, pII, 21 June 1997

Contents

Chapter I

Introduction

Contents

I. 1 The Aim of the PhD

The research undertaken in this PhD combined two areas of physics, to investigate the orbital angular momentum of light. The two established fields were "optical tweezers", which is the trapping and manipulation of micron-sized particles; and the generation of Laguerre-Gaussian laser modes. This combination not only transferred orbital angular momentum from a light beam to matter producing a novel optical tool, "optical spanners", but also resulted in improved optical tweezers.

The ability to manipulate and trap small particles using a laser beam has been studied since the early 1970's [1]. The optical tweezers create a 3-dimensional trap using a tightly focussed laser beam, giving full control over the trapped particle, be it synthetic or biological.

Laguerre-Gaussian modes form a complete set of laser modes. These modes possess orbital angular momentum [2], which is different to the spin angular momentum associated with the polarisation state of the light beam. In recent years, this well defined orbital angular momentum content of light has created much interest and at the start of this work, had not been experimentally quantified.

This research project set out to combine the optical tweezers with a Laguerre-Gaussian laser mode with five main objectives in mind:

- to construct a laser system and cylindrical lens mode converter for the production of Laguerre-Gaussian laser modes.

- to demonstrate the operation of a single beam gradient force, optical tweezers arrangement for the trapping and manipulation of particles in the size range 0.5 to 5 μm in diameter.

- to investigate the improvement in trapping efficiency of optical tweezers when a Laguerre-Gaussian laser mode is incorporated into the trapping arrangement.

- to use a Laguerre-Gaussian laser mode within the optical tweezers system, to transfer orbital angular momentum from the light beam to a trapped micron-sized particle and observe the rotation of the particle. This is now known as "optical spanners".

- to compare the resulting rotation of the trapped particles with that predicted by theory.

I. 2 The Outline of the Thesis

This thesis will describe the research undertaken, at the University of St. Andrews from 1994 to 1997, to transfer orbital angular momentum from light to matter.

Chapter II will describe the phase and intensity structure of Laguerre-Gaussian modes. It will cover the initial interest in the spin angular momentum of light in the 1930's [3, 4] through to the recent developments into the orbital angular momentum of light [2]. The Chapter will conclude with an overview of the methods of producing Laguerre-Gaussian laser modes, including the method that has been recently developed at St. Andrews using an optical fibre which has been published in *Applied Optics* [5].

Chapter III will review the development of optical tweezers, from the initial experiments of Arthur Ashkin in the early 1970's on optical levitation [6]

through to the single beam gradient force optical trap of today (optical tweezers) [7]. The main operating principles of the tweezers will be discussed as will the standard experimental arrangement. Some of the main applications of optical tweezers will be covered at the end of the Chapter.

Chapter IV will detail the experimental investigation into the intensity and phase structure of Laguerre-Gaussian laser modes, using a He-Ne laser in a Mach-Zehnder interferometer arrangement. The results of which have been published in the *American Journal of Physics* [8]. In addition, the second harmonic generation of Laguerre-Gaussian modes was also investigated and the findings published in the *Physics Review A* [9].

In Chapter V, the construction of a diode-pumped Nd:YLF laser will be described. To perform the optical trapping of particles with Laguerre-Gaussian laser modes, it was necessary to have a laser capable of producing high order modes at high laser powers, up to 100 mW. The elements of this laser system will be covered in this Chapter.

Chapter VI will cover the experimental operation of optical tweezers. Typical experimental parameters will be discussed and the experimental measurements of the minimum laser power required to obtain optical trapping of micron-sized silica spheres will be presented. By trapping with Laguerre-Gaussian modes it has been possible to trap the spheres with less laser power, and hence this area of the research is referred to as the improvement of optical tweezers. These experimental results have been accepted in January 1998 for publication in the *Journal of Modern Optics* [10]. The observations have been complemented by computer modelling the trapping forces involved, the results of which were published in the *Journal of Modern Optics* [11].

Chapter VII will detail the research on optical spanners, the main incentive behind this project. The experimental work demonstrates the transfer of orbital angular momentum from a Laguerre-Gaussian laser mode to a trapped particle using optical tweezers, resulting in an observable rotation of the particle. The optical spanners have also been used to demonstrate the mechanical equivalence of the spin and orbital angular momentum of light.

The well defined orbital angular momentum has been confirmed by directly comparing the orbital angular momentum to the spin angular momentum in the light beam. The details of this work have been published in *Optics Letters* [12] .

The concluding Chapter will give a summary of the thesis and an overview of the possible applications of optical spanners and where they might lead to in the future. The thesis will close with some comments on Optical Spanners and Optical Tweezers and their recent exposure in the media and to the general public. A full list of publications and conference papers attained during the PhD, some copies of the designs for the laser components and a copy of the computer modelling program will also be included at the end of the thesis in the appendices.

References

1. Ashkin, A., *Acceleration and trapping of particles by radiation pressure.* Phys. Rev. Lett., 1970. **24**: p. 156-159.

2. Allen, L., M.W. Beijersbergen, R.J.C. Spreeuw, and J.P. Woerdman, *Orbital angular momentum of light and the transformation of Laguerre-Gaussian laser modes.* Phys. Rev. A, 1992. **45**: p. 8185-8189.

3. Beth, R.A., *Direct detection of the angular momentum of light.* Phys. Rev., 1935. **48**: p. 471.

4. Beth, R.A., *Mechanical detection and measurement of the angular momentum of light.* Phys. Rev., 1936. **50**: p. 115-125.

5. McGloin, D., N.B. Simpson, and M.J. Padgett, *Transfer of orbital angular momentum from a stressed fiber-optic waveguide to a light beam.* Appl. Opt., 1998. **37**: p. 469-472

6. Ashkin, A. and J.M. Dziedzic, *Optical levitation by radiation pressure.* Appl. Phys. Lett., 1971. **19**: p. 283-285.

7. Ashkin, A., J.M. Dziedzic, J.E. Bjorkholm, and S. Chu, *Observation of a single-beam gradient force optical trap for dielectric particles.* Opt. Lett., 1986. **11**: p. 288-290.

8. Padgett, M., J. Arlt, N. Simpson, and L. Allen, *An experiment to observe the intensity and phase structure of Laguerre-Gaussian laser modes.* Am. J. of Phys., 1996. **64**: p. 77-82.

9. Dholakia, K., N.B. Simpson, M.J. Padgett, and L. Allen, *Second-harmonic generation and the orbital angular momentum of light.* Phys. Rev. A, 1996. **54**: p. R3742-R3745.

10. Simpson, N.B., D. McGloin, K. Dholakia, L. Allen, and M.J. Padgett, *Optical tweezers with increased axial trapping efficiency.* Accepted by J. of Mod. Opt., January 1998.

11. Simpson, N.B., L. Allen, and M.J. Padgett, *Optical tweezers and optical spanners with Laguerre-Gaussian modes.* J. of Mod. Opt., 1996. **43**: p. 2485-2491.

12. Simpson, N.B., K. Dholakia, L. Allen, and M.J. Padgett, *Mechanical equivalence of spin and orbital angular momentum of light: an optical spanner.* Opt. Lett., 1997. **22**: p. 52-54.

Chapter II

Laguerre-Gaussian Laser Modes and the Angular Momentum of Light

Contents

II. 1 Introduction

This Chapter will begin by discussing longitudinal and transverse laser modes. The common transverse modes encountered in laser cavities are Hermite-Gaussian modes which have rectangular symmetry. A second set of modes that have circular symmetry are less common and are called Laguerre-Gaussian laser modes.

The Chapter will then consider the angular momentum of light and review the early work performed involving the spin angular momentum of light. This preliminary research by Richard Beth in the 1930's [1] showed that the spin angular momentum is directly related to the circular polarisation of light and equal to $\hbar$ per photon. However, light can also possess orbital angular momentum in addition to the spin component.

For a beam that possesses an azimuthal phase term $\exp(-i\ell\phi)$ corresponding to a helical wavefront, it has been found that the orbital angular momentum in the beam is well defined and equivalent to $\ell\hbar$ per photon [2]. Laguerre-Gaussian modes are one example of such beams. Consequently, there has

been much experimental work to try to demonstrate the existence of orbital angular momentum.

There are various methods of producing beams with an orbital angular momentum content, typified by the Laguerre-Gaussian laser modes. There are two basic production techniques, both of which involve the transformation of a Hermite-Gaussian mode into a Laguerre-Gaussian mode. The first method is to convert a fundamental $TEM_{0,0}$ mode into a Laguerre-Gaussian mode directly, while the second is to convert a high order Hermite-Gaussian mode into its corresponding Laguerre-Gaussian mode. An overview of these different conversion techniques will be presented in this Chapter.

II. 2 Laser modes

This section of the Chapter will review laser modes and then discuss Gaussian modes. Hermite-Gaussian modes are rectangularly symmetric and are easily produceable from a laser and these can be transformed into circularly symmetric Laguerre-Gaussian modes. Both of these mode types are encountered in the experimental work of this PhD and they will be described in this section.

II. 2. 1 Longitudinal and transverse laser modes

All lasers essentially consist of a gain medium which amplifies the light by stimulated emission, and an optical resonator to provide the feedback needed to form an oscillator. The electromagnetic field within the laser cavity must satisfy a number of boundary conditions. In the steady state, there is the requirement that the field reproduces itself in phase after one round trip of the laser cavity. This gives rise to the longitudinal mode structure of the laser along the laser cavity. For a two-mirror linear cavity of optical length L, the longitudinal mode must satisfy the equation,

$$m\left(\frac{\lambda}{2}\right) = L \tag{2.1}$$

where λ is the operating wavelength of the laser and m is an integer defining the number of nodes along the cavity.

A secondary boundary condition constrains the transverse nature of the electromagnetic field and produces the transverse modes. In free space, there is a requirement that the electromagnetic field falls to zero away from the axis of the laser cavity and this leads to the observed intensity profile of the laser output. The analytical form of the allowed laser modes must satisfy these conditions and diverge at only a small angle with respect to the optical axis of the laser cavity system. This requires both the field amplitude and its derivative to fall to zero at a large distance from the axis of the cavity.

II. 2. 2 Hermite-Gaussian modes

Asymmetries in the laser cavity, such as the presence of a Brewster window, give rise to rectangular symmetry which results in the Hermite-Gaussian (HG) polynomials providing an accurate description. A fuller description, with many examples of transverse laser modes can be found in Siegman's book 'Lasers' [3].

These rectangularly symmetric modes are described by the product of two independent Hermite-Gaussian polynomials, for the field distributions in the x-direction and the y-direction. The two polynomials are characterised by integer subscripts m and n giving the order of the polynomials in the x and y directions respectively.

The electric field distribution of a transverse HG laser mode E_{HG} (x,y,z) is typically given by

$$E_{HG}(x,y,z) \propto \exp\left\{-\left(\frac{ik(x^2+y^2)}{2R}\right)\right\}\exp\left\{-\left(\frac{x^2+y^2}{\omega^2}\right)\right\}$$
$$\times\exp\{-i(m+n+1)\Psi\}\times H_n\left(\sqrt{2}\frac{x}{\omega}\right)\times H_m\left(\sqrt{2}\frac{y}{\omega}\right) \qquad (2.2)$$

where R is the radius of curvature of the near spherical wavefronts, k is the wavenumber of the electromagnetic wave, x and y are the transverse

positions within the beam, and ω is the beam radius at which the Gaussian term falls to 1/e of its on-axis value. The Gouy phase shift $\Psi(z)$ will be considered in more detail in section II. 5. 5.

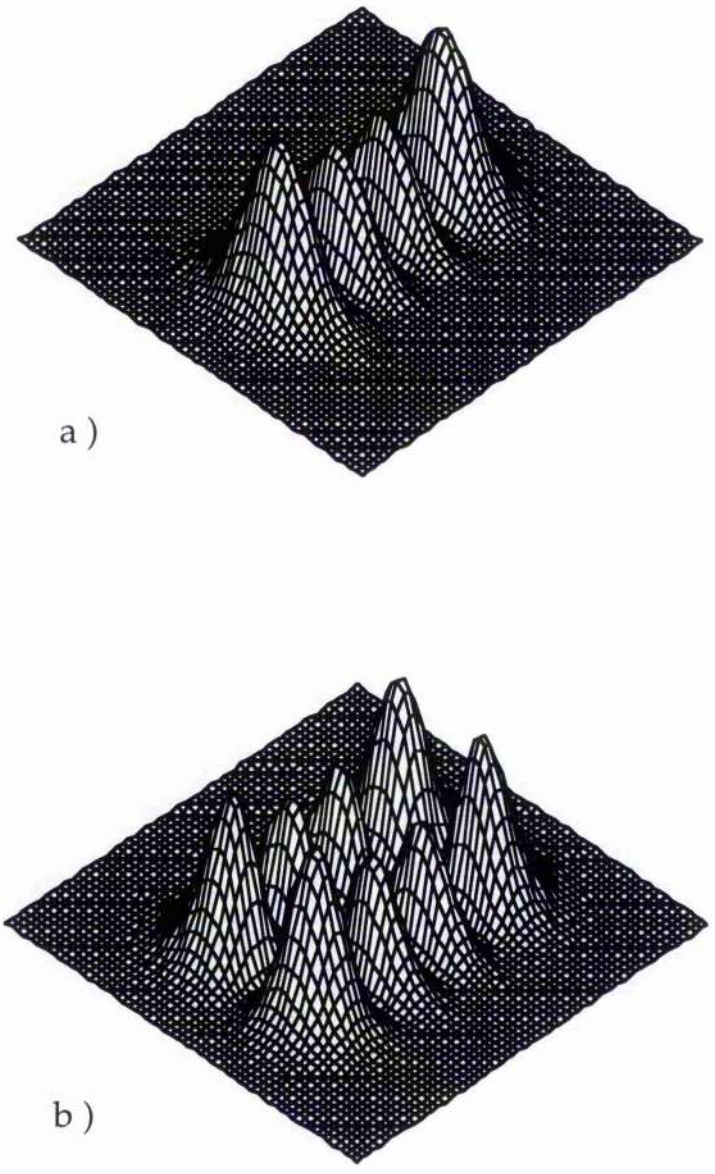

Figure II.a Examples of the intensity distribution of two HG modes
a) $HG_{3,0}$ b) $HG_{3,1}$

II. 2. 3 Laguerre-Gaussian modes

In a paper by Allen et al [2], an in-depth study is made of the electromagnetic theory of Laguerre-Gaussian (LG) modes which will not be entered into in any detail here but the main points will be described. The first thing to note is that Laguerre-Gaussian modes are not rectangularly symmetric, they are circularly symmetric. Hence the intensity distribution of these modes is of the form of rings.

For a laser system, it would then seem logical that given circular mirrors, the LG polynomials would give the most apt description of the transverse modes in a real laser, but this is not the case due to the presence of asymmetries as mentioned earlier.

The circularly symmetric LG modes $E_{LG}\ (r,\phi,z)$ are described by a single Laguerre polynomial with two indices. A superscript ℓ, describes the number of 2π cycles of phase around the circumference of the mode. This phase is the azimuthal phase which is responsible for the presence of the orbital angular momentum of $\ell\hbar$ per photon. A subscript p defines the number of nodes across the radial field distribution as p+1.

$$E_{LG}(r,\phi,z) \propto \exp\left\{-\left(\frac{ikr^2}{2R}\right)\right\}\exp\left\{-\left(\frac{r^2}{\omega^2}\right)\right\}\times\exp\{-i(2p+\ell+1)\Psi\}$$
$$\times\exp(-i\ell\phi)\times(-1)^p\left(\frac{r\sqrt{2}}{\omega}\right)^{\ell}\times L_p^{\ell}\left(\frac{2r^2}{\omega^2}\right) \qquad (2.3)$$

Equation 2.3 is the expression for the electric field distribution of a transverse LG laser mode $E_{LG}\ (r,\phi,z)$, where r is the radial position from the beam axis and ϕ is the azimuthal angle within the beam. Note the presence of the azimuthal phase term $\exp(-i\ell\phi)$ and also the presence of the Gouy phase $\Psi(z)$ which will be discussed further in section II. 5. 5.

Figure II.b shows two examples of LG modes, demonstrating their circular symmetry and intensity distribution.

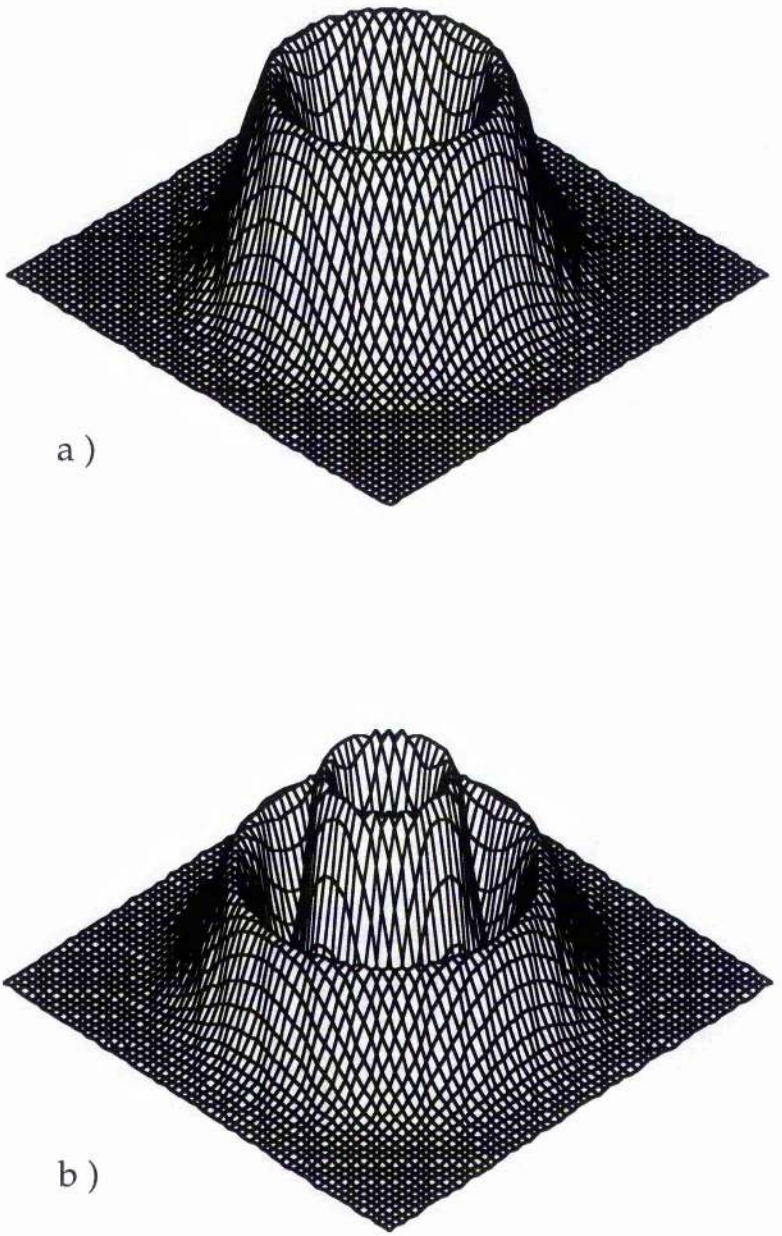

Figure II.b Examples of the intensity distribution of two LG modes
a) LG^3_0 b) LG^2_1

II. 2. 4 The Poynting vector

HG modes can be envisaged as surfaces of constant phase in a succession of discs at wavelength intervals. The Poynting vector $\underline{S}$, which represents the instantaneous electromagnetic power through a surface [4], points along the direction of propagation for these modes.

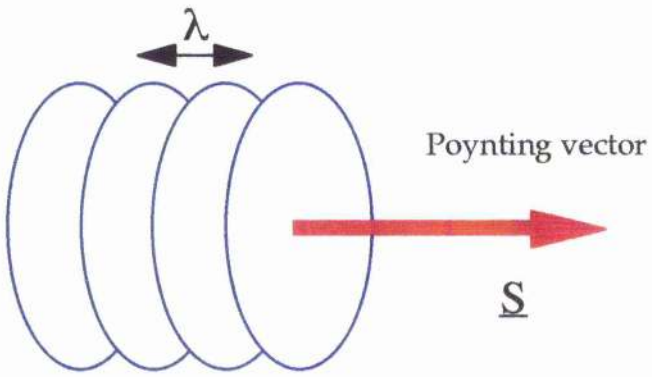

HG modes - plane wavefronts

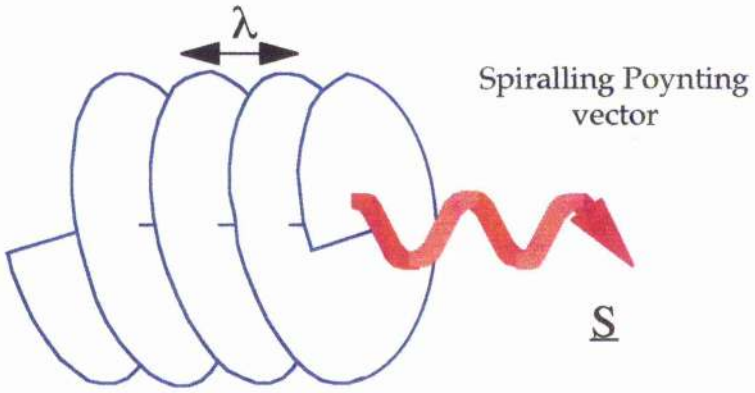

LG modes - helical wavefronts

Figure II.c The path of the Poynting vector for linearly polarised HG and LG modes

However, for LG modes with $\ell \neq 0$, these surfaces of constant phase form a helical path, such that the wavefronts are never perpendicular to the direction of propagation. Due to the nature of these wavefronts in a LG beam, the Poynting vector does not point along the direction of propagation but spirals like a corkscrew. The rotation of this vector in a LG mode [5] is proportional to a phase, called the Gouy phase.

The propagation of these LG modes follows that of standard Gaussian beams and can be described by the ABCD law of propagation [6]. The LG modes can also be described by the Wigner distribution function, which provides a representation of the focussing and twisting of the beam as it propagates [7].

II. 3 The angular momentum of light

Beginning with Maxwell's theories of electromagnetic radiation, it has been established that light carries both energy and momentum. This momentum may have linear and angular components, the angular momentum having a spin and orbital part. The spin angular momentum is associated with the polarisation state of the light and is a well established idea. The orbital angular momentum is associated with the phase structure of the beam and is less well understood.

II. 3. 1 Spin angular momentum

The concept of the angular momentum of light was studied more closely by Richard Beth in the early 1930's. He was the first to detect and measure the spin angular momentum content in light [8]. In a more detailed follow-up paper [1], he summarised the electromagnetic theory of the torque exerted by a beam of polarised light on a birefringent plate which altered the beam's state of polarisation. This theory will not be discussed in any detail here.

One of the main results to come out of the measurement of this torque, previously believed to be too small to measure experimentally, was that the torque could be accounted for by allocating an angular momentum of $\hbar$ to each photon of left circularly polarised light in a vacuum. Similarly for right

circularly polarised light, an angular momentum of -$\hbar$ could be assigned to each photon. From quantum theory, this angular momentum or spin of $\hbar$ or -$\hbar$ has its spin axis in the direction of propagation of the light.

At the start of the century, Poynting inferred from a mechanical analogy, that circularly polarised light should exert a torque equal to the light energy per unit volume times $\lambda/2\pi$ on unit area of a quarter-wave plate, which makes the light plane polarised [9]. From the quantum theory, incorporating the spin angular momentum values of $\hbar$, this result of Poynting is verified. Beth was able to then detect and measure the spin angular momentum of light.

To do this, he hung a one inch circular quartz wave plate on a 25 cm long fine quartz fibre and by directing polarised light through it, a resulting torque was observable. This was carried out in a vacuum and the radiating light obtained from a 3 mm tungsten ribbon filament. The change in the angular momentum of polarised light through the wave plate was detected and measured. The measured effect agreed with that predicted by wave theories and quantum theories of light. This is usually referred to as the measurement of the spin angular momentum of the photon of light and is $\pm\hbar$ depending on the polarisation state.

II. 3. 2 Orbital angular momentum

The orbital angular momentum term is not strictly speaking a photon property but is better understood in terms of the amplitude and phase of the electric field of the beam. The presence of an azimuthal phase term of the form $\exp(-i\ell\phi)$, results in the existence of the orbital angular momentum of $\ell\hbar$ per photon. Laguerre-Gaussian modes are examples of modes that carry this well defined orbital angular momentum of $\ell\hbar$ per photon [2, 10] in the direction of propagation. It is this momentum component that has created the recent interest in the Laguerre-Gaussian laser modes [2, 5, 11, 12].

The value of the orbital angular momentum of a paraxial beam of light is analogous to the angular momentum of the quantum harmonic oscillator and verifies the process of orbital angular momentum transfer from a light

beam to an astigmatic lens or diaphragm. This analogy between paraxial theory and quantum theory has enabled an eigenfunction description of the angular momentum of light to be formulated [13]. Other work has been performed to develop a general nonparaxial form of a beam based on Maxwell theory [14]. This examines the angular momentum properties of a light beam with near cylindrical symmetry, without using the paraxial approximation.

II. 4 Similar beams to LG beams

In some experimental work, beams with helical wavefronts are not referred to as Laguerre-Gaussian beams, but quite often as "optical vortices", "beams with phase singularities" or "beams with screw dislocations".

Singularities have been recognised as an important feature of the wave equation since the mid 1970's [15]. Phase singularities are basically wavefront dislocations of the phase of the wave, and can be broken down into two types. The first is the edge dislocation which is situated along a line in the wavefront plane and propagates along with the wave. The second is the screw dislocation or optical vortex of the form $\exp(im\phi)$, where m is the charge of the dislocation, referred to as the topological charge. This vortex is described by a spiralling of the wavefront around the line of defect. Note the similarity between this and the azimuthal phase term contained in the Laguerre-Gaussian beams and the equivalence of the azimuthal index ℓ and the topological m charge. The LG beams are actually a special case of these optical vortices, as the phase singularity is always centred on the beam axis.

The optical vortices can be formed within a smooth Gaussian beam causing a region of zero intensity similar to the ring modes of LG beams. When the screw dislocations contained within the beam have the same topological charge m, the positions of the vortices do not change as the beam propagates, they simply follow the host beam. They can be considered as dark beams propagating within the host Gaussian beam.

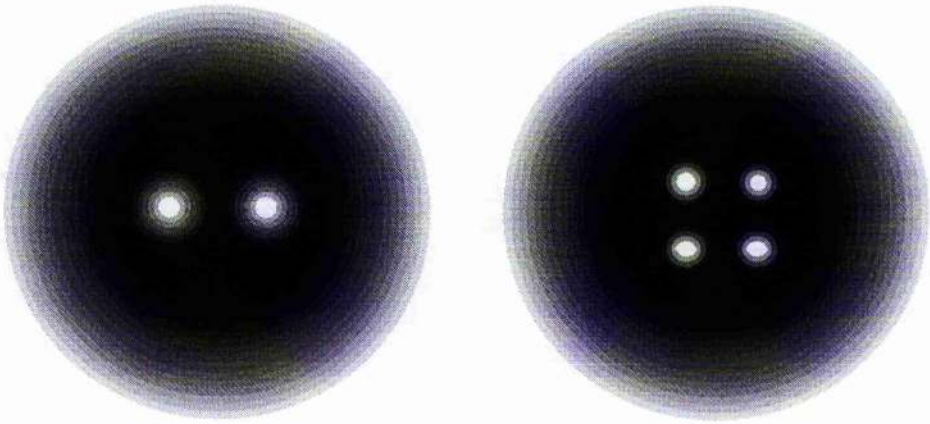

Second-order optical vortex
m=2

Fourth-order optical vortex
- the 'optical leopard'
m=4

Figure II.d Examples of intensity distribution of optical vortices

However, if the vortices have opposite charges associated with them, they will be attracted to each other. Vortex pairs can collide with each other and interfere destructively causing annihilation and the vortex pair will disappear. This has been observed experimentally by Basistiy et al [16]. This group has studied in some depth the phenomena of optical vortices and some of their properties [17], as have Brambilla and co-workers [18, 19] and Bazhenov and co-workers [20, 21].

Phase singularities can be investigated using interference techniques. One of the first studies was by Vaughan and Willetts in the late 1970's, who investigated the spatial wavefronts of a beam with a helical wave surface [22]. By examining the interference patterns using a Mach-Zehnder interferometer, the singularity is seen as a defect in the fringe pattern, where a new fringe line begins [23]. The rest of the interferogram will consist of uniform, straight fringes. Careful analysis of the interferograms can deduce the charge of the phase singularity (the topological charge).

The work on beams with phase singularities has not previously considered any associated orbital angular momentum with the phase dislocations, hence the current interest in the Laguerre-Gaussian modes.

II. 5 Laguerre-Gaussian laser mode production

There are various methods of producing Laguerre-Gaussian laser modes, and this section will give an overview of them. Some convert high order Hermite-Gaussian modes into corresponding Laguerre-Gaussian modes, while others convert a fundamental $TEM_{0,0}$ mode into higher-order LG modes and some produce LG modes almost directly from a laser cavity.

II. 5. 1 LG mode production from a laser

One of the first methods of producing a ring mode or doughnut $TEM_{0,1}^*$ mode was the interaction of two $TEM_{0,1}$ and $TEM_{1,0}$ modes from a laser [24]. By frequency-locking these two modes of a helium-neon laser in a single-longitudinal mode, Tamm was able to change the spectral composition of the laser signal if the beat frequency of the two interacting modes was reduced towards zero. The phases of the two modes were locked to a constant difference of $\pm\pi/2$ to produce a $TEM_{0,1}^*$ hybrid mode. This is not a pure LG mode but rather a superposition of $\ell = +1$ and $\ell = -1$ modes as there is no orbital angular momentum content. However, its intensity distribution is the same as a LG ring mode.

Lasers very rarely produce LG modes directly due to the presence of astigmatic elements in the cavity (such as Brewster plates) which cause all cylindrical symmetry to be lost. By using a CO_2 gas tube with plane-parallel, anti-reflection-coated windows, the main source of astigmatism can be removed [25]. The laser can then be tuned to particular LG mode ℓ index values and the corresponding ring modes are observed. Similar work was performed by Hennequin et al [26], who studied the production of LG modes in the cavity. Heckenberg and co-workers have also demonstrated the direct production of LG modes, using a 525 nm Na_2 vapour laser pumped by an Ar-ion laser [27]. This particular laser system had a velocity-selective optical pumping mechanism which resulted in very narrow gain linewidths so that only one set of transverse modes with specific mode indices of ℓ and p were chosen at a time.

The existence of laser states in the form of the helical wavefronts, akin to LG modes, have been demonstrated [28] and can be isolated using laser cavities with large Fresnel numbers. It is very difficult to force a laser to operate in these modes readily, so it is much more common to use techniques that convert HG modes into LG modes.

II. 5. 2 Mode production using filters/gratings and holograms

These techniques all use the same principle which is the illumination of a filter or grating with the resulting beam having an azimuthal phase term of the form $\exp(i\ell\phi)$, that of a helical waveform. A filter used for this mode production is called a "phase rotor filter" and is of the form of a mask which introduces a phase step, through which the laser light is transmitted [29] and is represented in figure II.e. The filter can be recorded by computer onto a photomask, which is then used to lay photoresist onto the phase filter using photolithography techniques. Coherent light transmitted through the phase rotor filter produces a magnified image of the Fraunhofer diffraction pattern which is of the form of a LG mode.

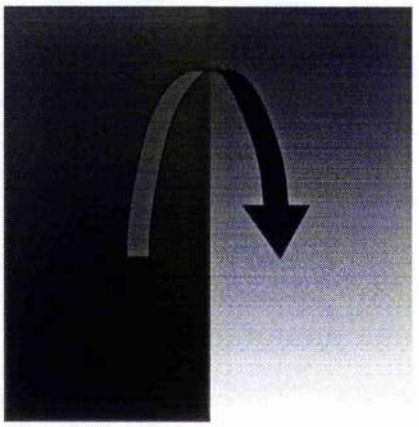

Figure II.e A typical amplitude mask for the rotor filter showing the change in transmitted amplitude around the mask

A similar technique of LG mode production is the use of diffraction gratings that have been synthesised with the aid of a computer [21]. Gratings can be computed in the form of an interference pattern with uniform straight

fringes with forks or branches in the lines, indicating the position of a phase singularity (see figure II.f). Photographs of the gratings from the computer screen are then reduced in size down to 2 x 2.5 mm^2 with a grating spacing of 0.1 mm. Modes are then obtained using a laser and observed on a screen in the far-field.

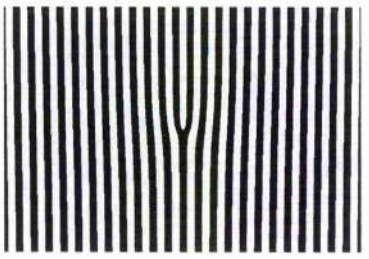

Figure II.f Diffraction grating element showing the branch/fork that introduces the phase singularity

This technique developed into a method which uses computer-generated holograms to convert a laser mode into a desired mode. This is quite an efficient method of mode production (~45% transmission efficient) and is flexible allowing any specific ℓ index to be produced, often a superposition of modes. However, to produce a pure mode with a specified p index, an amplitude mask is required and the efficiency drops to below a percent. The hologram is an interference pattern between a particular field and a reference one. When a $TEM_{0,0}$ mode (the reference) is passed through it, the output is the reconstructed field of interest.

Once again, the phase singularities are introduced by means of forks in the uniform interference fringes on the hologram [27]. The reconstructed mode will have the azimuthal phase the same as those associated with LG modes. The hologram itself is generated on a computer with the desired forks and fringe pattern, printed onto A4 paper and then reduced by photographing it to the size of half a 35 mm slide. The efficiency can be increased by bleaching the hologram.

Instead of producing the computer-generated holograms in the form of the uniform straight fringe patterns, it is also possible to produce the holograms in the form of Fresnel zone plates [30]. If the interference pattern of a plane

wave and a LG mode is recorded, the pattern is of the form of the spirals. These patterns are a variation on the Fresnel zone plate and will produce LG modes in the same way when illuminated by a He-Ne laser for example.

II. 5 .3 Mode production using spiral phaseplates

This is another method of converting a $TEM_{0,0}$ laser mode into one with a helical wavefront with a phase singularity on the beam axis. Again the output beam is a Laguerre-Gaussian beam with p=0, forming ring modes. For optical wavelengths, this method of producing LG modes was first demonstrated by Beijersbergen et al in 1994 [11].

The spiral phaseplate is a transparent plate whose thickness increases with the azimuthal angle around the circular plate (figure II.g). When a beam is passed through the plate, the resulting beam is dependent on the input beam. It can transform a non-helical beam into a helical one, but inputting a helical beam would result in the helicity of the beam being changed and not forming a non-helical beam.

The resulting beam is not a pure mode but a superposition of modes, so the spiral phaseplate is, in general, not a pure mode converter in the same way that the hologram gratings are not. If the LG mode has a modified helicity it is no longer a pure mode. Such a modified mode only exhibits the induced phase singularity in the far-field, while the near-field is the same as the input beam.

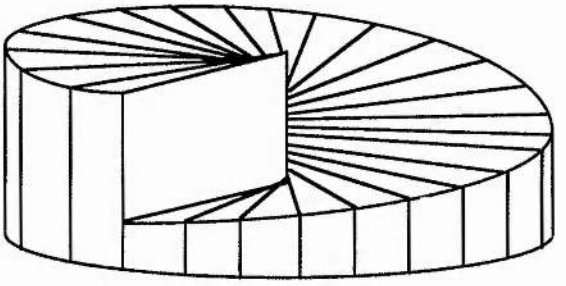

Figure II.g Spiral phaseplate

In the initial experiments by Beijersbergen, a He-Ne laser was used operating at 633 nm. Both the conversion of $TEM_{0,0}$ and LG^1_0 modes were investigated, resulting in the production of LG modes or modified LG modes respectively. By using a spiral phaseplate with different step heights, different modes were able to be produced. The input of an LG^1_0 mode was achieved using a cylindrical lens mode converter, see section II. 5. 5 for more details of this method of mode conversion.

A similar set of experiments were performed using millimetre-wave frequencies by Turnbull and co-workers in 1996 [31]. A spiral phaseplate was again used and the conversion of a $TEM_{0,0}$ mode into LG^1_0 and LG^2_0 modes was achieved.

II. 5 .4 Mode production using optical fibres

Recent work here at the University of St. Andrews has investigated a novel method of mode transformation of a $HG_{1,0}$ mode into a LG mode with ℓ=1. In this case, the mode converter was a short length of near single-mode, stressed optical fibre and the transmitted beam had a ring intensity distribution with a well defined azimuthal phase dependence. The experimental details were published in *Applied Optics* in January 1998 [32, 33].

The input beam was a $HG_{1,0}$ mode which could be considered as two orthogonal $HG_{1,0}$ modes. As the stress was changed on the fibre, the dimensions of the optical fibre waveguide were altered and the two orthogonal modes experienced different phase velocities. By carefully adjusting the stress, the difference in phase velocity caused the modes to be out of phase by 90° at the end of the fibre and a circularly symmetric ring mode was transmitted as the output mode.

The presence of the azimuthal phase dependence was confirmed using the same experimental technique that will be described in Chapter IV (section 2). As expected, there was a transfer of orbital angular momentum to the transmitted light of $\hbar$ per photon. This method of mode conversion is very

restrictive on the LG modes which are available as a pure ℓ mode can be produced but not a pure p mode.

II. 5 .5 Mode production using cylindrical lenses

The idea of using a cylindrical lens to convert a HG mode into a LG mode was considered in mathematical terms by Abramochkin and Volostnikov [34] who used a single lens but did not produce a structurally stable beam. Les Allen and co-workers [2] used a mode converter using two cylindrical lenses in their experimental work studying the structure of laser modes, as did Tamm and Weiss [35]. This is an experimental method of producing very pure LG modes with almost 100% efficiency.

In a follow up paper to the Allen paper [2], Beijersbergen et al [36] describe in more detail the operation of the "mode converter" and the basic principles can be explained here. There are direct relations between Hermite-Gaussian and Laguerre-Gaussian modes [37]. An LG mode can be written as a sum of HG modes and vice versa, so each mode type can be expressed in terms of the other [38] as they are both complete basis sets. There is a simple relationship between the indices of the transforming modes, which for an input HG mode of indices m and n, can convert into an LG mode of indices ℓ and p in the following way,

$$\ell = |m - n| \qquad p = \min(m, n). \tag{2.4}$$

It is by means of these two relations that the corresponding LG mode can be deduced from knowing the input HG mode. Basically, the cylindrical lens mode converter carries out these relations in the mode transformation.

An HG mode can be decomposed into a product of Hermite polynomials in the x and y axes if the mode's principle axes are orientated at 45° to the x and y axes. (For the cylindrical lens mode converter to operate correctly, the input HG mode must be aligned at 45° to the x and y axes of the lenses.) These mode components are in phase to form the original HG mode. To convert the mode into a LG mode, it is necessary to introduce a phase shift

between the decomposed HG mode components. This is achieved by introducing a Gouy phase to the Gaussian mode.

The Gouy phase Ψ, is the phase shift that a beam experiences when going through a beam waist, as compared to that of a plane wave of the same frequency. For an $HG_{m,n}$ mode, the Gouy phase is given by

$$\Psi(z) = (n+m+1)\arctan\left(\frac{z}{z_r}\right) \tag{2.5}$$

where z is the distance along the beam axis from the beam waist and z_r is the Rayleigh range. Similarly, the Gouy phase shift for an LG^{ℓ}_{p} mode is given by

$$\Psi(z) = (2p+\ell+1)\arctan\left(\frac{z}{z_r}\right). \tag{2.6}$$

In the mode converter, the Gaussian beam is focussed by a cylindrical lens and it becomes an elliptical Gaussian beam. Consequently, the Rayleigh ranges in the x-z and y-z planes are not equal and the corresponding Gouy phase shift for this situation is

$$\Psi(z) = \left(m+\frac{1}{2}\right)\arctan\left(\frac{z}{z_{r(x-z)}}\right)+\left(n+\frac{1}{2}\right)\arctan\left(\frac{z}{z_{r(y-z)}}\right) \tag{2.7}$$

The different Rayleigh ranges of the decomposed components of the initial HG mode as they pass through the cylindrical lens, mean that the component modes will undergo different Gouy phase shifts. Upon recombination of the HG mode components, the corresponding LG mode will be formed if the difference in the Gouy phase shifts of the component HG modes is $\pi/2$ (figure II.h). This occurs when the separation d, of the two cylindrical lenses if focal lengths f is given by [36] ,

$$2d = f\sqrt{2} \tag{2.8}$$

and the Rayleigh range of the incident beam is

$$z_r = \left(1 + \frac{1}{\sqrt{2}}\right) f. \tag{2.9}$$

The incident Rayleigh range of the HG mode can be adjusted by adding a spherical lens of the appropriate focal length before the cylindrical lens mode converter. Beijersbergen [36] presents the images of various input modes and the mode conversions of the HG modes into their corresponding LG modes.

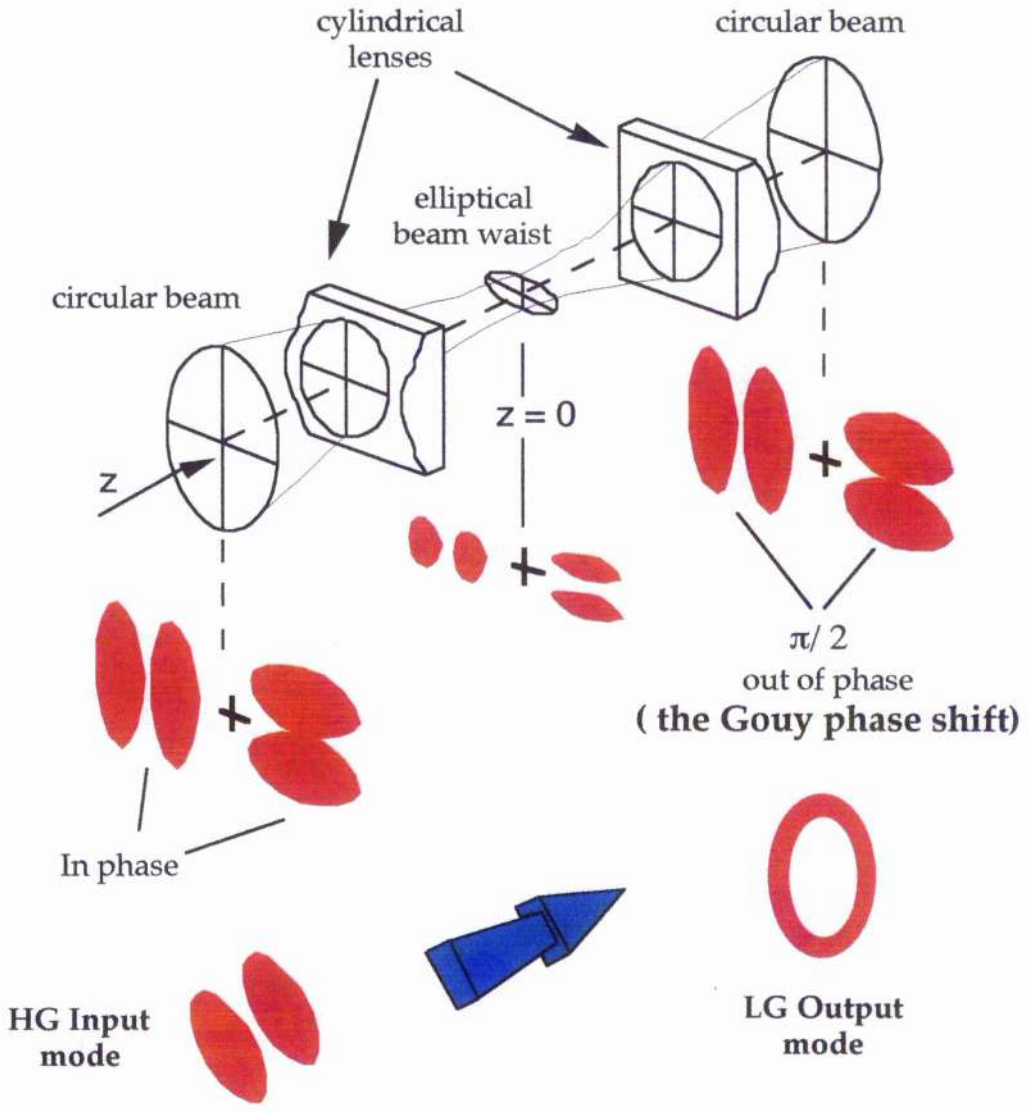

Figure II.h The cylindrical lens mode converter

II. 6 Conclusions

The aim of this chapter was to introduce the concepts of orbital angular momentum of light and the family of laser modes that possess this angular momentum content, Laguerre-Gaussian modes.

It is because of this link between LG modes and the orbital angular momentum of light that such interest has arisen in these modes. By using cylindrical lens mode converters, very pure LG modes can be produced and used in different experimental areas to investigate other physical properties. Areas of interest are the focussing of atomic beams [39], the behaviour of atoms in the presence of the orbital angular momentum of LG modes [40], the second harmonic generation of LG beams in nonlinear media [41] and of course, the transfer of the orbital angular momentum from a LG beam to matter which is covered in this PhD work.

References

1. Beth, R.A., *Mechanical detection and measurement of the angular momentum of light.* Phys. Rev., 1936. **50**: p. 115-125.

2. Allen, L., M.W. Beijersbergen, R.J.C. Spreeuw, and J.P. Woerdman, *Orbital angular momentum of light and the transformation of Laguerre-Gaussian laser modes.* Phys. Rev. A, 1992. **45**: p. 8185-8189.

3. Siegman, A.E., *Lasers.* 1986, Mill Valley, CA: University Science Books.

4. Jackson, J.D., *Classical Electrodynamics.* 1962, New York: Wiley.

5. Padgett, M.J. and L. Allen, *The Poynting vector in Laguerre-Gaussian laser modes.* Opt. Comm., 1995. **121**: p. 36-40.

6. Taché, J.P., *Derivation of ABCD law for Laguerre-Gaussian beams.* Appl. Opt., 1987. **26**(14): p. 2698-2700.

7. Gase, R., *Representation of Laguerre-Gaussian modes by the Wigner distribution function.* IEEE J. of Quant. Elec., 1995. **31**: p. 1811-1818.

8. Beth, R.A., *Direct detection of the angular momentum of light.* Phys. Rev., 1935. **48**: p. 471.

9. Poynting, J.H., Proc. R. Soc. Lond., Ser. A, 1909. **82**: p. 560.

10. Van-Enk, S.J. and G. Nienhuis, *Commutation rules and eigenvalues of spin and orbital angular momentum of radiation fields.* J. of Mod. Opt., 1994. **41**: p. 963-977.

11. Beijersbergen, M.W., R.P.C. Coerwinkel, M. Kristensen, and J.P. Woerdman, *Helical-wavefront laser beams produced with a spiral phaseplate.* Opt. Comm., 1994. **112**: p. 321-327.

12. Babiker, M., W.L. Power, and L. Allen, *Light-induced torque on moving atoms.* Phys. Rev. Lett., 1994. **73**: p. 1239-1242.

13. Van-Enk, S.J. and G. Nienhuis, *Eigenfunction description of laser beams and orbital angular momentum of light.* Opt. Comm., 1992. **94**: p. 147-158.

14. Barnett, S.M. and L. Allen, *Orbital angular momentum and nonparaxial light beams.* Opt. Comm., 1994. **110**: p. 670-678.

15. Nye, J.F. and M.V. Berry, *Dislocations in wave trains.* Proc. R. Soc. Lond. A, 1974. **336**: p. 165-190.

16. Basistiy, I.V., V.Y. Bazhenov, M.S. Soskin, and M.V. Vasnetsov, *Optics of light beams with screw dislocations.* Opt. Comm., 1993. **103**: p. 422-428.

17. Basistiy, I.V., M.S. Soskin, and M.V. Vasnetsov, *Optical wavefront dislocations and their properties.* Opt. Comm., 1995. **119**: p. 604-612.

18. Brambilla, M., F. Battipede, L.A. Lugiato, V. Penna, F. Prati, C. Tamm, and C.O. Weiss, *Transverse laser patterns. I. Phase singularity crystals.* Phys. Rev. A, 1991. **43**(9): p. 5090-5113.

19. Brambilla, M., L.A. Lugiato, V. Penna, F. Prati, C. Tamm, and C.O. Weiss, *Transverse laser patterns. II. Variational principle for pattern selection, spatial multistability, and laser hydrodynamics.* Phys. Rev. A, 1991. **43**(9): p. 5114-5120.

20. Bazhenov, V.Y., M.V. Vasnetsov, and M.S. Soskin, *Laser beams with screw dislocations in their wavefronts.* JETP Lett., 1990. **52**: p. 429-431.

21. Bazhenov, V.Y., M.S. Soskin, and M.V. Vasnetsov, *Screw dislocations in light wavefronts.* J. of Mod. Opt., 1992. **39**: p. 985-990.

22. Vaughan, J.M. and D.V. Willetts, *Interference properties of a light beam having a helical wave surface.* Opt. Comm., 1979. **30**: p. 263-267.

23. White, A.G., C.P. Smith, N.R. Heckenberg, H. Rubinsztein-Dunlop, R. McDuff, and C.O. Weiss, *Interferometric measurements of phase singularities in the output of a visible laser.* J. of Mod. Opt., 1991. **38**(12): p. 2531-2541.

24. Tamm, C., *Frequency locking of two transverse optical modes of a laser.* Phys. Rev. A, 1988. **38**(11): p. 5960-5963.

25. Slekys, G., C.O. Weiss, D.Y. Tang, and M.F.H. Tarroja, *Helical-wave emission of lasers.* J. Opt. Soc. Am. B, 1994. **11**(10): p. 2089-2094.

26. Hennequin, D., C. Lepers, E. Louvergneaux, D. Dangoisse, and P. Glorieux, *Spatio-temporal dynamics of a weakly multimode CO2 laser.* Opt. Comm., 1992. **93**: p. 318-322.

27. Heckenberg, N.R., *Laser beams with phase singularities.* Opt. and Quant. Elec., 1992. **24**: p. S951-S962.

28. Coullet, P., L. Gil, and F. Rocca, *Optical vortices.* Opt. Comm., 1989. **73**: p. 403-408.

29. Khonina, S.N., V.V. Kotlyar, M.V. Shinkaryev, V.A. Soifer, and G.V. Uspleniev, *The phase rotor filter.* J. of Mod. Opt., 1992. **39**(5): p. 1147-1154.

30. Heckenberg, N.R., R. McDuff, C.P. Smith, and A.G. White, *Generation of optical phase singularities by computer-generated holograms.* Opt. Lett., 1992. **17**: p. 221-223.

31. Turnbull, G.A., D.A. Robertson, G.M. Smith, L. Allen, and M.J. Padgett, *The generation of free-space Laguerre-Gaussian modes at millimetre-wave frequencies by use of a spiral phaseplate.* Opt. Comm., 1996. **127**: p. 183-188.

32. McGloin, D., N.B. Simpson, and M.J. Padgett. *The transfer of orbital angular momentum from a light beam to a stressed fibre-optic waveguide.* in *National Quantum Electronics Conference - QE13.* September 1997. poster P6-2, Cardiff, UK.

33. McGloin, D., N.B. Simpson, and M.J. Padgett, *Transfer of orbital angular momentum from a stressed fiber-optic waveguide to a light beam.* Appl. Opt., 1998. **37**: p. 469-472.

34. Abramochkin, E. and V. Volostnikov, *Beam transformations and nontransformed beams.* Opt. Comm., 1991. **83**: p. 123-135.

35. Tamm, C. and C.O. Weiss, *Bistability and optical switching of spatial patterns in a laser.* J. Opt. Soc. Am. B, 1990. **7**: p. 1034-1038.

36. Beijersbergen, M.W., L. Allen, H.E.L.O.v.d. Veen, and J.P. Woerdman, *Astigmatic laser mode converters and transfer of orbital angular momentum.* Opt. Comm., 1993. **96**: p. 123-132.

37. Danakas, S. and P.K. Aravind, *Analogies between two optical systems (photon beam splitters and laser beams) and two quantum systems (the two-dimensional oscillator and the two-dimensional hydrogen atom).* Phys. Rev. A, 1992. **45**: p. 1973-1977.

38. Kimel, I. and L.R. Elias, *Relations between Hermite and Laguerre Gaussian modes.* IEEE J. of Quant. Elec., 1993. **29**: p. 2562-2567.

39. McClelland, J.J. and M.R. Scheinfein, *Laser focusing of atoms: a particle-optics approach.* J. Opt. Soc. Am. B, 1991. **8**(9): p. 1974-1986.

40. Power, W.L., L. Allen, M. Babiker, and V.E. Lembessis, *Atomic motion in light beams possessing orbital angular momentum.* Phys. Rev. A, 1995. **52**: p. 479-488.

41. Dholakia, K., N.B. Simpson, M.J. Padgett, and L. Allen, *Second-harmonic generation and the orbital angular momentum of light.* Phys. Rev. A, 1996. **54**: p. R3742-R3745.

Chapter III

Review of Optical Tweezers

Contents

III. 1 Introduction

This Chapter will review the origins of the Optical Tweezers technology and describe how the technique has developed over the last 20 years. The work began with Arthur Ashkin at the Bell Telephone Laboratories in the USA who first demonstrated the possibility of trapping and manipulating micron-sized particles.

The first work performed by Ashkin and his co-workers used the radiation pressure of a laser to accelerate horizontally and trap a particle against a wall or surface [1]. This then progressed to using two opposing laser beams and trapping a particle in the optical potential well where the two propagating beams overlapped.

Optically trapping was also achieved by using just one laser directed in an upward direction, thus using the radiation pressure of the laser beam itself to counteract the gravitational forces pulling the particle downwards. This technique was called *Optical Levitation* [2].

The crucial breakthrough came with a technique which enabled the trapping laser to be used in a downward direction. It was not the radiation pressure that provided the optical trapping forces, but the gradient forces of a tightly focussed laser beam as it passed through the trapped particle. This technique, known as the "single beam gradient force optical trap" [3], is now commonly referred to as *Optical Tweezers.*

The principles of Optical Tweezers will now be discussed. In particular, the axial and transverse trapping forces will be considered. The standard arrangement for the operation of tweezers will also be described, along with the laser requirements and the types of particles that can be expected to be "tweezed".

The Chapter will conclude with an overview of the current applications of tweezers' systems in the world today, which are mainly in the field of biology.

III. 2 Trapping using radiation pressure

The first observation of the acceleration and trapping of micron-sized particles was published in 1970 by Arthur Ashkin of the Bell Telephone Laboratories [1]. The experiments were performed using transparent latex spheres of diameters 0.6, 1.3 and 2.7 μm suspended in water. The laser used was an argon ion laser operating in a $TEM_{0,0}$ mode, with a beam waist of 12 μm at a wavelength of 515 nm. The laser was directed horizontally and focussed through a glass cell containing the solution of the spheres, with a microscope positioned to observe the trapping.

III. 2. 1 The acceleration of spheres using light

As the laser beam propagated through the sample cell (of a thickness 120μm), there were interactions between the beam and the spheres (fig III.a). The spheres underwent Brownian motion in the water solution until the laser beam was directed into the sample cell with only milliWatts of laser power. When the beam hit a sphere that was positioned off the beam propagation axis, the sphere was drawn in to the beam axis and accelerated along the axis

in the direction of the light propagation. It reached a terminal velocity of the order of microns per second until it collided with the wall of the sample cell where it remained trapped against the surface in the laser beam.

This phenomenon occurred for all of the sphere sizes that Ashkin used in this early work, with the larger size spheres requiring more laser power to achieve the same terminal velocities. In a similar experiment, again by Ashkin [1], 5 μm diameter water drops were accelerated in air with a single beam. This motion was clearly visible, as the laser with 50 mW of laser power was able to move the water droplets at velocities of 2.5 mm per second.

The observation of spheres being attracted in to the laser beam axis and being accelerated along the beam in the direction of propagation, was due to radiation pressure forces from the refraction and reflection of the rays of light as they passed through the sphere. This will be considered in more detail in section III. 5. The refraction and reflection results in a net radial force inwards to the beam axis and a net forward force along the beam axis, thus the sphere is observed to be accelerated inwards and forwards.

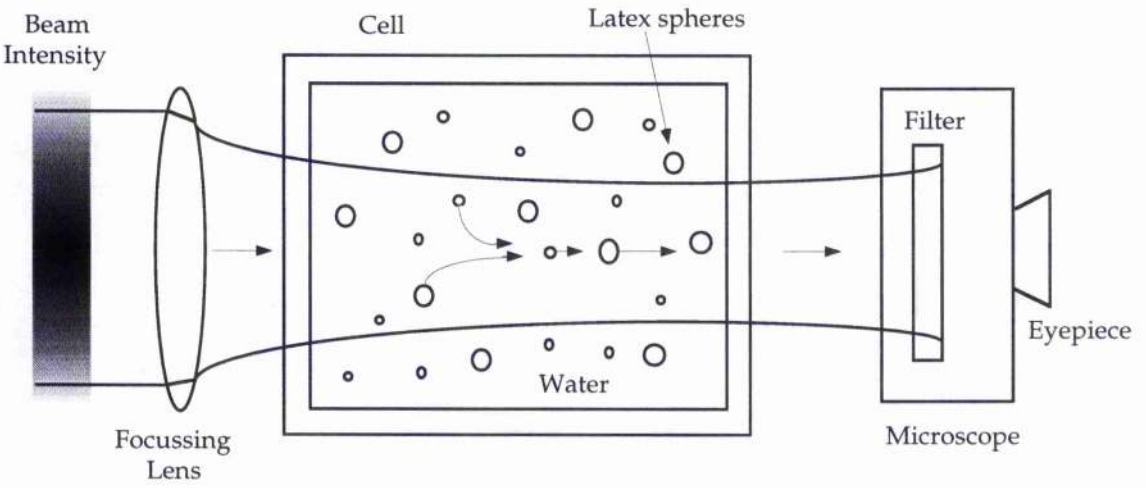

Figure III.a Acceleration of particles using a focussed laser beam

For the case of the latex spheres in water, the spheres have a higher refractive index (n_s = 1.58) than their surrounding medium, i.e. the water (n_w = 1.33). This results in the sphere acting as a converging or focussing lens and the spheres experience the inward radiation pressure force to the beam axis. However, if the magnitude of the refractive indices are reversed, the sign of the radial radiation pressure force is also reversed resulting in the sphere being pushed sideways out of the beam. Now the sphere acts as a diverging lens on the beam as it passes through.

Ashkin confirmed this experimentally by using a solution of 8 μm diameter air bubbles (n_s = 1.00) in an 80% mixture of glycerol in water of refractive index n_g = 1.44. The bubbles were always pushed out of the laser beam but still experienced the accelerating force along the beam axis at the same time.

This radial inward force on high refractive index spheres, was the experimental observation that started the interest in the whole field of optical trapping of particles. Ashkin believed that it would be possible to construct an "optical potential well" based on radiation pressure alone.

III. 2. 2 Trapping in an "optical potential well"

Ashkin went on to perform an experiment which comprised of two opposing laser beams of the same parameters, with their beam waists positioned as shown in figure III.b. The laser and spheres in suspension were the same as those used in his first experiment as described in section III. 2. 1.

When one of the spheres (of high refractive index) fell within the laser beams, it experienced forces that attracted it in to the beam axis and experienced an acceleration along the direction of beam propagation as before. However, at the point of symmetry of the two beams, there was a region of stable equilibrium where the accelerating sphere experienced an opposing force and the sphere remained trapped at that equilibrium point. Any displacement from this region resulted in a restoring force pulling the sphere back to the "optical potential well".

This was observed by Ashkin [1] with the argon ion laser operating in the $TEM_{0,0}$ mode at a few 10's of milliWatts to produce the two opposing beams and a sample cell containing 2.7 μm diameter latex spheres in a water solution as before. When particles drifted close to either of the beams, they were drawn in and accelerated to the equilibrium point where they stopped and remained trapped.

The accelerating and trapping of micron-sized spheres had been achieved and this work paved the way for the development of further trapping techniques.

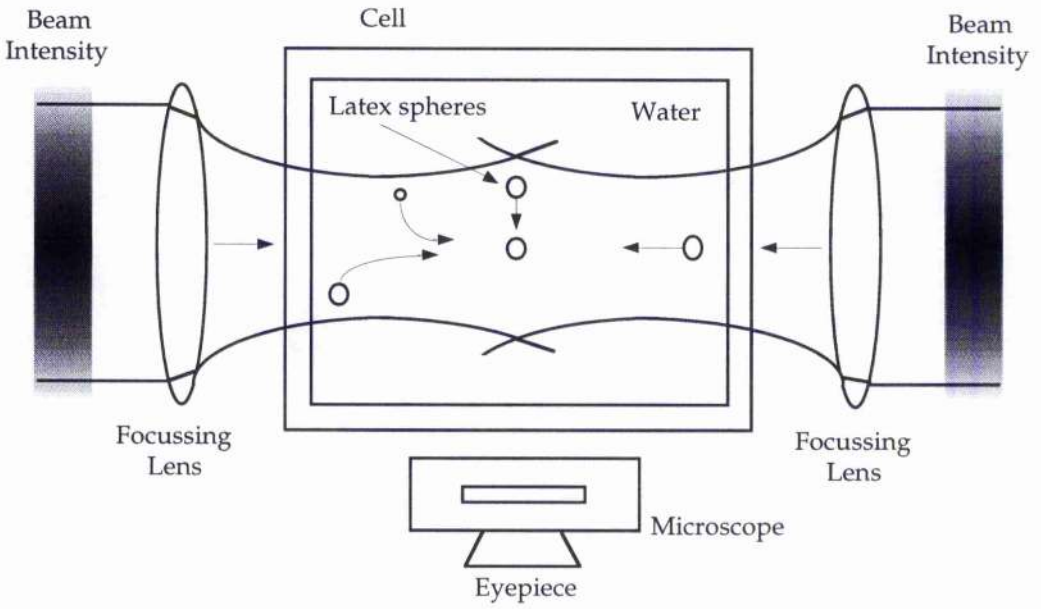

Figure III.b Trapping of particles in a stable optical potential well

III. 3 Optical levitation

The trapping of particles then took another step forwards, with the development of a technique called "optical levitation". Again it was Arthur Ashkin, along with Joseph Dziedzic, at the Bell Laboratories who pioneered this work in 1971 [2]. Using a laser beam that was directed vertically upwards, they were able to balance the gravitational forces of the trapped particle with the radiation pressure of the laser beam and suspend the particle in the surrounding medium.

A single, vertically directed, focussed, continuous-wave laser beam was used to raise a glass sphere off the bottom of a sample cell and levitate it in a very controlled manner. The laser had a wavelength of 515 nm and was operating at about 250 mW in a $TEM_{0,0}$ mode with a beam waist of 25 μm. The spheres were made of transparent glass and 20 μm in diameter and sealed in a sample cell containing air as the suspending medium.

An acoustic wave was required to loosen the spheres off the base of the cell. They were then forced upwards by the radiation pressure forces of the diverging Gaussian beam until these forces were balanced by the gravitational forces on the sphere. An equilibrium position was reached above the beam waist, where the sphere was completely suspended in air - hence the term "optical levitation". It was then possible to move the beam around the cell, all the while keeping the particle trapped at the equilibrium position within the laser beam. This was a very stable situation which could be maintained for hours if required.

When the air pressure in the sample cell was decreased down to a vacuum of 133 N/m^2 or 1 Torr (compared with atmospheric pressure of 101,325 N/m^2 or 762 Torr), optical levitation could still achieved. However, the equilibrium position dropped down to a point nearer the base of the cell. This was due to an additional downward force caused by a temperature difference at the top and bottom of the sphere, resulting in a downward radiometric force. Additionally, at low pressures, the particles became less stable both vertically and horizontally, due to their Brownian motion becoming increasingly dominant.

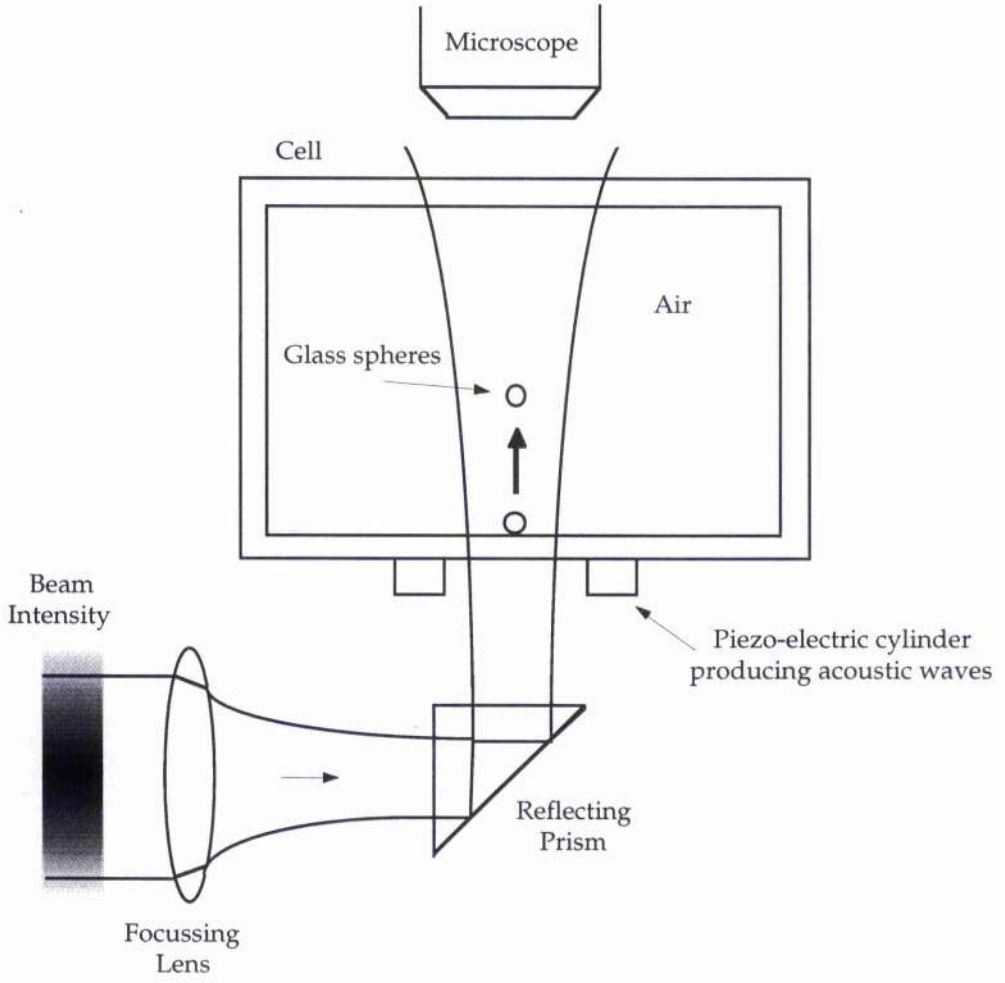

Figure III.c The optical levitation experimental set-up

By introducing a secondary laser to the system in the horizontal direction (figure III.d), it was determined that the horizontal restoring forces were much stronger than the vertical restoring forces about the equilibrium point of the trap, i.e. the radial forces were larger than the axial forces.

This horizontal beam had adjustable power and was used to find the maximum power that would still allow the sphere to remain trapped within the vertical, levitating laser beam. The sphere was displaced horizontally as the power was increased up to 125 mW, which almost pushed the sphere out

of the trap. The weak vertical stability was very susceptible to minor power fluctuations whereas the transverse trapping was extremely stable.

Ashkin and Dziedzic did try other laser modes in their optical levitation arrangement, namely the $TEM_{0,1}$ and $TEM^{*}_{0,1}$ (doughnut) modes. These were successful but they found the fundamental $TEM_{0,0}$ mode to be the optimum mode for their optical levitation systems.

All of Ashkin's early work on radiation pressure and optical levitation is succinctly covered in the one article written in *Scientific American* by Ashkin himself [4], which describes and summarises his pioneering experiments.

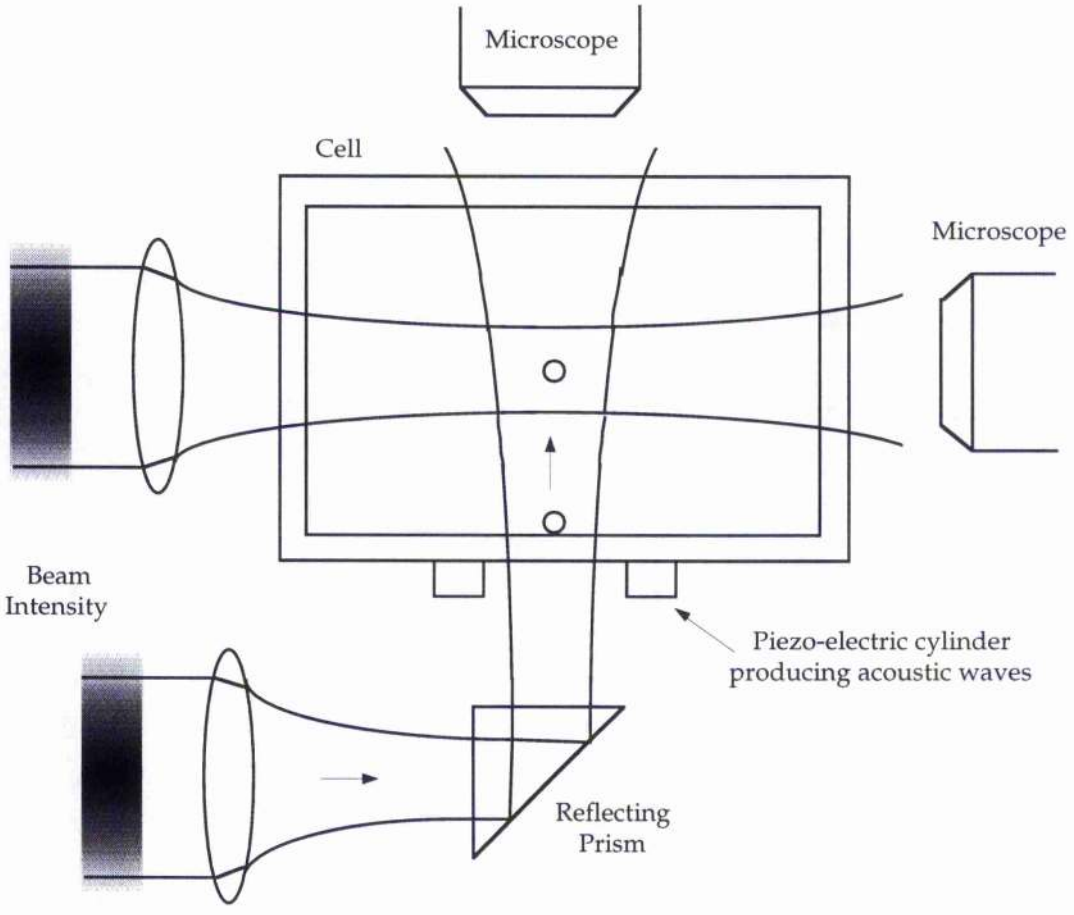

Figure III.d Two laser system to investigate the radial forces

III. 3. 1 Improving optical levitation

Work continued with $TEM^{*}_{0,1}$ (doughnut) modes in optical levitation experiments and trapping was achieved with transparent, hollow dielectric spheres [5, 6]. In this instance, the wavelength of the laser was 488 nm and the doughnut mode meant that there was an intensity minimum on the beam propagation axis. The hollow, dielectric spheres were partially reflecting, thin-walled (1.5 μm thickness) and of a diameter 45 μm. Approximately three times as much laser power was required to levitate a 40 μm hollow sphere compared to an equivalently weighted 24 μm solid sphere.

As Ashkin had already discovered, the axial stability was somewhat limited due to laser power fluctuations, so attempts were made to improve it. By incorporating a short focal length lens with a long working distance into the trapping set-up, the vertical gradient of the light intensity was increased. By increasing the effective convergent angle of the beam by a factor of 10, Ashkin found that the stability of the vertical trap also improved by a factor of about 10. Not only did this high numerical aperture lens system improve the vertically trapping and stability, but it also brought with it the possibility of a second trapping region along the beam axis.

With the high numerical aperture system, the focussed beam waist (~2 μm) was considerably less than the size of the sphere (~20 μm) and a second region of stability was formed below the beam waist. For vertical stability, the force vertically must increase if there is a displacement on the trapped particle downwards. For the smaller beam waist situation, the vertical force has a minimum at the beam focus while above and below the focus, the beam diverges quickly and surface reflections and refractions give a larger force. This results in there being two regions of stability, one above and one below the beam focus. The focussed beam provided two trapping regions and much more vertically stability.

III. 3. 2 Experiments using optical levitation

Ashkin and Dziedzic then proceeded to experiment further with optical levitation to study many situations and phenomena. They succeeded in observing levitation in high vacuum conditions down to pressures of 10^{-6} Torr, using very low absorption particles such as silicone oil drops and fused quartz spheres [7]. Optical levitation was used to observe a new nonlinear photoelectric effect in glass by measuring very low emission rates [8] and also to observe optical resonances in radiation pressure on dielectric spheres [9]. They developed an electronic feedback system to control the laser power and lock an optically levitated sphere in space [10] and Roosen and Imbert in 1976 demonstrated a method for optical levitation using two horizontal $TEM_{0,0}$ laser beams [11].

In the early 1980's, Ashkin and Dziedzic used the levitation technique to prove an optical radiation Earnshaw theorem [12]. This said that a small dielectric particle could not be trapped using the scattering forces of radiation pressure alone, gradient forces are also required to allow trapping. A couple of years later, they published a paper demonstrating a new principle of radiation pressure trapping of dielectric particles by using alternating light beams [13]. Trapping was possible due to the alternating scattering force fields and they believed that this technique could be used in atom trapping to overcome the limitations of the optical Earnshaw theorem.

They also successfully extended the trapping to nonspherical particles so that the light scattering from them could be studied [14]. The particles were constructed from combinations of spheres to create spheroids, teardrops, spherical doublets, triplets, quadruplets and spheres within spheres. By using optical levitation, detailed studies were made of the light scattering in the near and far field with very high resolution.

In 1984, work was performed using single mode optical fibres to achieve optical levitation [15]. The fibres enabled less complicated optical paths to be constructed in the experiments. In the early 1990's, fibre optics were used once more to demonstrate a stable 3-dimensional optical trap [16].

There has also been significant work concentrating on the modelling of the radiation pressure forces involved in optical levitation. Some are based on light scattering theories, which produce exact numerical solutions but tend to be very mathematical and complex. By using a geometrical optics approach, simpler and still adequately accurate models can be derived. For example, Gauthier and Wallace produced a geometrical optics model that compared very favourably with published experimental work [17].

III. 4 The single beam gradient force optical trap - "optical tweezers"

The next major advancement in the trapping of micron-sized particles was the development of the single beam gradient force optical trap. It was this arrangement that became known as "optical tweezers".

Once more, it was Arthur Ashkin and Joseph Dziedzic with their co-workers, John Bjorkholm and Steven Chu at the AT&T Bell Laboratories, who demonstrated the first trapping of dielectric particles using this system [3]. It had been proposed as an atom trap in 1978 but it was not until 1986 that it was applied to trap micron-sized particles up to 10 μm in size. This could be said to be the birth of "optical tweezers" as we know them today.

The main new feature of this approach was the use of the gradient force to form a 3-D trap using a single laser beam. The gradient force is proportional to the intensity gradient which points in the direction of the +ve gradient i.e. from low to high intensity. By contrast, the scattering force is proportional to the optical intensity but points in the direction of propagation of the incident light.

In the early single beam trap, using optical levitation, the axial stability depended on the balancing of the scattering force with gravity and the axial gradient force was small. In this new all-optical single beam system, the axial gradient force is very large and dominates the stability in the axial direction without the need for gravity.

The presence of the backward gradient force is most obvious when trapping Mie particles, those particles that have a diameter larger than the wavelength of the trapping laser. A geometrical optics approach can be used for these particles to describe the reflection and the refraction of the light through the particle. This will be considered in more detail in section III. 5. The basis of this trapping is the refraction of light through a trapped sphere, producing a net backward trapping force acting on the sphere towards the beam's focus. This trapping mechanism also applies for Rayleigh particles, i.e. those particles whose diameter is smaller than the wavelength of the light being used. However, a ray optics approach cannot be used to describe these interactions.

In the first demonstration of the single beam gradient force optical trap, the apparatus that was used comprised of an argon ion laser at 515 nm operating at ~100 mW, which was directed through a high numerical aperture (NA 1.25) water-immersion microscope objective. This created a very tightly focussed laser beam that was focussed into a sample containing glass spheres of about 10 μm in size (Mie particles) suspended in a water solution. They used a second laser to optically levitate the spheres off the bottom of the cell, as in section III. 3, to move them into the focus of the trapping beam (figure III.e).

Successful trapping was also observed with Rayleigh particles down to a sphere size of 25 nm. Once a particle was trapped it ceased to exhibit Brownian motion, and there was complete control over the sphere. The translation of the particle could be achieved in two ways. Either the laser can be translated dragging the sphere with it, or the cell can be translated relative to the fixed, trapped sphere. The manipulation was compared to manoeuvring particles with a pair of tweezers, hence the term "optical tweezers" which was first coined by Ashkin and Dziedzic in 1987 [18].

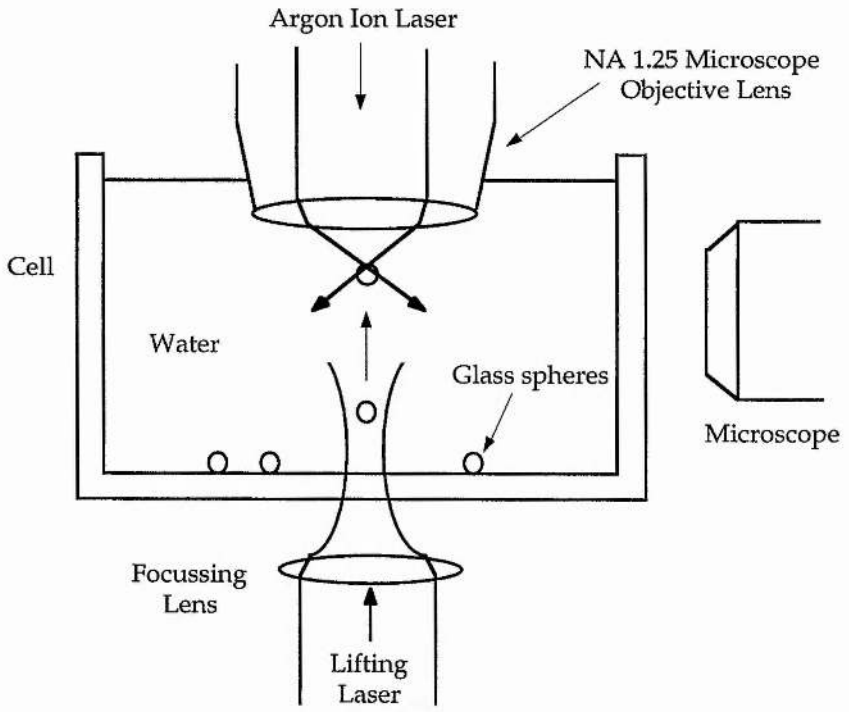

Figure III.e The single beam backward gradient force optical trap

This was the last major advancement in the development of the optical tweezers. The majority of the work with the tweezers from then on was concentrated on their application within biology and the manipulation of cells and bacteria, which will be discussed in section III. 7. For developing the optical tweezers, Ashkin and Dziedzic were awarded the 1993 Rank Prize in optoelectronics.

The tweezers' experimental arrangements have been improved over the years, the most significant development being the introduction of diode lasers as the trapping laser. Until the early 1990's, most of the tweezers' systems used a Nd:YAG or an argon ion laser as the trapping beam, but using a diode laser brings added advantages. The most obvious advantage is the small size of the diode laser, which helps to make the tweezers more portable. In 1990, Ashkin and Dziedzic recommended using the diode wavelength range 0.8-1.8 μm within optical tweezers [19], as this would reduce the optical damage to living biological samples.

Increasing absorption of light by the trapped particle reduces the backward gradient force and increases the risk of optical or thermal damage to the particle. The near infra-red region of the spectrum is most desirable for trapping biological applications, as the ultra-violet and short visible wavelengths have a strong absorption in biological materials and using infra-red would have a strong absorption in water. Also the near infra-red laser diodes have good spatial coherence which is vital for tightly focussing the laser beam by the high numerical aperture microscope objective lens. They are also considerably cheaper than Nd:YAG and argon ion lasers.

Sato et al demonstrated optical trapping of micron-sized polystyrene latex spheres, glass spheres and yeast cells, using a 1.3 μm InGaAsP diode laser operating at ~5 mW [20]. Similar work was accomplished by Afzal and Treacy [21] who described how to construct a simple optical tweezers system using a laser diode at 840 nm, and also by Bakker-Schut and co-workers [22] using a 780 nm diode laser.

III. 5 The principles behind optical tweezers

A basic understanding of the techniques of optical levitation and the single beam backward gradient force trap (optical tweezers) comes from the reflection and refraction of the rays of the beam as they interact with the particle. Both techniques can be understood by considering the radial forces and the axial forces acting on the particle, also known as the x-y and z trapping forces. If the particle is larger than the wavelength of the laser, the Mie regime, then a ray optics approach can be used to explain the phenomenon. The majority of trapping applications are in this regime.

III. 5. 1 The x-y trapping forces (radial forces)

There are two cases of x-y trapping that must be considered. The first is encountered more regularly as this is the trapping of a particle whose refractive index is higher than the surrounding supporting medium. Typically, especially in the early work of the 1970's and 80's, this tends to be glass or silica spheres ($n \approx 1.6$) suspended in water ($n = 1.33$). In this case, the sphere (taken as an idealised, symmetrical particle), acts as a converging lens

and experiences a force drawing it to the beam axis. This can be explained in terms of the refraction of rays of a near-collimated propagating beam through Mie particles (figure III.f).

By considering two rays incident on the sphere, the radial forces can be understood. The ray nearer the beam axis is a stronger ray as it has a larger intensity. It initially undergoes a Fresnel reflection and a refraction at the first interface. This results in a radiation pressure force F_{R1} caused by the reflection and a refraction force F_{D1} caused by the deflection of the ray as indicated on figure III.f. It then experiences a similar reflection and refraction at the interface of the sphere as the ray emerges resulting in the forces F_{R2} and F_{D2} . All forces result in a forward acceleration in the +z direction. The radial components of F_{R1} and F_{R2} approximately cancel, but the radial components of F_{D1} and F_{D2} add to give a net radial force inwards to the beam axis and the higher laser light intensity.

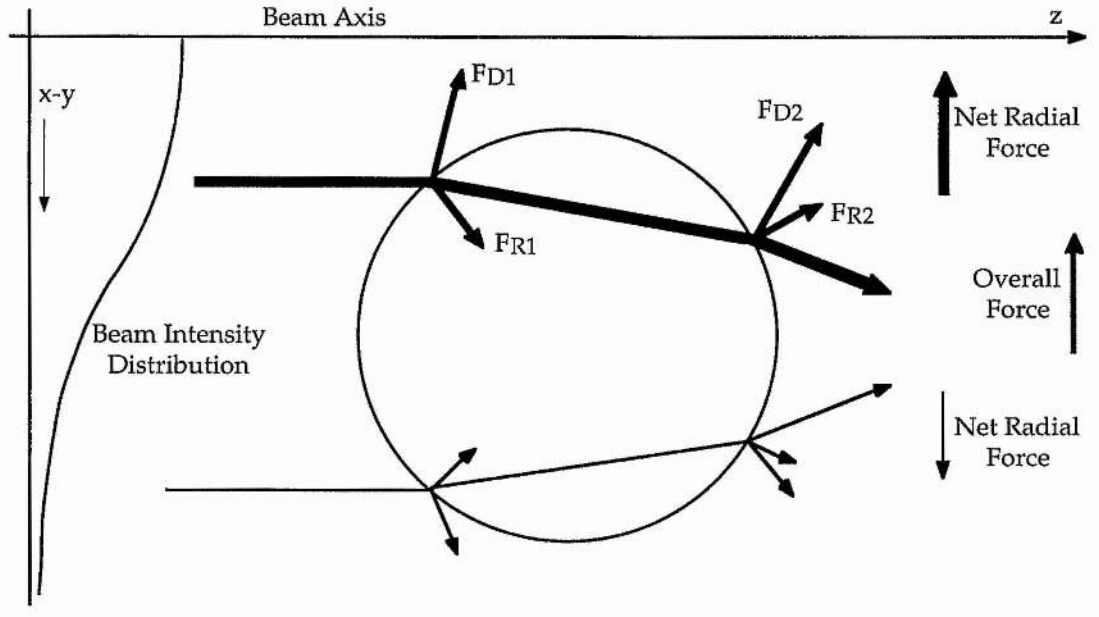

Figure III.f Radial forces acting on high index Mie particle off the beam axis

The second, weaker ray experiences similar reflections and refractions resulting in a net outward radial force. Due to this ray having a weak intensity associated with it, there is an overall net radial force experienced by the sphere which is directed inwards, drawing the sphere to the region of high light intensity. Once the sphere is on the axis, the radial components cancel completely and the sphere remains "trapped" on the beam axis. If the sphere is deflected off axis, it will experience radial, restoring forces and the sphere will return to the beam axis.

There is a second case that must be considered also, which is the x-y trapping forces acting on a Mie particle, whose refractive index is less than that of the surrounding supporting medium. For these particles, the sign of the radial forces, due to the refraction of rays, is reversed as the sphere is now behaving as a diverging lens. Usually this results in an overall net radial force on the sphere acting away from the beam's axis, which causes the sphere to be pushed out of the beam. Higurashi and co-workers demonstrated the optical trapping of low refractive index particles, using particles of index 1.525 in a suspending medium of index 1.605 [23].

The geometrical optics explanation is valid for Mie particles, but for particles that are smaller in size than the laser wavelength (Rayleigh particles) it is not possible to use this approach. For Rayleigh particles, a full numerical, complicated analysis has to be applied to understand the interactions of the beam with the sphere but the particles experience similar radial forces depending on the refractive indices.

III. 5. 2 The z trapping forces (axial forces)

As described in the previous sub-section, the interaction of the rays results in an acceleration of the particle in the +z direction. For optical levitation, this force is used to balance that due to gravity to give a stable trap. Within optical tweezers, the single beam backward gradient force trap, the beam is tightly focussed with a high numerical aperture microscope objective lens. In this case, the radial trapping forces occur in the same way as before, but the axial forces are very different.

For spherical Mie particles, the reflection and refraction of the rays of the laser beam can be described by ray optics as before. For the extremal rays, the forces due to refraction F_R are directed back along the negative z direction (figure III.g). The component of the gradient forces along the beam axis can therefore be defined as being "backward", as there is a large net force acting against the forces of the radiation pressure. It is this z trapping force that balances the forces due to gravity and radiation pressure to create the trapping along the beam axis. Combined with the radial trapping, this forms a complete 3-dimensional trap and is the basic principle of optical tweezers.

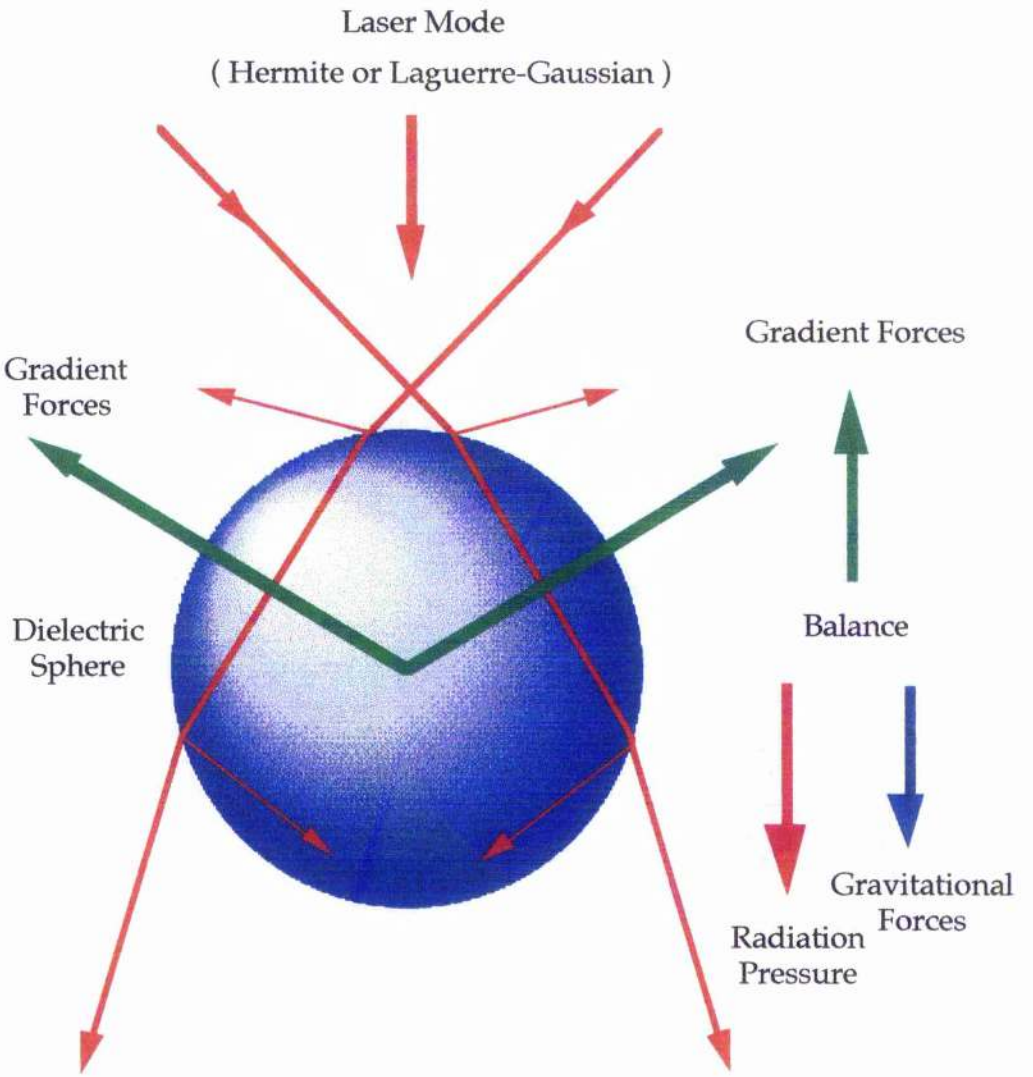

Figure III.g Diagram showing the backward gradient force

There is a strong gradient, axial force that exists for Rayleigh particles also. A numerical analysis for the axial gradient force component does give solutions that can be associated with lenslike properties of the trapped particle, similar to those experienced by Mie particles.

For a Rayleigh particle of radius r, whose diameter is less than the wavelength λ of the laser, there is a scattering force F_{scat} in the direction of the incident radiation of intensity I_0. If the supporting medium has a refractive index of n_s and the effective index is n_e (which is the index of the particle divided by the index of the medium), then the scattering force is given by [3]

$$F_{scat} = \left(\frac{I_0}{c}\right)\left(\frac{128 \cdot \pi^5 \cdot r^6}{3 \cdot \lambda^4}\right)\left(\frac{n_e^{\,2} - 1}{n_e^{\,2} + 2}\right)n_s. \tag{3.1}$$

The force in the direction of the intensity gradient, the gradient force F_{grad}, is given by [3]

$$F_{grad} = -\left(\frac{n_s^{\,3} \cdot r^3}{2}\right)\left(\frac{n_e^{\,2} - 1}{n_e^{\,2} - 2}\right)\nabla E^2. \tag{3.2}$$

A stable position for a Rayleigh particle in the optical trap will occur when the gradient force is equal to the scattering force. For a Gaussian beam of spot size ω_0, this will occur along the z-axis of the beam at a position given by [3]

$$z = \frac{\pi \omega_0^{\,2}}{\sqrt{3}\lambda}. \tag{3.3}$$

In the standard arrangement of the optical tweezers, the region of balance for the forces on the particle is just below the focus of the tightly focussed laser beam. Any movement from this position will result in restoring forces on the particle to bring it back into the optical trap.

The more extreme rays, that are towards the edges of the trapped sphere, will provide a stronger z trapping force than those that are incident in the middle areas of the sphere. This is due to the larger angle of incidence onto the sphere caused by the high numerical aperture objective lens. Those rays that are very close to being on the beam axis create very little backward gradient

forces and large radiation pressure forces. Therefore it is beneficial to accentuate the extremal rays and increase the amount of z trapping that's possible. This can be achieved by having a large numerical aperture beam, and a 1.3 NA is quite standard in most optical tweezers arrangements. An alternative method of increasing the z trapping is to reduce the on-axis rays, so that the radiation pressure is vastly reduced. This method is one that has been investigated in more depth during the course of the research in this PhD.

III. 6 The standard tweezers experimental set-up

The experimental set-up for optical tweezers is very straight forward. It consists of four main sections which will each be described in turn in the following sections. Optical tweezers are now available as a commercial product based on a solid state device [24] and further details about the simple construction of optical tweezers may be found in published papers by Afzal and Treacy [21], Steven Block [25] and Berns, Wright and Steubing [26].

III. 6. 1 The microscope objective system

The microscope objective is ideally a high numerical aperture, water or oil immersion objective lens in a microscope set-up. However, a dry lens has now been demonstrated for tweezing particles in air [27]. Typically, the lens is of 100x magnification with an NA of 1.3. It is usually combined with a secondary tube lens to form an image behind the back aperture plane. To observe the image for use as a microscope, the sample cell is illuminated from beneath by a white light source.

The objective lens will usually be either be a water or oil immersion lens, which means that the lens must always be in a surrounding medium of either water or oil respectively to allow correct refractive index matching of the lens and the sample cell. The collimated beam must fill the back aperture of the objective lens to obtain a small focussed spot size.

III. 6. 2 The beam steering optics

The arrangement of lenses directing the beam from the laser source to the microscope objective will vary in each system depending on the experimental circumstances. Traditionally, a beam expansion telescope is incorporated into the path of the beam. This is to allow full control over the size of the beam entering the back aperture of the objective lens (figure III.h).

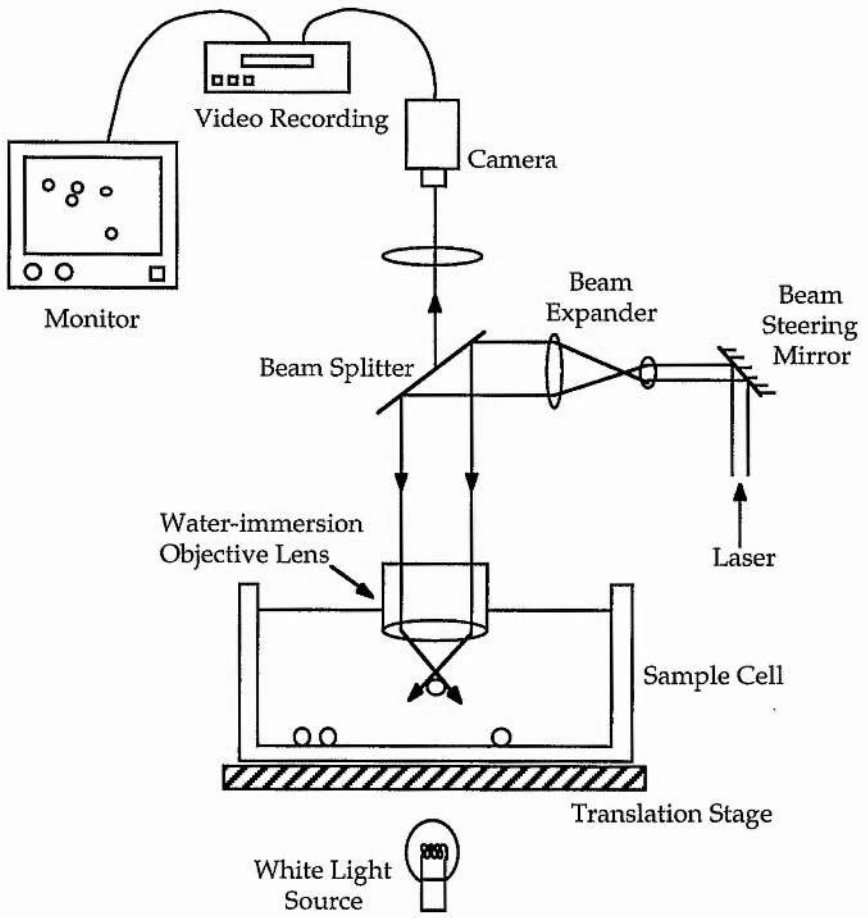

Figure III.h Schematic diagram of the beam steering optics and viewing system

There are two methods of translating a trapped particle within the sample cell. The first is the translation of the stage upon which the sample cell is fixed. In this case, the particle remains trapped in one position and the surrounding particles move relative to it.

Another method is to keep the sample cell stationary and move the trapped particle around the cell. This is achieved by using beam steering mirrors before the beam hits the beam splitter and enters the objective lens. The mirrors enable the angle of incidence of the beam into the back aperture of the objective lens to be changed, thus altering the position of the beam focus within the sample cell. By carefully adjusting these mirrors it is possible to translate the particle around the sample cell at will. This creates a much finer control than moving the stage of the cell and very precise experiments can be performed using this method of manipulation. In other systems, the moving of the mirrors may be replaced by incorporating acousto-optic modulators as beam deflectors.

The beam is usually directed into the microscope objective lens by a beam splitter. This is fully reflecting at the laser wavelength to direct the laser through the objective lens and is transparent at visible wavelengths to allow the viewing of the sample cell using the same microscope optics. Above the beam splitter is either an eyepiece for viewing, or alternatively a camera linked to a monitor and video recording equipment. The recording of optical tweezers experiments is particularly useful for further study of trapping experiments when the video footage can be used to take measurements of particle sizes and distances translated over a set timescale.

III. 6. 3 The trapping laser

Optical tweezers were originally constructed with Nd:YAG or argon ion lasers for the trapping of particles. These tended to be large and cumbersome in the laboratory, as well as being expensive. Diode lasers now provide a much more convenient and accessible laser source due to their size and cost.

High laser powers are not required for optical trapping. In most cases, the optical tweezers only require a few mW for operation. Also, the selection of

the laser wavelength again depends on the particles being investigated. It may be necessary to have some absorption of the laser by the sample particle but there must be transmission through the particle otherwise it will be impossible to achieve optical trapping. For the investigation of biological samples, ultra-violet and infra-red wavelengths are unsuitable due to their high absorption, so the majority of optical tweezers arrangements incorporate a near infra-red laser into the tweezers set-up.

III. 6. 4 The specimen particles and the sample cell

The sample cells also vary in their design. It is very common for a microscope slide to be used as the basis of an experimental cell. A well is created on the slide, either by building up walls or by creating a small trough-like structure. The solution with suspended particles is placed in this well and a coverslip, is placed over the top, making a sealed cell (figure III.i). The sample cell is usually of the order of 50 - 100 μm in depth. A drop of oil or water must be placed on top of the coverslip to match the refractive indices of the oil/water immersion objective lens to the coverslip. If the sample consists of water, the water immersion objective lens may sometimes be lowered straight into the specimen solution.

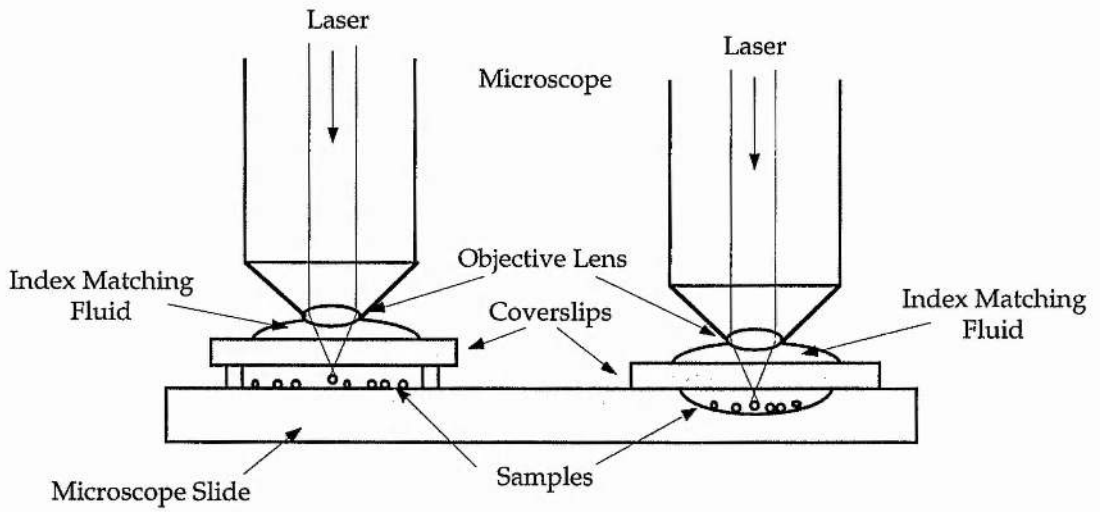

Figure III.i Typical sample cells for use in optical tweezers

The sample particles are usually of the order of a few microns in size and suspended in a solution. Different solutions can be used, but water is the most common. The choice depends on the solution properties required, such as viscosity, density and the likelihood of any reaction with the particles. The particles may be synthetic such as silica or glass spheres, or of a biological nature. To achieve optical trapping in the way described earlier, the particles must be at least partially transparent to allow trapping to take place.

III. 7 Applications of optical tweezers

Optical tweezers are now quite common in the fields of cell biology, biophysics and microbiology [25, 26, 28-31]. This is the major application of tweezers to date. The first successful trapping of a biological specimen was reported in 1987 [18]. Once more it was Ashkin and Dziedzic who took the development of optical tweezers to the application stage.

III. 7. 1 Biological applications

Ashkin's group trapped tobacco mosaic viruses which were suspended in an aqueous solution. These viruses were cylindrical in shape with a length of ~0.3 μm, effectively asymmetric Rayleigh particles. They were successfully trapped using an argon ion laser of wavelength 515 nm operating at ~150 mW with no obvious damage to the viruses themselves. In these samples, two types of bacteria were seen after a few days and were identified as rod-like motile bacteria, with rotating tails for propulsion, of lengths 0.5 and 1.5 μm. These too were successfully trapped with only a few milliWatts of laser power. Full details of this first demonstration of optical trapping of biological particles can be found in Ashkin and Dziedzic's paper, reference [18].

However, long exposure in the optical trap, even at only a few milliWatts of the green laser radiation, still caused optical damage to the biological specimens. Ashkin termed this optical damage "opticution", the death of a biological sample by light. He therefore decided to use a near infra-red laser to reduce the harmful effects caused by absorption. He was then able to

successfully trap and manipulate red blood cells, yeast and individual organelles inside the cell walls of algae using optical tweezers [32].

Optical tweezers create forces of the order of picoNewtons. Forces of this size are of the correct magnitude to move and reposition cells [33], bend membranes and stop bacteria swimming freely. The study of biological structures is now greatly enhanced by the ability to manipulate samples with the aid of optical tweezers. For example, Steven Block at Harvard University used tweezers to make measurements of the elasticity of bacterial flagella or tails [34].

The tweezers technology has also been combined with other laser techniques, in particular, with a pulsed ultra-violet laser to create an "optical scalpel". This allows the cutting or ablation of biological material on a microscopic scale. The fusion of cells has been performed by using optical tweezers to bring together two cells and then cutting their membranes to allow their fusion with ultra-violet light [35]. Berns and colleagues have combined optical tweezers and optical scalpels successfully [36] and also tried to use optical tweezers for in vitro fertilisation. Recently, Bruer, Gahagan, Swartzlander Jnr and Weathers from the Worcester Polytechnic Institute in Massachusetts, reported the cutting open of a plant cell with a laser scalpel and inserting a single bacterium into the cell using optical tweezers [37].

Another useful application of the tweezers has been to use micron-sized spheres as "handles" to hold molecules and biological structures. One of the most publicised experiments in this field was by Steven Block, now at Princeton University and his colleagues, who attached microspheres to the ends of a DNA strand [38]. The molecule was stretched and then released. The relaxation was used to make detailed experimental observations of the polymer behaviour. Similar work has also been undertaken by Justin Molloy and colleagues at York University [39] and Bob Simmons and co-workers at King's College, London [40-42], to measure the forces of individual muscle fibres.

Multiple optical traps are also possible. These allow particles of different shapes and sizes to be orientated at will, which is not possible with a single

trap. Double tweezers systems have been used to construct arrays of latex particles into an ordered structure [43] and also to study the resonance of thermal hopping over time-varying potential barriers [44]. Similarly, dual-traps have been developed within optical tweezers forming two fully steerable 3-D traps [45]. Automated cell sorters using optical traps have also been constructed successfully [46].

III. 7. 2 Non-biological applications

To date, there has been little published work on applications of optical tweezers outside of the biological field. However, investigations are underway into confocal microscopy and tweezers technology. The last few years has seen the development of the scanned probe optical microscope using an optical trap to position a microscopic probe light source very close to a selected object [47]. An extension of this was to trap, with infra-red light, a frequency doubling crystal, thus producing an optical probe light source in the visible region creating two-colour optical microscopy [48].

Optical tweezers have been used to hold a micron-sized ball lens (a micro-objective) to image areas of samples otherwise inaccessible using conventional microscope techniques [49]. This micro-objective is able to view the side aspect of an object as well as the plan view that is usually obtained.

Another line of research has been to use optical tweezers to hold a stylus for a scanning force microscope [50, 51]. Spring constants have been measured of particles held in the effective harmonic oscillator of an optical trap with a view to developing this into an operational scanning force microscope.

Various studies of particle properties have been made possible due to the introduction of optical tweezers techniques. For example, the investigation of Brownian motion has been undertaken, by studying a 1 μm particle in an optical trap [44].

III. 8 Conclusions

This Chapter has aimed to provide a general overview of the development of optical tweezers beginning at their elementary roots in the early 1970's. Starting with Ashkin's first experimental work of accelerating and trapping particles, the further development into the single beam gradient force optical trap has now allowed full and complete control over trapped particles to allow full manipulation.

The basic principles of the trapping of particles by the laser beam have been studied, along with the traditional experimental arrangements for the operation of optical tweezers. The Chapter concluded with a review of the applications of tweezers in the world today, mainly in the fields of micro-biology and the manipulation of biological particles.

This introductory Chapter has demonstrated the simplicity of optical tweezers and also the great potential that they hold for the manipulation of micron-sized objects.

References

1. Ashkin, A., *Acceleration and trapping of particles by radiation pressure.* Phys. Rev. Lett., 1970. **24**: p. 156-159.

2. Ashkin, A. and J.M. Dziedzic, *Optical levitation by radiation pressure.* Appl. Phys. Lett., 1971. **19**: p. 283-285.

3. Ashkin, A., J.M. Dziedzic, J.E. Bjorkholm, and S. Chu, *Observation of a single-beam gradient force optical trap for dielectric particles.* Opt. Lett., 1986. **11**(5): p. 288-290.

4. Ashkin, A., *The pressure of laser light.* Scient. Amer., 1972. **226**: p. 63-71.

5. Ashkin, A. and J.M. Dziedzic, *Stability of optical levitation by radiation pressure.* Appl. Phys. Lett., 1974. **24**: p. 586-588.

6. Roosen, G. and C. Imbert, *The TEM(*01) mode laser beam - a powerful tool for optical levitation of various types of spheres.* Opt. Comm., 1978. **26**(3): p. 432-436.

7. Ashkin, A. and J.M. Dziedzic, *Optical levitation in high vacuum.* Appl. Phys. Lett., 1976. **28**: p. 333-335.

8. Ashkin, A. and J.M. Dziedzic, *Observation of a new nonlinear photoelectric effect using optical levitation.* Phys. Rev. Lett., 1976. **36**(5): p. 267-270.

9. Ashkin, A. and J.M. Dziedzic, *Observation of resonances in the radiation pressure on dielectric spheres.* Phys. Rev. Lett., 1977. **38**(23): p. 1351-1354.

10. Ashkin, A. and J.M. Dziedzic, *Feedback stabilization of optically levitated particles.* Appl. Phys. Lett., 1977. **30**(4): p. 202-204.

11. Roosen, G. and C. Imbert, *Optical levitation by means of two horizontal laser beams: a theoretical and experimental study.* Phys. Lett., 1976. **59A**(1): p. 6-8.

12. Ashkin, A. and J.P. Gordon, *Stability of radiation-pressure particle traps: an optical Earnshaw theorem.* Opt. Lett., 1983. **8**(10): p. 511-513.

13. Ashkin, A. and J.M. Dziedzic, *Observation of radiation-pressure trapping of particles by alternating light beams.* Phys. Rev. Lett., 1985. **54**(12): p. 1245-1248.

14. Ashkin, A. and J.M. Dziedzic, *Observation of light scattering from non spherical particles using optical levitation.* Appl. Opt., 1980. **19**: p. 660-668.

15. Pochelle, J.-P., J. Raffy, Y. Combemale, M. Papuchon, G. Roosen, and M.T. Plantegenest, *Optical levitation using single mode fibres and its application to self-centering of microlenses.* Appl. Phys. Lett., 1984. **45**(4): p. 350-352.

16. Constable, A., J. Kim, J. Mervis, F. Zarinetchi, and M. Prentiss, *Demonstration of a fiber-optical light-force trap.* Opt. Lett., 1993. **18**: p. 1867-1869.

17. Gauthier, R.C. and S. Wallace, *Optical levitation of spheres: analytical development and numerical computations of the force equations.* J. Opt. Soc. Am. B, 1995. **12**: p. 1680-1686.

18. Ashkin, A. and J.M. Dziedzic, *Optical trapping and manipulation of viruses and bacteria.* Science, 1987. **235**: p. 1517-1520.

19. Ashkin, A. and J.M. Dziedzic, U.S. Patent No. 4 893 886, 1990.

20. Sato, S., M. Ohyumi, H. Shibata, H. Inaba, and Y. Ogawa, *Optical trapping of small particles using a 1.3 micron compact InGaAsP diode laser.* Opt. Lett., 1991. **16**: p. 282-284.

21. Afzal, R.S. and E.B. Treacy, *Optical tweezers using a laser diode.* Rev. Sci. Instrum., 1992. **63**: p. 2157-2163.

22. Bakker-Schut, T.C., E.F. Schipper, B.G.d. Grooth, and J. Greve, *Optical-trapping micromanipulation using 780-nm diode lasers.* Opt. Lett., 1991. **18**: p. 447-449.

23. Higurashi, E., O. Ohguchi, and H. Ukita, *Optical trapping of low-refractive-index microfabricated objects using radiation pressure exerted on their inner walls.* Opt. Lett., 1995. **20**: p. 1931-1933.

24. LaserTweezers, Cell Robotics Inc., 2715 Broadbent Parkway NE, Albuquerque, NM 87107, USA, .

25. Block, S.M., *Optical Tweezers: A New Tool for Biophysics,* in *Non Invasive Techniques in Cell Biology,* J.K. Foskett and S. Grinstein, Editor^Editors. 1990, A Wiley & Sons, Inc.: p. 375-402.

26. Berns, M.W., W.H. Wright, and R. Wiegand-Steubing, *Laser microbeam as a tool in cell biology.* Int. Rev. Cytology, 1991. **129**: p. 1-44.

27. Omori, R., T. Kobayashi, and A. Suzuki, *Observation of a single-beam gradient-force optical trap for dielectric particles in air.* Opt. Lett., 1997. **22**(11): p. 816-818.

28. Block, S.M., *Making light work with optical tweezers.* Nature, 1992. **360**: p. 493-495.

29. Block, S.M., *Laser light traps for biology.* Physics Today, 1989. **40**: p. S17-S18.

30. Schütze, K. and A. Clement-Sengewald, *Catch and move - cut or fuse.* Nature, 1994. **368**: p. 667-669.

31. Kuo, S.C. and M.P. Sheetz, *Optical tweezers in cell biology.* Trends in Cell Biology, 1992. **2**: p. 116-118.

32. Ashkin, A., J.M. Dziedzic, and T.M. Yamane, *Optical trapping and manipulation of single cells using infrared laser beams.* Nature, 1987. **330**: p. 769-771.

33. Aufderheide, K.J., Q. Du, and E.S. Fry, *Directed positioning of micronuclei in Paramecium tetraurelia with laser tweezers - absence of detectable damage after manipulation.* J. Eukary. Microbiol., 1993. **40**: p. 793-796.

34. Block, S.M., D.F. Blair, and H.C. Berg, *Compliance of bacterial flagella measured with optical tweezers.* Nature, 1989. **338**: p. 514-518.

35. Weigand-Steubing, R., Cytometry, 1991. **12**: p. 505-510.

36. Liang, H., W.H. Wright, S. Cheng, W. He, and M.W. Berns, *Micromanipulation of chromosomes in PTK-2 cells using laser microsurgery (optical scalpel) in combination with laser-induced optical forces (optical tweezers).* Exp. Cell Res., 1993. **204**: p. 110-120.

37. Buer, C.S., K.T. Gahagan, G.A. Swartzlander-Jr, and P.J. Weathers. *Transformation of Ginko biloba using optical tweezers and scissors.* in *XVII Conference on Lasers and Electro-Optics - CLEO '97.* 1997. Paper no CTuD6, Baltimore, USA.

38. Wang, M.D., H. Yin, R. Landick, J. Gelles, and S.M. Block, *Stretching DNA with optical tweezers.* Biophys. J., 1997. **72**: p. 1335.

39. Molloy, J.E., J.E. Burns, J. Kendrick-Jones, R.T. Tregear, and D.C.S. White, *Movement and force produced by a single myosin head.* Nature, 1995. **378**: p. 209-212.

40. Finer, J.T., R.M. Simmons, and J.A. Spudich, *Single myosin molecule mechanics: piconewton forces and nanometre steps.* Nature, 1994. **368**: p. 113-119.

41. Tskhovrebova, L., J. Trinick, J. Sleep, and R. Simmons, *Optical tweezer measurements of force and extension in individual titin molecules.* J. of Muscle Res. and Cell Motility, 1996. **17**(1): p. 113.

42. Simmons, R.M., J.T. Finer, S. Chu, and J.A. Spudich, *Quantitative measurements of force and displacement using an optical trap.* Biophys. J., 1996. **70**(4): p. 1813-1822.

43. Misawa, H., K. Sasaki, M. Koshioka, N. Kitamura, and H. Masuhara, *Multibeam laser manipulation and fixation of microparticles.* Appl. Phys. Lett., 1992. **60**(3): p. 310-312.

44. Simon, A. and A. Libchaber, *Escape and synchronization of a Brownian particle.* Phys. Rev. Lett., 1992. **68**(23): p. 3375-3378.

45. Fällman, E. and O. Axner, *Design for fully steerable dual-trap optical tweezers.* Appl. Opt., 1997. **36**(10): p. 2107-2113.

46. Buican, T.N., M.J. Smyth, H.A. Crissman, G.C. Salzman, C.C. Stewart, and J.C. Martin, *Automated single-cell manipulation and sorting by light trapping.* Appl. Opt., 1987. **26**: p. 5311-5316.

47. Malmqvist, L. and H.M. Hertz, *Trapped particle optical microscopy.* Opt. Comm., 1992. **94**: p. 19-24.

48. Malmqvist, L. and H.M. Hertz, *Two-color trapped-particle optical microscopy.* Opt. Lett., 1994. **19**(12): p. 853-855.

49. Sasaki, M., T. Kurosawa, and K. Hane, *Micro-objective manipulated with optical tweezers.* Appl. Phys. Lett., 1997. **70**: p. 785-787.

50. Ghislain, L.P. and W.W. Webb, *Scanning-force microscope based on an optical trap.* Opt. Lett., 1993. **18**(19): p. 1678-1680.

51. Friese, M.E.J., H. Rubinsztein-Dunlop, N.R. Heckenberg, and E.W. Dearden, *Determination of the force constant of a single-beam gradient trap by measurement of backscattered light.* Appl. Opt., 1996. **35**: p. 7112-7116.

Chapter IV

Experiments with Laguerre-Gaussian Laser Modes

Contents

IV. 1 Aim of the experiments

Within this PhD project, two experiments were undertaken to investigate the properties of Laguerre-Gaussian (LG) laser modes. The first studied the intensity and phase structure of the modes by means of an interferometer, so that the azimuthal phase dependence could be visualised. The interference fringes obtained gave information about the order of the mode and confirmed the azimuthal phase dependence which is the origin of the orbital angular momentum associated with these modes.

The second experiment made a first investigation into second harmonic generation using Laguerre-Gaussian laser modes. As each mode was doubled in frequency, it was also transformed to a higher order mode. This was consistent with the orbital angular momentum of the mode being directly proportional to the azimuthal mode index.

These experiments were additional to the main application of using Laguerre-Gaussian laser modes in the optical tweezers arrangement (the optical spanners), but it was felt that useful information about the modes could be gleaned from these relatively simple and quick experiments.

IV. 2 Visualisation of the phase structure

This section of the Chapter describes an easily reproducible experiment which allowed the amplitude and phase structure of various transverse laser modes to be investigated. The experimental details and the results were published in the *American Journal of Physics* in January 1996 [1].

IV. 2. 1 The production of high-order LG modes

Laser cavities usually operate in the fundamental mode which has a standard Gaussian profile. This $TEM_{0,0}$ mode can be selected by including an aperture on the cavity axis, forcing oscillation in the fundamental mode as the losses are the lowest.

To force the laser cavity to operate in a higher order Hermite-Gaussian (HG) mode, this is easily achieved by inserting a cross wire into the cavity itself. The wires form the nodes in the transverse HG mode. By fine adjustment of the position of the cross wires in the cavity, various HG modes can be forced to oscillate. The corresponding high order Laguerre-Gaussian (LG) mode is then produced by the introduction of an extra-cavity cylindrical lens mode converter (see section II. 5. 5).

The cylindrical lens mode converter was initially demonstrated by Tamm and Weiss [2], and then more recently by Beijersbergen and co-workers [3]. The LG^{ℓ}_{p} mode produced by this method is related to the $HG_{m,n}$ mode out of the laser cavity by two simple relationships, as follows,

$$\ell = |m - n| \qquad p = \min(m, n). \tag{4.1}$$

Taking the $HG_{1,1}$ mode as an example, when the principle axis of the input HG mode is inclined at 45° to the main axis of the cylindrical lens, the mode can be considered as a superposition of two HG modes that are in phase (see figure IV.a). The cylindrical lenses introduce a Gouy phase shift between these two orthogonal modes and upon superposition, the modes have a phase difference of $\pi/2$ and the resultant mode upon recombination is a LG mode.

In this experiment, a cylindrical lens mode converter of this type was used to produce the different high order LG modes, the order of which could be deduced by using the expressions of 4.1.

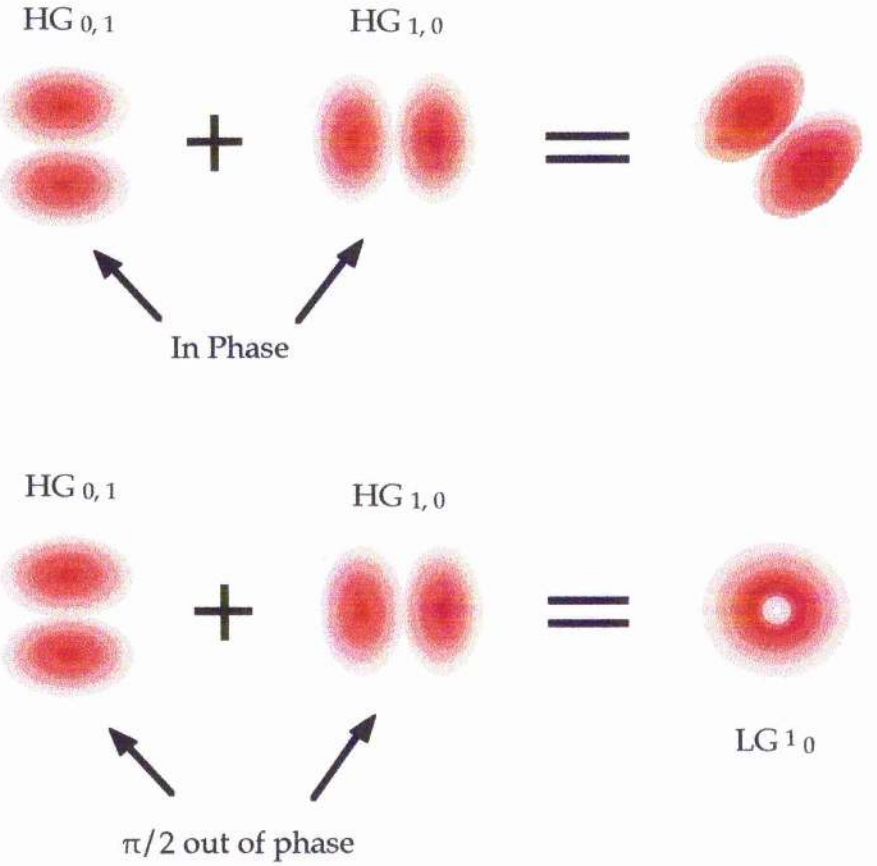

Figure IV.a The formation of a LG mode by the superposition of HG modes

IV. 2. 2 Experimental arrangement

The design of the cylindrical lens mode converter was based on the details given in section II. 5. 5 and from the work of Beijersbergen [3]. It had the following specifications

- two cylindrical lenses of focal length 25.4 mm
- cylindrical lens separation of 18.0 mm (between the principal planes).

The lenses were mounted with their plane faces cemented to a tube to set the correct separation of their principal planes. The two lens arrangement (the mode converter) could now be rotated with the lenses remaining fixed at a separation of 18.0 mm.

To focus the laser beam into the mode converter, a lens was required just before the converter. The optimum focal length of this coupling lens could be calculated from the diameter of the input beam and its wavefront curvature. It was found that a single lens with a focal length of 250 mm was the optimum lens to use.

For the laser source itself, an unmounted He-Ne tube was used with a Brewster window and an external output coupler. The output coupler had to be separable so that by positioning it 100 mm from the Brewster window, an x-y translation stage carrying a cross-wire (made from 10μm diameter tungsten wire) could be inserted into the laser cavity. With careful adjustment of the cross-wire and alignment of the output coupler, the laser could be forced to oscillate in a variety of higher order HG modes. This particular He-Ne laser operated at a wavelength of 633 nm with an output power of 3 mW.

To investigate the phase structure of LG modes, it was necessary to extend the experimental arrangement beyond that of the mode converter and the production of the modes themselves. The experimental arrangement to observe the intensity and phase structure of the LG modes was as shown in figure IV.b. It was based on a Mach-Zehnder interferometer set-up, with the mode converter and input lens in one arm and a beam expansion telescope in the other. The purpose of the lens after the mode converter, of focal length 160 mm, was to form a second beam waist outside the interferometer.

This was so that the mode structure could be examined at various positions either side of this beam waist.

The beam expansion telescope consisted of two lenses (of focal lengths 40 mm and 300 mm) to give an expanded, collimated output beam. This beam was an expanded form of the input HG mode. Although having a Hermite-Gaussian intensity profile, the large Rayleigh range that the expanded mode now had, meant that the mode had a near-planar wavefront. This expanded HG mode was used as a phase reference for the examination of the LG modes. The LG mode could now be interfered with effectively a plane wave, and the interferograms studied.

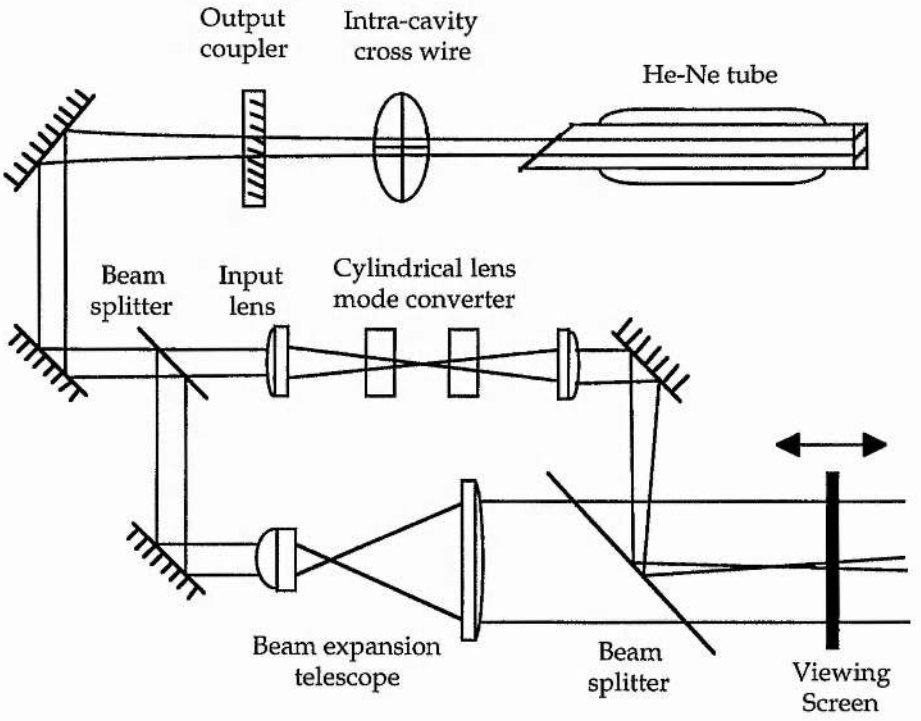

Figure IV.b The experimental arrangement for the observation of the intensity and phase structure of LG modes using a Mach-Zehnder interferometer.

IV. 2. 3 Observation of the intensity and phase structure of LG modes

An initial experiment was performed with the beam expander arm blocked. This meant that the expanded HG mode was not observed and the intensity structure of the LG modes themselves could be observed. After selecting a high order HG mode from the laser, the intensity distribution of the beam after it was transmitted by the mode converter was examined. These intensity distributions were observed simply by placing a screen in the beam path. They were also recorded by using a CCD (charge-coupled-device) array interfaced to a framegrabbing card running on a computer so that they could be recorded.

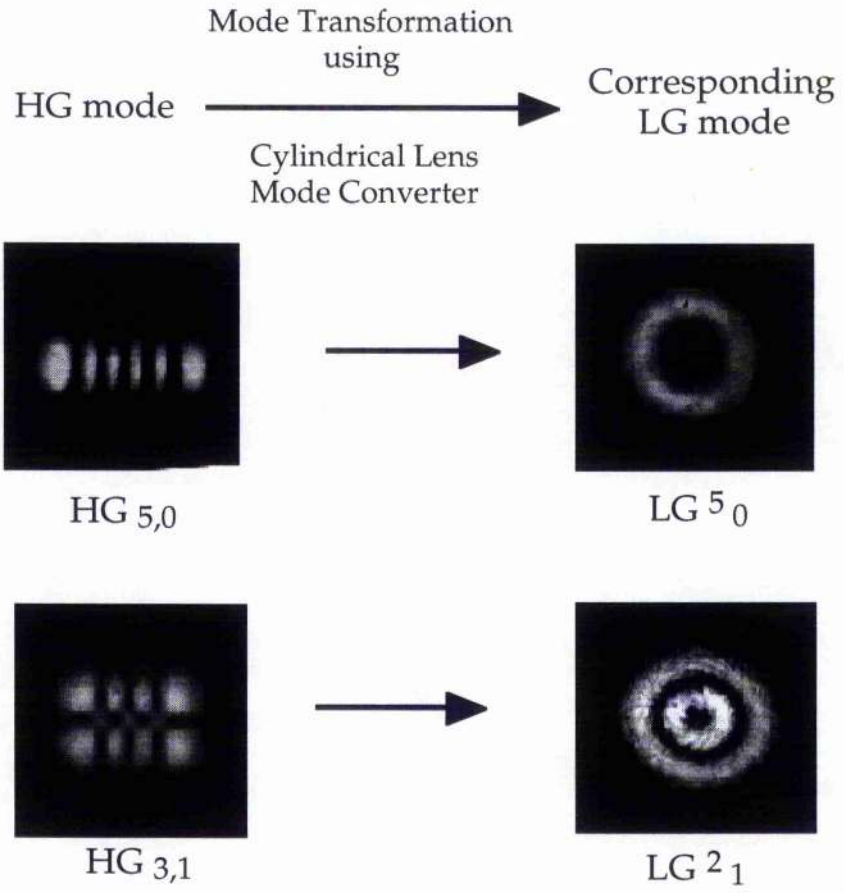

Figure IV.c Photographs of input HG modes and the output LG modes after mode transformation by the cylindrical lens mode converter.

Basically, these images confirmed the results presented in the work by Beijersbergen et al [3]. At this stage, it was a case of checking that the cylindrical lens mode converter was transforming the HG modes into LG modes correctly. Figure IV.c shows images taken of two input HG modes and the resulting output LG modes from the mode converter.

Once the various intensity patterns of the input HG and output LG modes had been observed and confirmed, the beam telescope arm of the Mach-Zehnder interferometer was unblocked. This allowed the LG mode to be superimposed onto the expanded HG mode, aligned such that the LG mode fell within one of the greatly expanded HG modal lobes. The resulting interference pattern could be observed on the screen. The expanded HG mode acted as a plane-wave reference and the observed interference fringes revealed the relative phase variations of the LG mode being studied.

Figure IV.d shows images of the intensity and interference patterns obtained for several higher order HG modes and their corresponding LG modes after mode conversion. In all cases the number of radial fringes was equal to ℓ and the number of radial nodes was equal to p+1. For the LG modes with multiple ring amplitudes (e.g. the LG^2_1, which is obtained from the $HG_{3,1}$), the azimuthal position of the fringe maxima and minima is reversed between successive rings, corresponding to the change of phase between successive rings of the Laguerre-Gaussian distribution. Note also that in the special case of the $m = n$ HG mode, there is an on-axis intensity for the corresponding LG mode, and no azimuthal phase dependence. Consequently, these fringes are circular and not spiral demonstrating a constant azimuthal phase. The radii of the fringes can be calculated from the wavefront curvature of the beam and are analogous to Newton's rings.

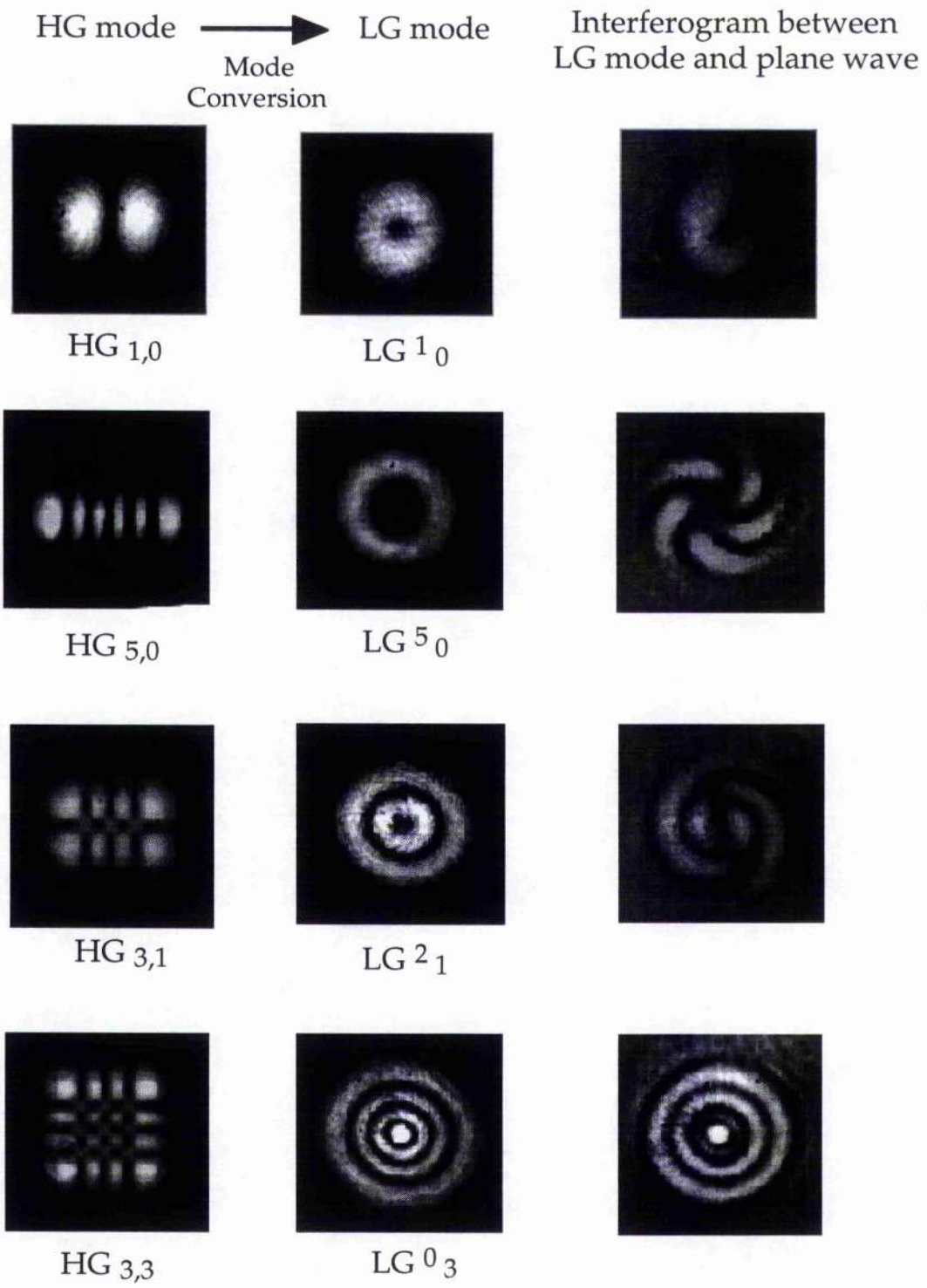

Figure IV.d Photographs of HG modes, the corresponding LG modes and the interferograms between LG modes and a plane-wave reference.

The propagation of the LG modes was also investigated. When the CCD array was moved along the propagating beam, the interference patterns were observed at various positions about the beam waist (figure IV.e). At the beam waist itself, the 6π azimuthal phase change around the LG^3_0 mode gave rise to three dark radial fringes. No spiral fringes were observed as there was no radial phase dependence. Away from the beam waist, spiral fringes were observed.

These arise from the combination of the radial phase variation due to wavefront curvature, and the tangential phase variation due to the azimuthal phase dependence. The sense of the spiral is reversed either side of the waist in accordance with the curvature of the wavefronts, thus changing the radial phase dependence.

The sense of the spirals could also be reversed by changing the sense of the azimuthal phase variation. This is most readily achieved by rotating the mode converter about the optical axis by 90° (i.e. from +45° to -45° with respect to the input mode). Alternatively, the input HG mode could be rotated by 90°, changing its orientation with respect to the cylindrical lens mode converter. Either of these procedures changed the sense of the spirals.

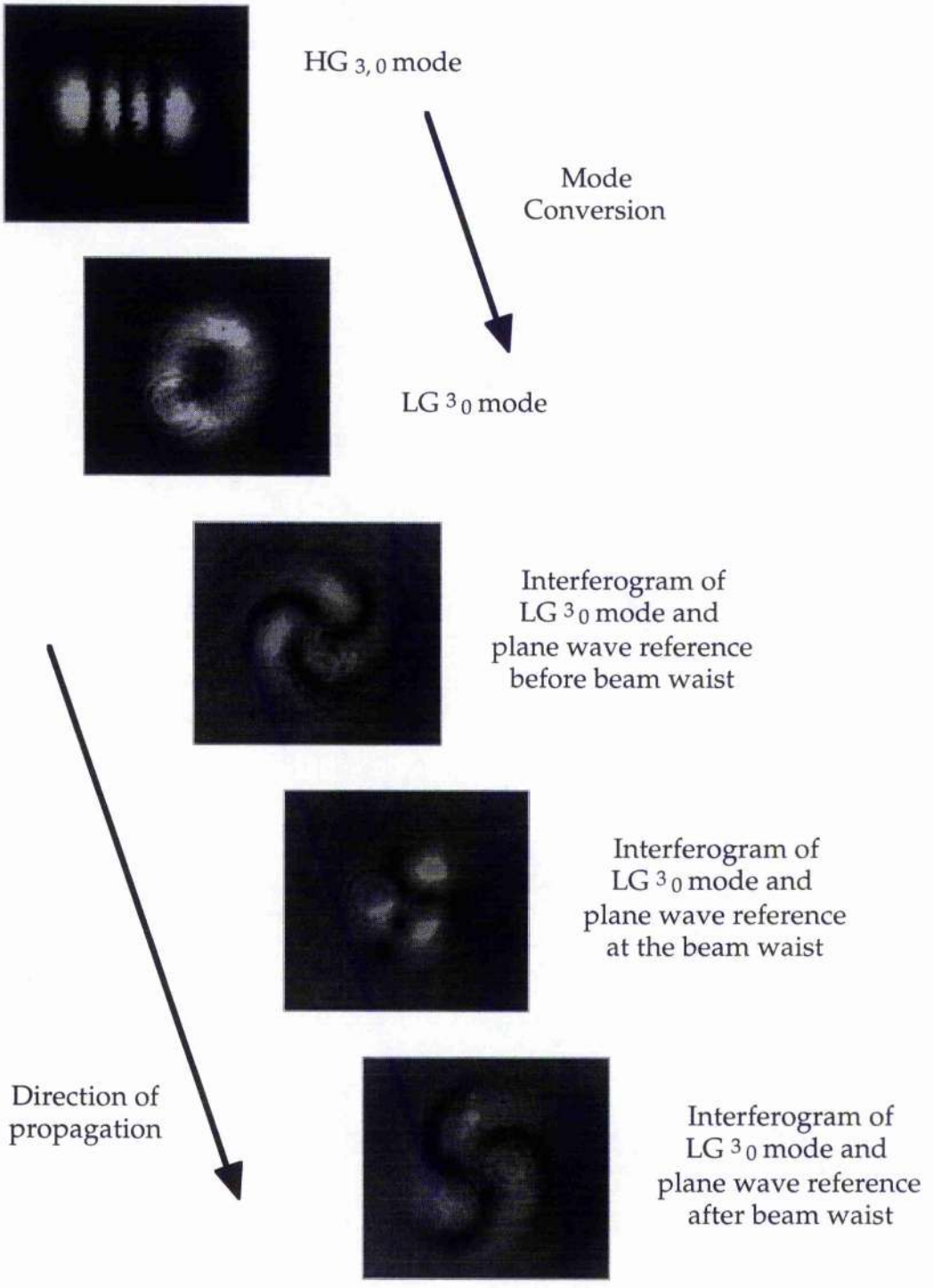

Figure IV.e Photographs of input $HG_{3,0}$ mode and corresponding LG^{3}_{0} mode and the interferograms as it propagates through the beam waist.

IV. 3 Second harmonic generation using LG laser modes

This section will describe an experiment that we performed to investigate the second harmonic generation using Laguerre-Gaussian laser modes. I performed the initial proof-of-principle experiment, while the bulk of the subsequent results and analysis were undertaken by Kishan Dholakia. The experimental details and the results are presented here for completeness and were published in the *Physical Review A* in November 1996 as a rapid communication [4]. Our work was also presented as a Postdeadline Paper at *QELS '96* in Anaheim, USA [5] and also at the *IEEE/LEOS Meeting of the Scottish Chapter* at Heriot-Watt University [6]. The experiment sought to observe the second harmonic generation (SHG) of non-zero order LG light beams and show that the modes become converted to a higher order. This is consistent with the fact that the modes possess orbital angular momentum which is conserved in the nonlinear process.

This type of experiment was initially carried out in 1993 by Basistiy et al [7], who frequency doubled a beam that contained a phase dislocation along its axis to a beam containing two phase dislocations. At the time they failed to understand the mechanism of this process and the work we have carried out investigated more fully this process with respect to the orbital angular momentum of light.

IV. 3. 1 SHG and orbital angular momentum of light

LG modes have been shown theoretically to possess a well-defined orbital angular momentum of $\ell\hbar$ per photon [8] where ℓ is the azimuthal phase index of the mode. This is in addition to any spin angular momentum due to their state of polarisation. Upon frequency doubling, the resulting higher mode order can be explained by considering the orbital angular momentum content of the input and output beams.

If the input beam, of frequency ω, has an amplitude E^{ω}, then the second harmonic of frequency 2ω, will have an amplitude $E^{2\omega}$ proportional to the square of the input amplitude,

$$E^{2\omega} \propto \left(E^{\omega}\right)^2 \tag{4.2}$$

which for a fundamental Gaussian mode means that the spot size is reduced by a factor of $\sqrt{2}$ compared to the input fundamental beam's spot size,

$$E^{2\omega} = \left(E_1 \exp\left(\frac{-r^2}{\omega^2}\right)\right)^2 = E_1^2 \exp\left(\frac{-2r^2}{2\omega^2}\right). \tag{4.3}$$

If this same approach is considered for a Laguerre-Gaussian laser beam, whose amplitude is given by Equation 2.3, then for a simplified case at the beam waist for a p=0 mode, the amplitude is

$$E^{\omega} = E_0 \exp\left[\frac{-r^2}{\omega^2}\right] \exp[-i\ell\phi] \left(\frac{r\sqrt{2}}{\omega}\right)^{\ell}. \tag{4.4}$$

Upon squaring for the second harmonic generation process, the harmonic is a p=0 LG mode with the ℓ index of the azimuthal phase term becoming 2ℓ as follows,

$$E^{2\omega} = \left(E_1 \exp\left(\frac{-r^2}{\omega^2}\right) \exp(-il\phi) \left(\frac{r\sqrt{2}}{\omega}\right)\right)^2 = E_1^2 \exp\left(\frac{-2r^2}{2\omega^2}\right) \exp(-i2l\phi) \left(\frac{r\sqrt{2}}{\omega}\right)^2. \tag{4.5}$$

Not only has the frequency doubled but so has the angular momentum per photon ($\ell\hbar$ » $2\ell\hbar$). This can be thought of as two photons combining their energies of $\hbar\omega$ to form a single photon of energy $2\hbar\omega$. At the same time, the two units of $\ell\hbar$ orbital angular momentum have combined to form a photon with orbital angular momentum of $2\ell\hbar$. This is not possible for circularly polarised light as a second harmonic can't have spin angular momentum of $2\hbar$.

IV. 3. 2 Experimental arrangement

A cross wire was used inside the laser cavity to force the laser to oscillate in a variety of higher order HG modes. The laser used in this experiment was a diode-pumped Nd:YAG laser operating at 1064 nm with a linearly polarised

output power of 100 mW. The HG mode was transformed into its corresponding LG mode by means of a cylindrical lens mode converter [3], as described in section II. 5. 5. This LG mode was then frequency doubled using a crystal of lithium triborate 20 mm in length. The crystal was temperature tuned to give noncritical, type-I phase matching for a second harmonic at 532 nm. The experiment was also performed using a KTP crystal, which was angle-tuned to give critical type-II phase matching. The LG mode was optimally focussed into the nonlinear crystal to maximise the power output of the second harmonic, which was typically a few μW.

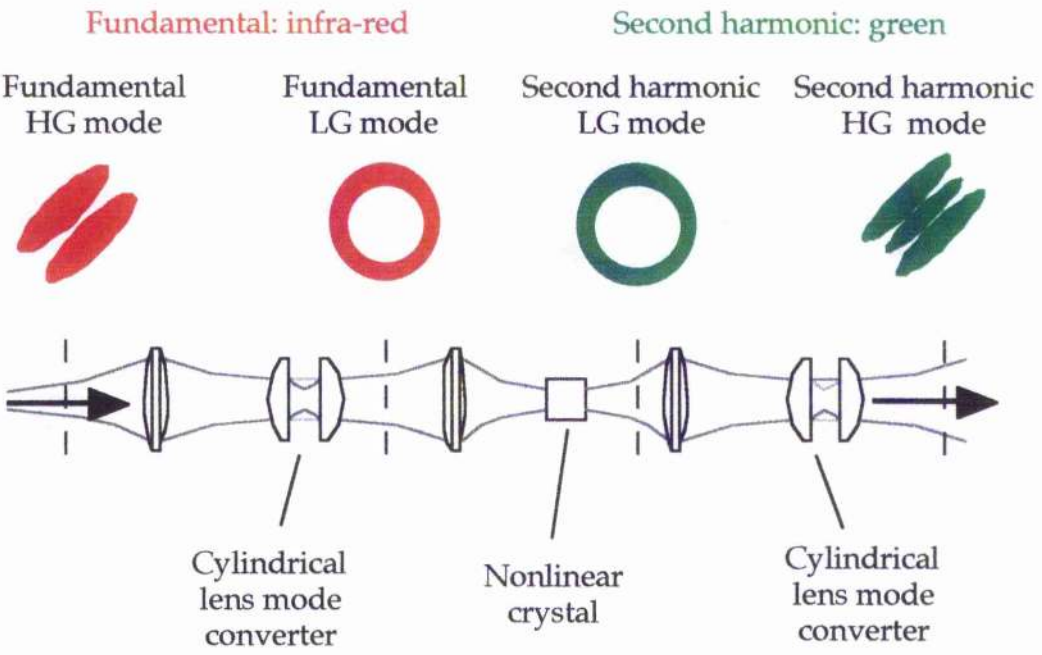

Figure IV.f Experimental arrangement for the observation of the frequency doubling of LG modes.

To investigate the order of the frequency doubled mode, a second cylindrical lens mode converter was incorporated into the arrangement to transform the fundamental and second harmonic LG modes back into their corresponding HG modes (see figure IV.f). The Rayleigh range is unchanged by the nonlinear process which meant it was possible to use the same mode

converter to transform both the fundamental and the second harmonic back to their corresponding HG modes. It was easier to determine the indices from the HG mode rather than from the LG mode itself. By using equations 4.1 it was possible to infer the indices and the order of the LG modes.

By selecting appropriate filters, it was possible to observe the fundamental modes or the second harmonic modes. The images of the modes were recorded using a CCD array and a framegrabbing application.

IV. 3. 3 Observation of frequency doubled LG modes

This experiment restricted the modes under consideration to LG modes with index $p = 0$. To produce a LG mode with a zero p index, the input HG mode had to have an index m=0, as p=m. Upon frequency doubling, ℓ doubled which meant that the corresponding HG mode followed ℓ=2(n-m). As m=0 it followed that n doubled in the second harmonic HG mode. This can be summarised in the following form for HG(m,n) and LG(ℓ ,p) modes,

Input HG mode	$m = 0$	$n = \mathrm{N}$
Input LG mode	$\ell = n - m = \mathrm{N}$	$p = \min(m,n) = 0$
SHG LG mode (ℓ doubles)	$\ell = 2\mathrm{N}$	$p = 0$
SHG HG mode	$m = \min(\ell,p) = 0$	$n = \ell - m = 2\mathrm{N}$

Figure IV.g shows the intensity images obtained for such a SHG process described above. The Nd:YAG laser produced a $HG_{0,1}$ mode @ 1064 nm and this was transformed, using the mode converter, into a LG^1_0 mode. This mode was frequency doubled using a lithium niobate (LBO) crystal to produce a LG^2_0 mode @ 532 nm. Using the second mode converter, the indices of the LG mode were confirmed by determining the HG mode's indices to be $HG_{0,2}$. The second harmonic generation of many LG modes were investigated, all with $p = 0$. The azimuthal mode index was changed and for all values of $\ell = 0, 1, 2, \ldots, 7$ it was found that ℓ doubles upon SHG. The same behaviour was observed when frequency doubling using a KTP crystal and these images are shown in figure IV.h.

The doubling of the ℓ index upon frequency doubling is consistent with the conservation of the orbital angular momentum contained in the LG modes, which is $\ell\hbar$ per photon.

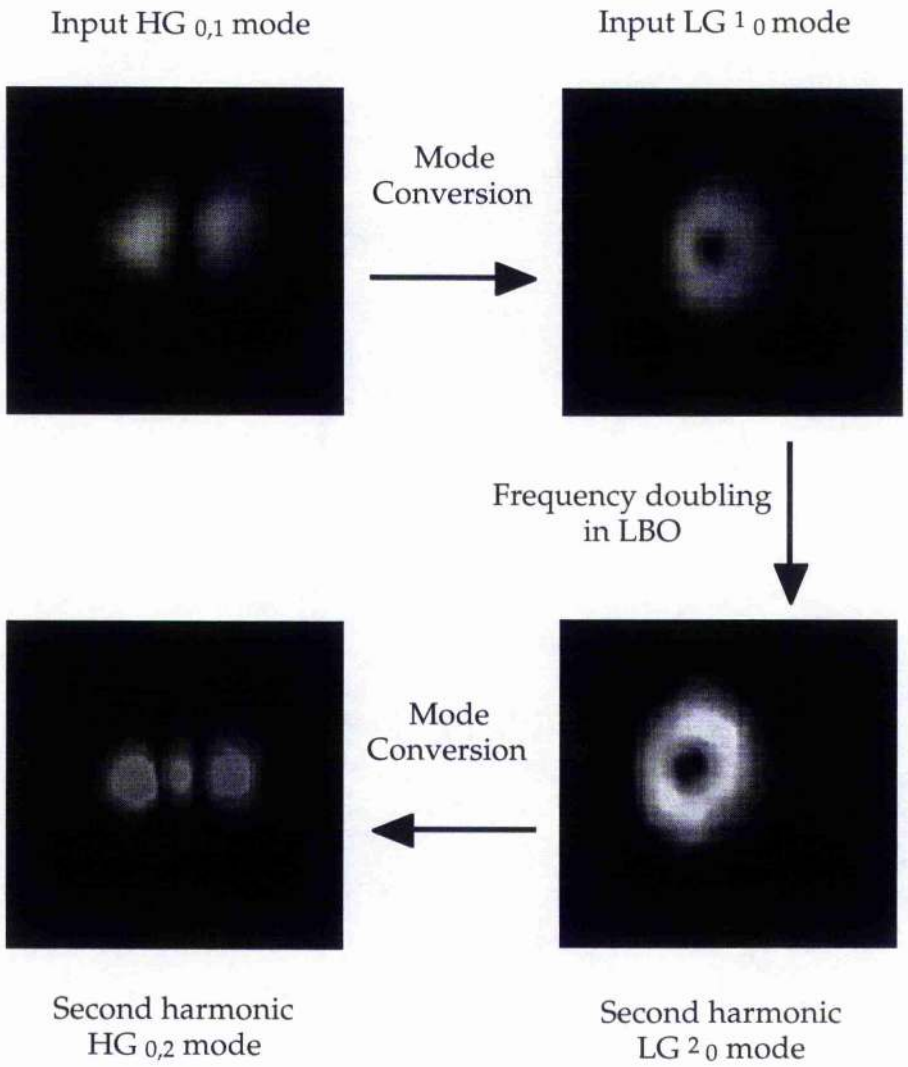

Figure IV.g Second harmonic generation in lithium niobate for a $HG_{0,1}$ mode converted into a LG^1_0 mode (type I phase matching).

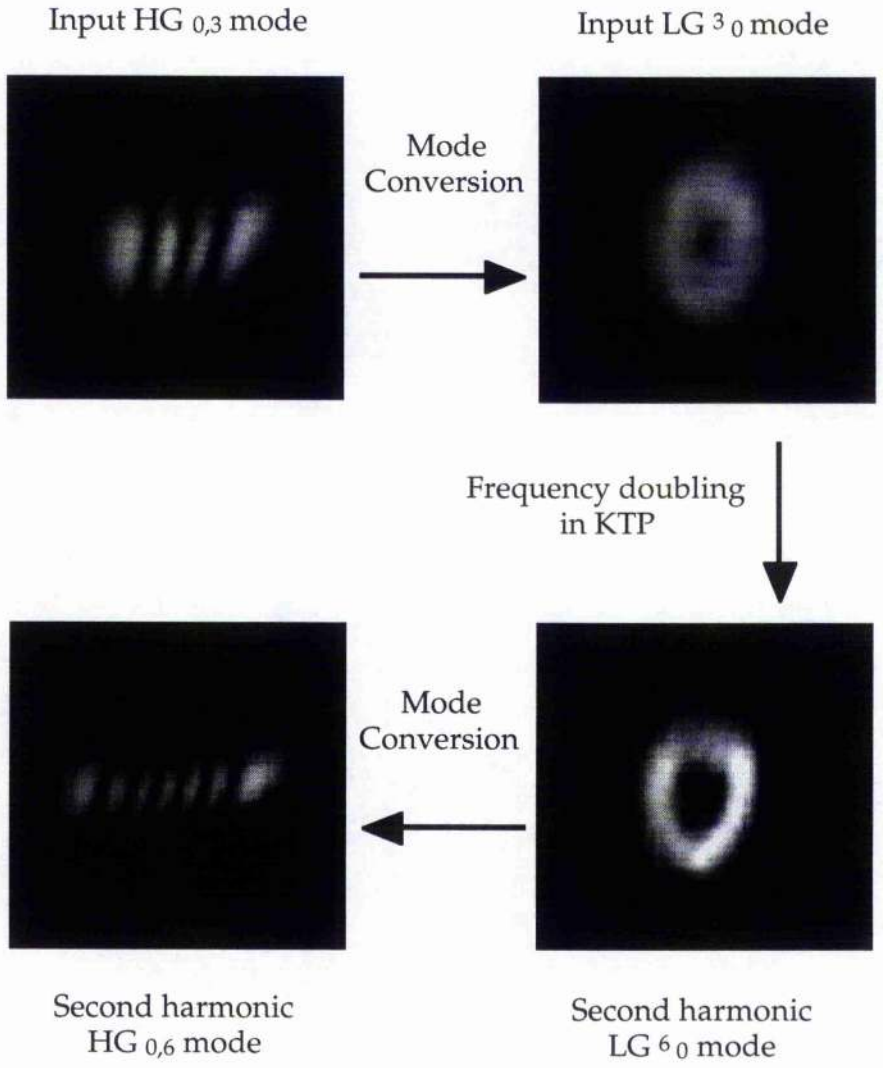

Figure IV.h Second harmonic generation in KTP for a $HG_{0,3}$ mode converted into a LG^{3}_{0} mode (type II phase matching).

IV. 4 Conclusions

The first experiment presented in this Chapter describes our investigation into the intensity and phase structure of Laguerre-Gaussian transverse laser modes. By using a cylindrical lens mode converter, very pure, high order LG modes were produced and by means of a Mach-Zehnder interferometer arrangement, the phase of the LG mode was compared to that of a plane wave. The resulting interferograms demonstrated the presence of an azimuthal phase dependence in the LG modes, which is directly linked to the orbital angular momentum content within the laser mode.

The second experiment concerned frequency doubling using LG modes with $p = 0$ and $\ell = 0, 1, 2, ..., 7$. Upon doubling, it was found that the ℓ index of the mode doubles as well as the frequency. The effects cannot be explained in terms of spin angular momentum (the polarisation state of the beam) but can be associated with the conservation of the orbital angular momentum of light, which is directly proportional to ℓ. This experimental work is consistent with the fact that linearly polarised Laguerre-Gaussian laser modes contain an angular momentum term and complements the results found by He et al [9].

References

1. Padgett, M., J. Arlt, N. Simpson, and L. Allen, *An experiment to observe the intensity and phase structure of Laguerre-Gaussian laser modes.* Am. J. of Phys., 1996. **64**: p. 77-82.

2. Tamm, C. and C.O. Weiss, *Bistability and optical switching of spatial patterns in a laser.* J. Opt. Soc. Am. B, 1990. **7**: p. 1034-1038.

3. Beijersbergen, M.W., L. Allen, H.E.L.O.v.d. Veen, and J.P. Woerdman, *Astigmatic laser mode converters and transfer of orbital angular momentum.* Opt. Comm., 1993. **96**: p. 123-132.

4. Dholakia, K., N.B. Simpson, M.J. Padgett, and L. Allen, *Second-harmonic generation and the orbital angular momentum of light.* Phys. Rev. A, 1996. **54**: p. R3742-R3745.

5. Dholakia, K., N.B. Simpson, M.J. Padgett, and L. Allen. *Second harmonic generation and the orbital angular momentum of light.* in *VI Quantum Electronics and Laser Science Conference - QELS '96.* June 1996. POSTDEADLINE PAPER no. QPD6, Anaheim, USA.

6. Dholakia, K., N.B. Simpson, L. Allen, and M.J. Padgett. *Non-linear optics with Laguerre-Gaussian beams.* in *IEEE/LEOS Meeting of Scottish Chapter.* September 1996. Heriot-Watt, UK.

7. Basistiy, I.V., V.Y. Bazhenov, M.S. Soskin, and M.V. Vasnetsov, *Optics of light beams with screw dislocations.* Opt. Comm., 1993. **103**: p. 422-428.

8. Allen, L., M.W. Beijersbergen, R.J.C. Spreeuw, and J.P. Woerdman, *Orbital angular momentum of light and the transformation of Laguerre-Gaussian laser modes.* Phys. Rev. A, 1992. **45**: p. 8185-8189.

9. He, H., M.E.J. Friese, N.R. Heckenberg, and H. Rubinsztein-Dunlop, *Direct observation of transfer of angular momentum to absorptive particles from a laser beam with a phase singularity.* Phys. Rev. Lett., 1995. 75(5): p. 826-829.

Chapter V

Laser Construction

Contents

V. 1 Reason for new laser system

The previous Chapter described experiments investigating Laguerre-Gaussian laser modes. The first experiment, to visualise the intensity and phase structure of LG modes, was performed with a small He-Ne laser. This operated at 633 nm and had an output power of ~ 3 mW only. To optically trap particles in the optical tweezers, a new laser was required that could produce up to a few 100's mW of laser power in a high order HG mode.

At St. Andrews, optical tweezers had already been successfully demonstrated using a small commercial Nd:YAG laser in a fundamental $TEM_{0,0}$ mode. However, it was impossible to force this laser to operate in a high order HG mode as the laser was a self-contained system with no means to insert a cross wire into the laser cavity.

It was decided to construct a fibre-coupled diode pumped Nd:YLF crystal laser. The introduction of the fibre would enable the pump beam to be accurately aligned and also help to maintain some circular symmetry in the mode which was desirable. The laser cavity would be accessible so that it would be possible to force the laser into high order HG modes.

V. 2 Nd:YLF laser arrangement

A Neodymium : Lithium Yttrium Fluoride crystal (Nd:YLF) was used, of dimensions 3 x 3 x 4 mm with coated end-faces and doping of 1.1%. This crystal absorbed at 797 nm, emitted at 1047 nm and behaved in a very similar way to a Nd:YAG crystal. The crystal was end-pumped by a laser diode and heating effects during this process were reduced by water-cooling the crystal to keep the operating temperature constant and to avoid damage to the crystal.

The laser diode operated at 797 nm (temperature tuneable) with a maximum optical power output of 10 W (continuous wave). Having the diode fibre-coupled was a great advantage as it provided greater manipulation of the diode output when focussing into the Nd:YLF crystal. Also, the circular output obtained from the fibre, of core diameter of 400 μm, helped to reduce some of the rectangular symmetry from the laser cavity.

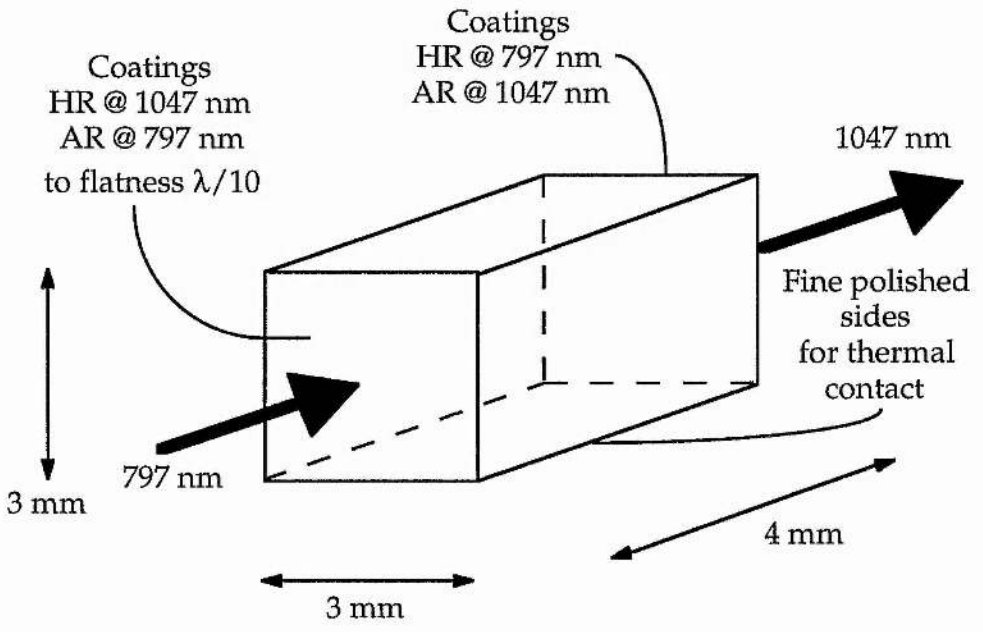

Figure V.a Dimensions and coatings of the Nd:YLF crystal

A temperature controller monitored the running temperature of the laser diode by means of a small thermistor and a Peltier unit, inserted into the cooling arrangement of the laser diode. The temperature was stabilised to within 0.1°C of a specified operating temperature, as a change in temperature of 1°C would result in a wavelength shift of 0.3 nm, so it was imperative to keep the diode at a constant operating temperature. The diode was also water-cooled to assist in the controlling of the operating temperature.

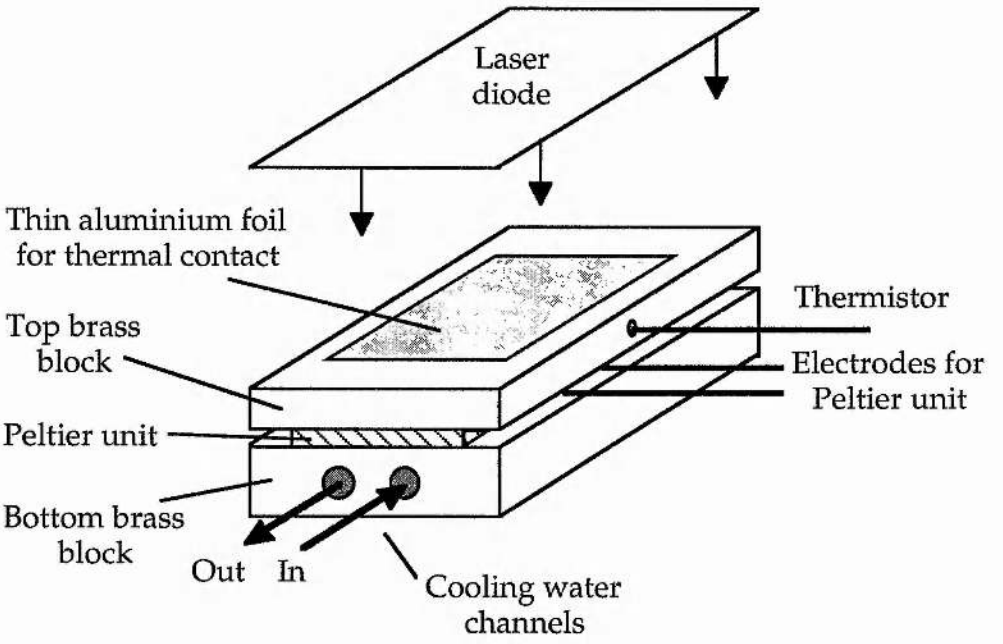

Figure V.b The water-cooling system of the laser diode

The output from the fibre had a beam divergence of about 50°. This was directed through an aspheric glass condenser lens of focal length 8.5 mm, producing a near collimated beam. A second identical lens focussed the beam into the Nd:YLF crystal. The end face of the crystal formed one end of the laser cavity, while the other was formed by an output coupler lens of radius of curvature 0.2 m and of 97% reflection at 797 nm. These created a laser cavity of length 15 cm. A Brewster plate was inserted within the laser cavity to set the polarisation.

It was found that by adjusting the orientation of the output coupler, it was possible to select a high order HG mode quite readily. This was partly due to the circular beam profile from the fibre, which reduced some of the rectangular symmetry within the cavity allowing more control over the range of HG modes possible. The highest order HG mode that was observed by this method was a $HG_{18,0}$ mode.

To assist with the alignment of all the components in this laser system, they were mounted in Spindler & Hoyer (S&H) mounts. This method of construction eliminated many of the alignment problems as all components were fixed to 6 mm diameter steel rods by means of the S&H mounts. The advantage of using such a precise positioning method, apart from the accuracy of alignment and the self-centring of components, was that it was possible to use specific S&H components that were already in mounting plates. Examples of these were lenses, x-y positioners, apertures and steerable mirrors.

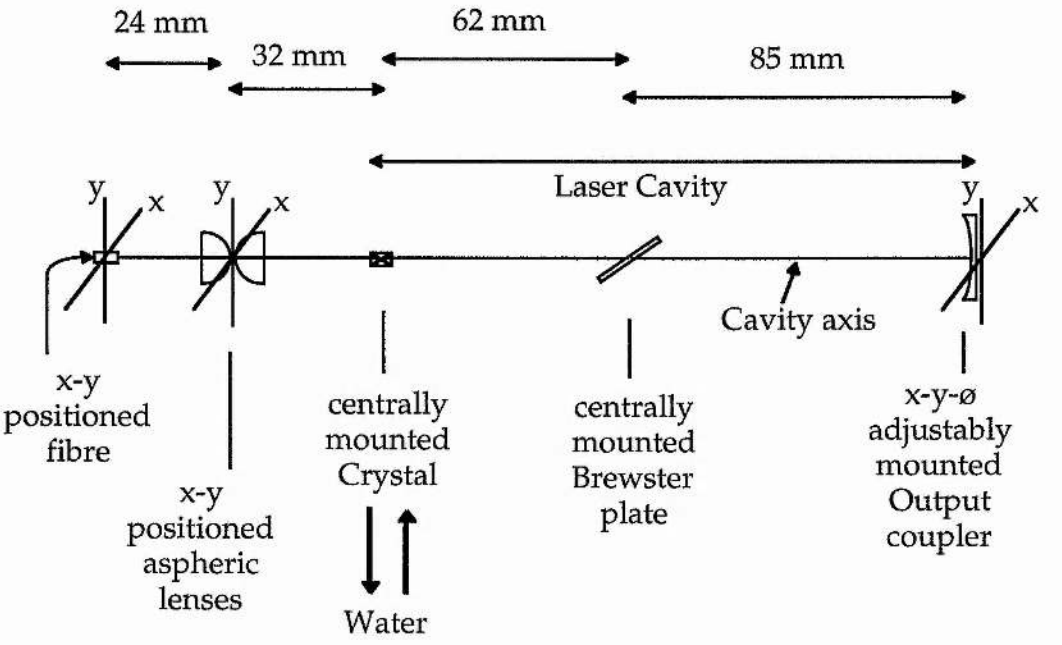

Figure V.c The arrangement of the laser components in the cavity

V. 3 Optimising the laser output

V. 3. 1 Maximising the laser power output

By fine adjustment of the positions of the components in the laser cavity, the output of the 1047 nm laser radiation from the cavity was maximised. Figure V.c shows the final positions of the components. The output power of the cavity of the 1047 nm radiation and the optical power levels of the input laser diode were measured for a given value of current driving the laser diode (see figure V.d). It was found that at low driver currents there was a conversion efficiency of ~3% to produce a few 10's mW of 1047 nm radiation. At high laser diode driver currents (up to 20A) the conversion efficiency was ~10% producing up to 650 mW @ 1047 nm from 6.5 W @ 797 nm from the laser diode. Consequently, it was desirable to operate the diode at currents over 14 Amps to obtain the best conversion efficiency.

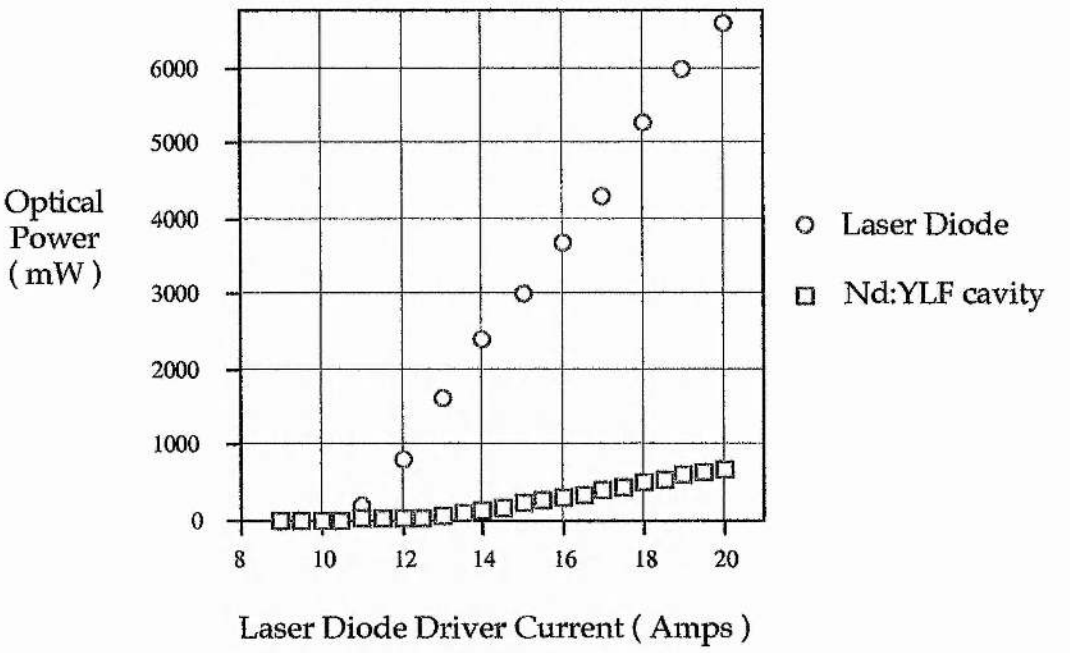

Figure V.d Plot showing the output laser power levels of the diode and the Nd:YLF cavity

V. 3. 2 Changing the Rayleigh range of the laser beam

In order to convert the high order HG modes, obtained from the Nd:YLF cavity, into the corresponding LG modes, it was necessary to propagate the laser beam with the correct Rayleigh range for the cylindrical lens mode converter to operate correctly. To use the mode converter for the laser operating at 1047 nm it was therefore necessary to alter the Rayleigh range of the Nd:YLF laser to match that required by the converter.

For varying large distances from the output coupler z, the distance between the nodes x, of various high order HG modes was measured and from this, the beam radius ω for each mode, was calculated.

$HG_{2,0}$ mode	x = centre of middle lobe to middle of node	= 0.5 ω
$HG_{3,0}$ mode	x = centre of middle node to middle of 2nd node	= 0.866025 ω
$HG_{4,0}$ mode	x = centre of middle lobe to middle of 2nd node	= 1.16721 ω

For large z, the beam radius can be described by,

$$\omega = \frac{\omega_0 \cdot z}{Z_r} = \omega_0 \cdot z \cdot \left(\frac{\lambda}{\pi \cdot \omega_0^{\,2}} \right) = \left(\frac{z \cdot \lambda}{\pi \cdot \omega_0} \right). \tag{5.1}$$

The beam waist radius was then calculated for each of the different HG modes from the Nd:YLF laser, using the gradient of a plot of ω against z (figure V.e). The Rayleigh ranges Z_r could then be calculated for the beams using the deduced values of ω_0.

$$\omega_0 = \left(\frac{z}{\omega} \right) \left(\frac{\lambda}{\pi} \right) = \left(\frac{1}{gradient} \right) \left(\frac{\lambda}{\pi} \right) \tag{5.2}$$

$$Z_r = \frac{\pi \cdot \omega_0^2}{\lambda} \tag{5.3}$$

It was found that the Rayleigh range of the Nd:YLF laser was 25 mm and that required for the incoming beam of the mode converter was 44 mm. By inserting a 200 mm focal length lens at a distance 15 cm from the beam waist

(or 7 cm outside the output coupler), the Rayleigh range of the Nd:YLF laser was appropriately changed so that it could then be used with the cylindrical lens mode converter, to produce the LG modes needed for the work within optical tweezers.

Figure V.e also demonstrates an important point that is worth noting. By changing the modes of the Nd:YLF laser, the associated Rayleigh ranges of the beams were not changed. This was most useful as it meant that any of the Nd:YLF beams with different mode profiles could be focussed into the cylindrical lens mode converter without needing to change any of the focussing optics.

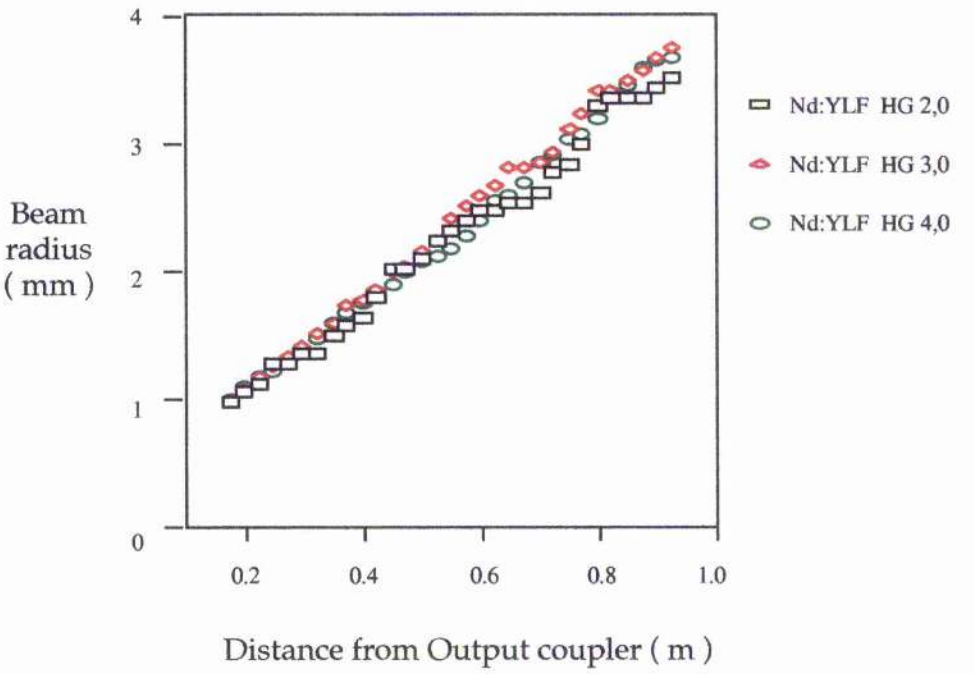

Figure V.e Plot showing the beam radius of various modes at distances from the output coupler

V. 4 Conclusions

This Chapter outlined the need for a new laser system and briefly described the various components of the fibre-coupled laser diode pumped Nd:YLF laser. Examples of some of the component designs are included in Appendix II. Upon completion of the construction of the laser, it was capable of producing high order HG modes of 1047 nm wavelength, up to powers of 650 mW. An additional lens was incorporated into the system so that the beam had an appropriate Rayleigh range for correct operation in the cylindrical lens mode converter.

The work described in this Chapter was my first major achievement of the PhD project. It was necessary to have this laser up and running as soon as possible, for the investigation of optical tweezers and LG modes depended on its construction. To have a stable, reliable and efficient laser source was paramount and this was successfully achieved after 12 months of the project work. It was then possible to begin the principal research of the PhD.

Chapter VI

Improved Optical Tweezers

Contents

VI. 1 Aim of the experiments

The work described in this Chapter combined the technique of optical tweezers, which has been discussed in Chapter III, along with Laguerre-Gaussian (LG) laser modes (Chapters II and IV). The experimental arrangement of the tweezers, with the LG modes incorporated into the system, will be described. This will also include typical experimental parameters for the operation of the tweezers' system, such as particle size, laser powers required for tweezing and the estimated velocity of the trapped particles through the suspending media.

The improvement in the operation of the optical tweezers when using LG modes was investigated both theoretically and experimentally. In this work, the trapping forces were compared for a traditional $TEM_{0,0}$ mode and a high order $p = 0$ LG mode. Due to the lack of on-axis rays, it has been found from our research that LG modes produce a much stronger axial force in the optical trap and consequently, a more efficient optical trap. The ability to trap particles optically with less laser power will have significant importance for the trapping of biological specimens. This is due to reducing the risk of damage to the specimen through thermal effects and its eventual death, sometimes referred to as the "opticution" of a specimen.

VI. 2 Modelling the z-trapping forces within tweezers

Whilst the Nd:YLF laser system was being assembled and constructed, it gave sufficient time and opportunity to be able to perform some theoretical modelling of the axial forces involved in the optical tweezers. As the radial trapping forces are typically an order of magnitude larger than the axial or z-trapping forces [1], the whole performance of the optical tweezers could be inherently improved by improving the axial forces. It was believed that this could be achieved using high order LG modes. The modelling results were published in the *Journal of Modern Optics* in December 1996 [2].

In particular, the tweezers' forces on a Mie particle were investigated and compared for those arising from a fundamental $TEM_{0,0}$ laser mode and from a high order LG laser mode. More specifically, LG modes with zero intensity on the beam axis were of interest as the lack of these on-axis rays should increase the trapping efficiency of the beam. To carry out such computer modelling it was necessary to be able to compare the performance of tweezers with different laser modes. This meant that the beam radius of each mode under consideration had to be adjusted so that each experienced a similar amount of aperturing.

VI. 2. 1 Beam truncation for direct comparison of modes

The modes under consideration for this modelling were a fundamental $TEM_{0,0}$ laser mode (which is identical to a LG^0_0 mode), and various high order LG modes with zero on-axis intensity and indices $p = 0$ and $\ell \neq 0$. Figure VI.a shows the intensity of these modes after normalisation to unit power as their beam radius ω increases, including the $\ell = 0$ case (the fundamental $TEM_{0,0}$ mode). The radius r of the maximum intensity of these modes is given by [3]

$$r = \omega \frac{\sqrt{2\ell}}{2}. \tag{6.1}$$

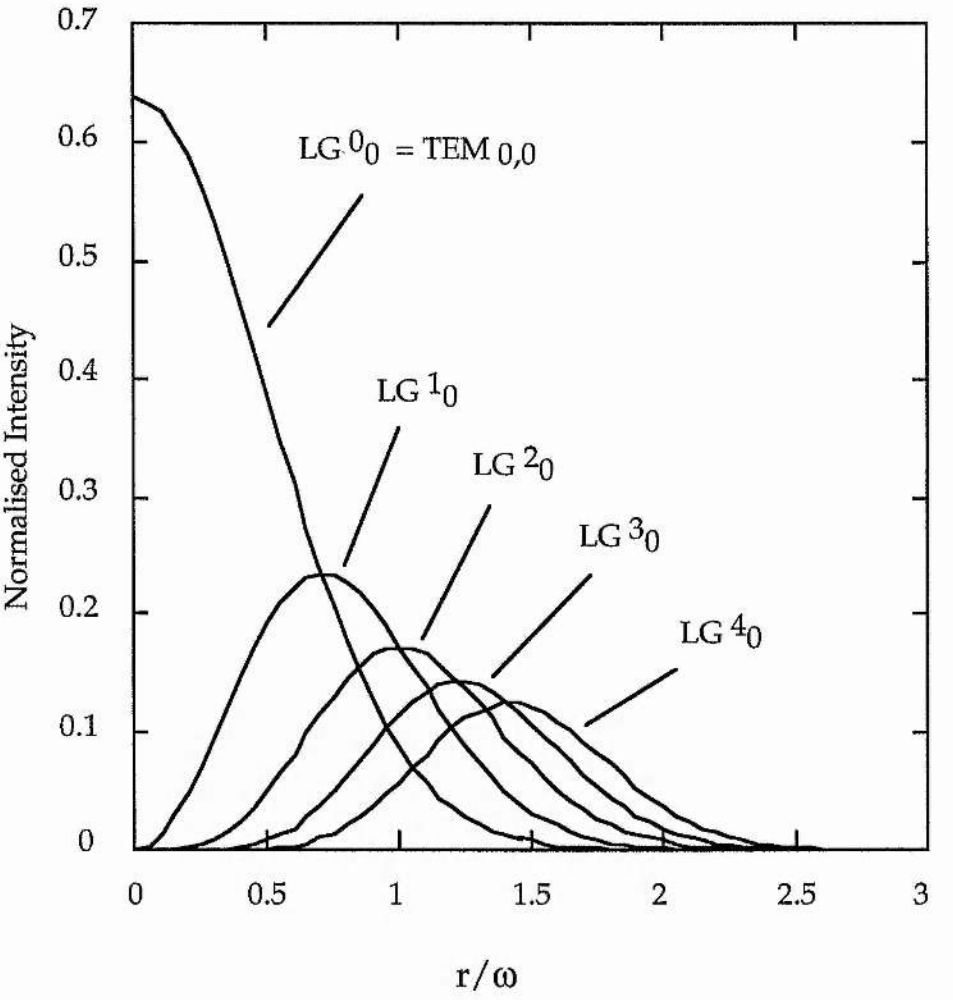

Figure VI.a Intensity distribution of p=0 LG modes as a function of beam radius

For the computer modelling, it was decided to truncate all the modes at a radius corresponding to 1.8ω which would still allow all the modes to keep their main intensity characteristics. This was equivalent to aperturing the modes by a lens.

VI. 2. 2 Modelling of the axial trapping forces

The gradient forces experienced by a particle can be calculated, but they depend on the size of the particle. For Rayleigh particles, smaller than the

trapping laser wavelength, the equations for the forces can be solved analytically and calculated [4]. However, for Mie particles, larger than the trapping laser wavelength, the trapping forces within the optical tweezers must be calculated numerically. Our modelling considered particles several times larger than the trapping wavelength, i.e. Mie particles. The approach taken in the modelling followed a similar approach as that taken by Gussgard et al in their theoretical modelling [5]. The details of the programs written for the modelling can be found in Appendix III.

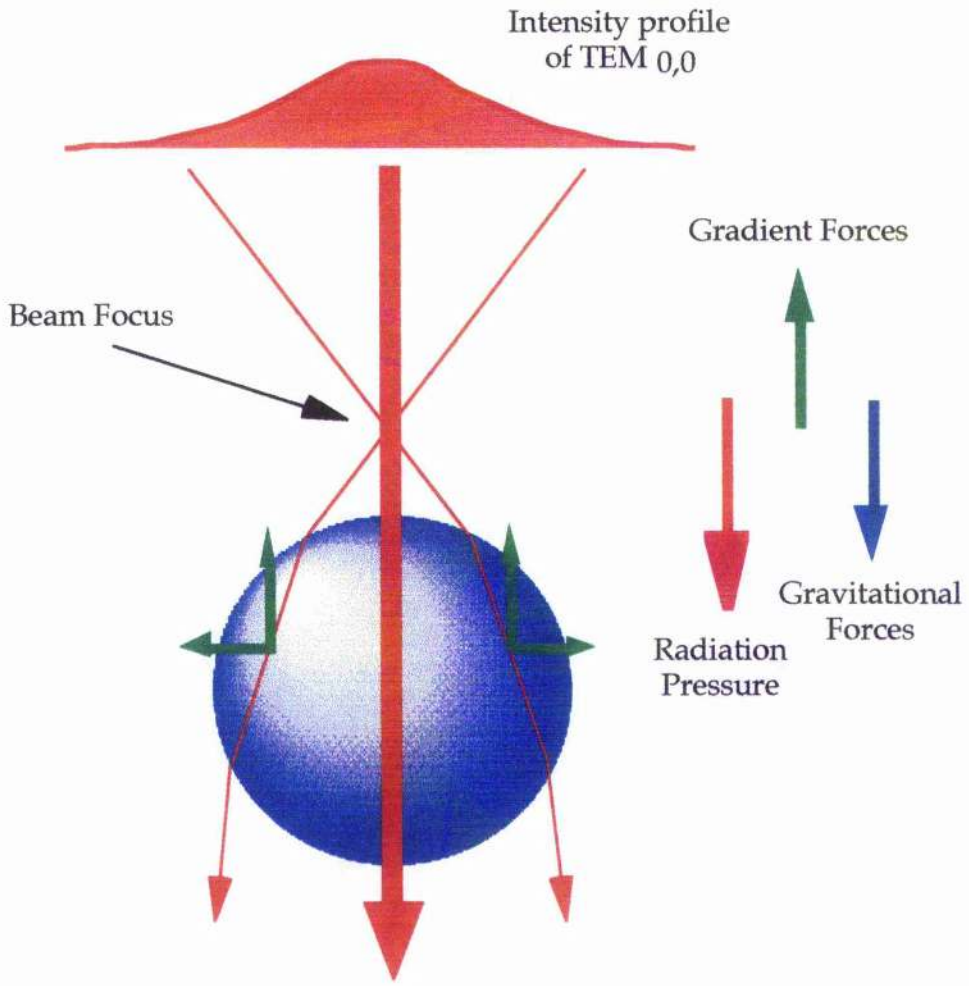

Figure VI.b The z-trapping of a particle using a $TEM_{0,0}$ mode

Let us firstly reconsider the axial trapping case in terms of a geometrical optics approach. For a trapping laser operating in a $TEM_{0,0}$ mode, the ray optics show that the on-axis rays are detrimental to the z-trapping and that the trapping along the z-axis is due to the extremal rays of the mode (figure VI.b). These rays have radial components that approximately cancel, but the z components sum to give the gradient force.

By reducing the intensity of the on-axis rays, the trapping can be greatly improved as the extremal rays would have a much greater effect. This can be achieved by using the family of modes with $p = 0$ and $\ell \neq 0$ as they have zero intensity on the beam axis (figure VI.c).

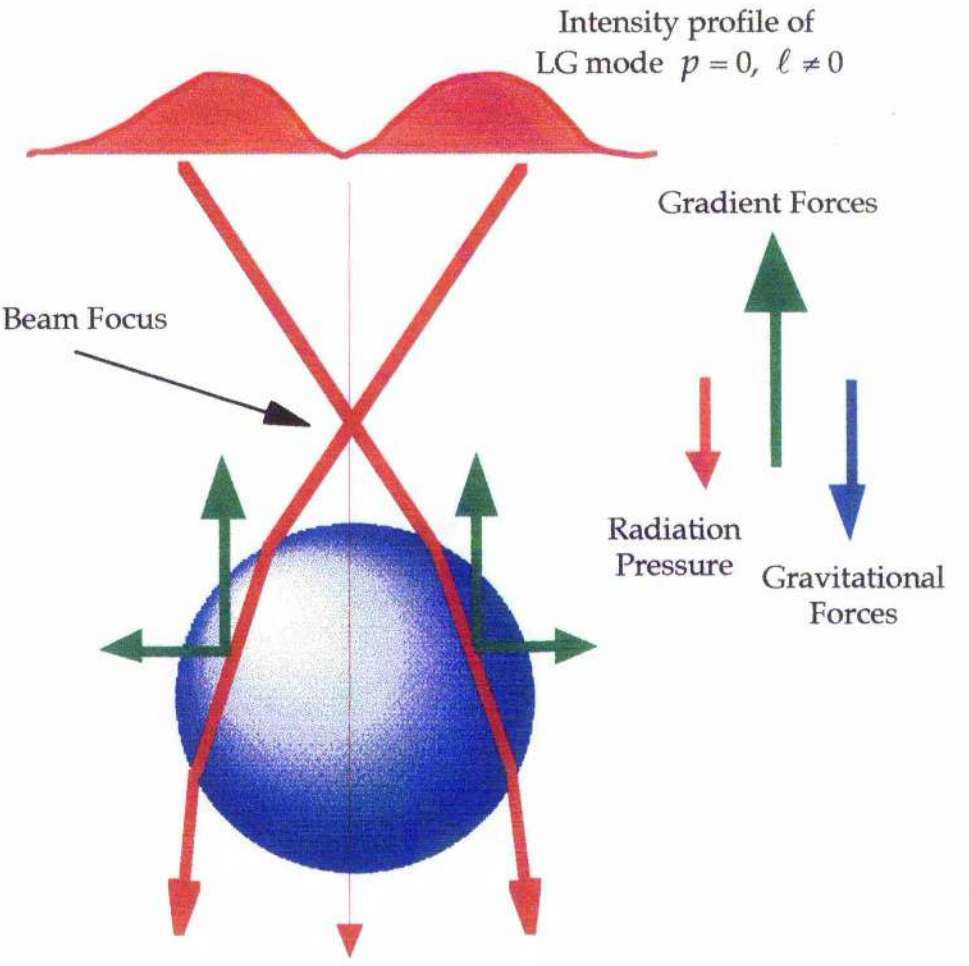

Figure VI.c The z-trapping of a particle with an LG mode of $p = 0$ and $\ell \neq 0$

In the model, the incident Gaussian beam (be it $TEM_{0,0}$ or Laguerre) was represented by 500 concentric rings of rays. These rings were defined to converge at the centre of curvature of the wavefronts. For each ray (or ring of rays), the curvature of the Gaussian beam was calculated at the point where the beam first intersected the sphere. Each ring of rays was individually weighted to give the appropriate radial intensity distribution for the required beam profile ($TEM_{0,0}$ or Laguerre) as shown in figure VI.d.

As the rays underwent refractions upon entering and leaving the sphere, there was a net momentum transfer which resulted in the gradient forces that acted upon the sphere against the propagation direction of the beam. Similarly, as the rays experienced reflections, there was a radiation pressure force and a scattering force which acted along the direction of propagation of the beam. By allowing the refractive index of the sphere to be close to that of the surrounding media, it was acceptable to use the average value of the perpendicular and parallel Fresnel coefficients when calculating the intensity of the reflected light. There was no overall force in the radial direction due to the symmetry of the sphere on the beam axis.

There was a position along the beam axis where the gradient forces balanced the scattering and gravitational forces, and an equilibrium was achieved. There was a small range along the beam axis where the gradient forces were dominant causing a net backward force and this resulted in what is known as a trapping region.

To calculate the axial trapping forces that occur within the optical tweezers, each ring of rays was taken in turn and the net momenta change calculated. This was done by calculating the momenta of the photons in the reflected and transmitted rays and taking the axial components. These were summed and the momenta changes for all of the rays were summed to obtain a net momenta change for the beam in the z-direction as it interacted with the sphere. The z-trapping force was directly related to this momenta change and was calculated as a function of sphere position along the beam axis.

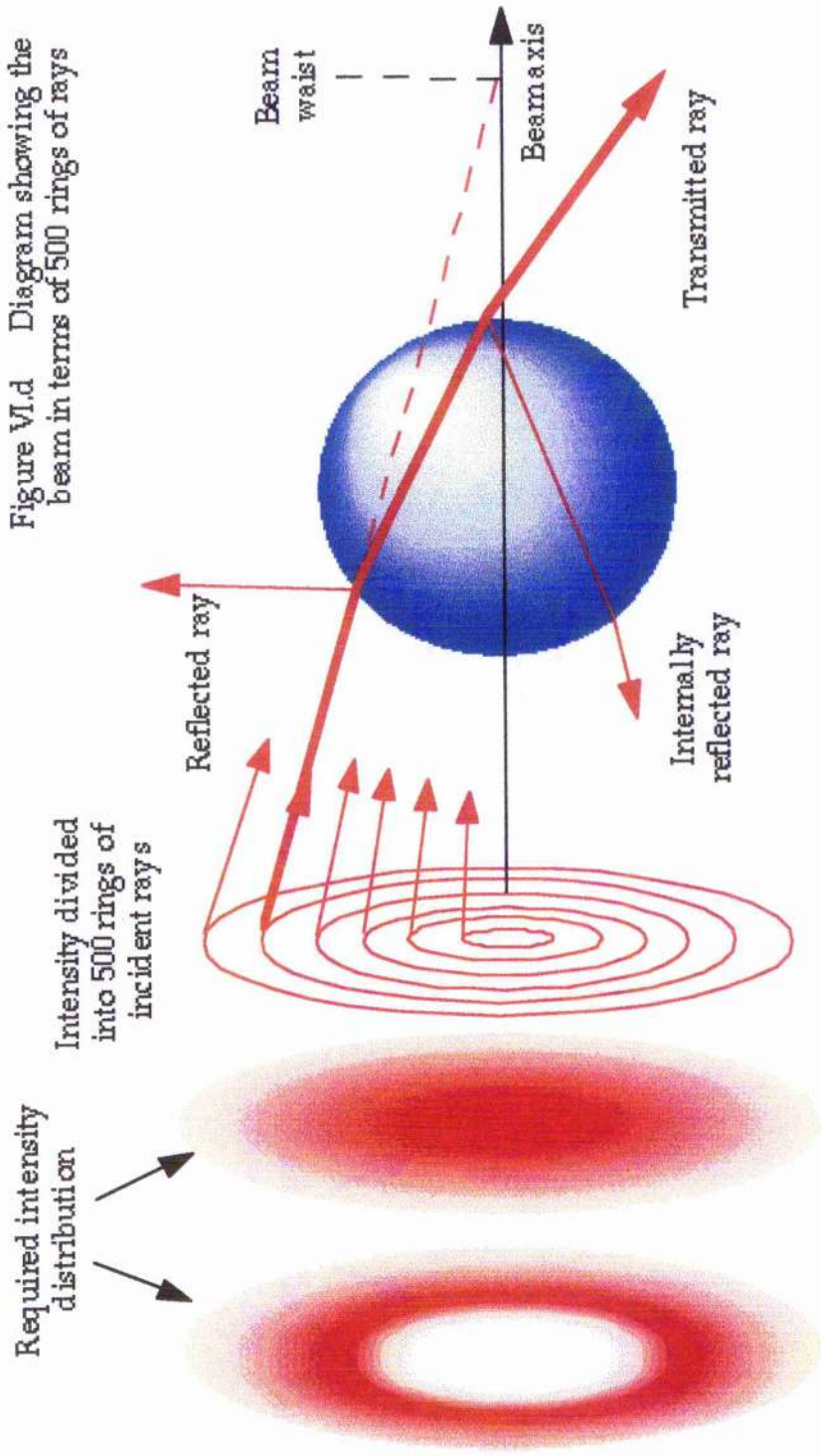

Figure VI.d Diagram showing the beam in terms of 500 rings of rays

VI. 2. 3 Modelling results

A set of experimental circumstances were assumed for the purpose of the computer modelling of the z-trapping forces. A laser wavelength of 532 nm was used with a microscope objective lens of numerical aperture 1.3. The Mie particle to be trapped was assumed to be an 8 μm diameter silica sphere which was suspended in water. The focussing of the laser beam in this case produced a beam waist for the fundamental mode in water of 0.42 μm. The axial trapping forces were calculated, using ray optics, for the $TEM_{0,0}$ mode and high order LG modes of $p = 0$ and $\ell = 1$, 2, and 4. They were calculated as a function of the sphere's position along the beam axis with respect to the beam waist of the beam, with the beam propagating in the positive z-direction. Figure VI.e shows the modelling results for the experimental parameters described.

When the gradient forces of the refracting rays balance the radiation forces of the reflecting rays, the net axial trapping force is zero. When the radiation forces are dominant, there is a net positive z-trapping force which forces the particle away from the beam waist in the direction of the beam propagation. Due to the optical tweezers geometry, the positive z-direction is pointing vertically downwards and thus gravity acts in this direction also. Where the gradient forces exceed the radiation forces, there is a net negative z-trapping force which acts on the particle, drawing it towards the beam focus in the opposite direction to the propagation and against gravity.

Figure VI.e shows that there is a trapping region between 4 and 10 μm below the beam waist in the tweezers set-up. When the sphere is in these positions, it experiences a force pulling it back up towards the beam focus. It can be clearly seen that as the ℓ index of the LG mode increases, the axial trapping force increases in magnitude up to 4 times that of the fundamental $TEM_{0,0}$ mode. This was expected due to the absence of the non-refracting on-axis, high intensity rays in the high order LG modes. This meant that there was considerably less radiation pressure (due to the reflection of rays) acting on the sphere, which resulted in the gradient forces being increasingly dominant and thus producing a very large net negative trapping force.

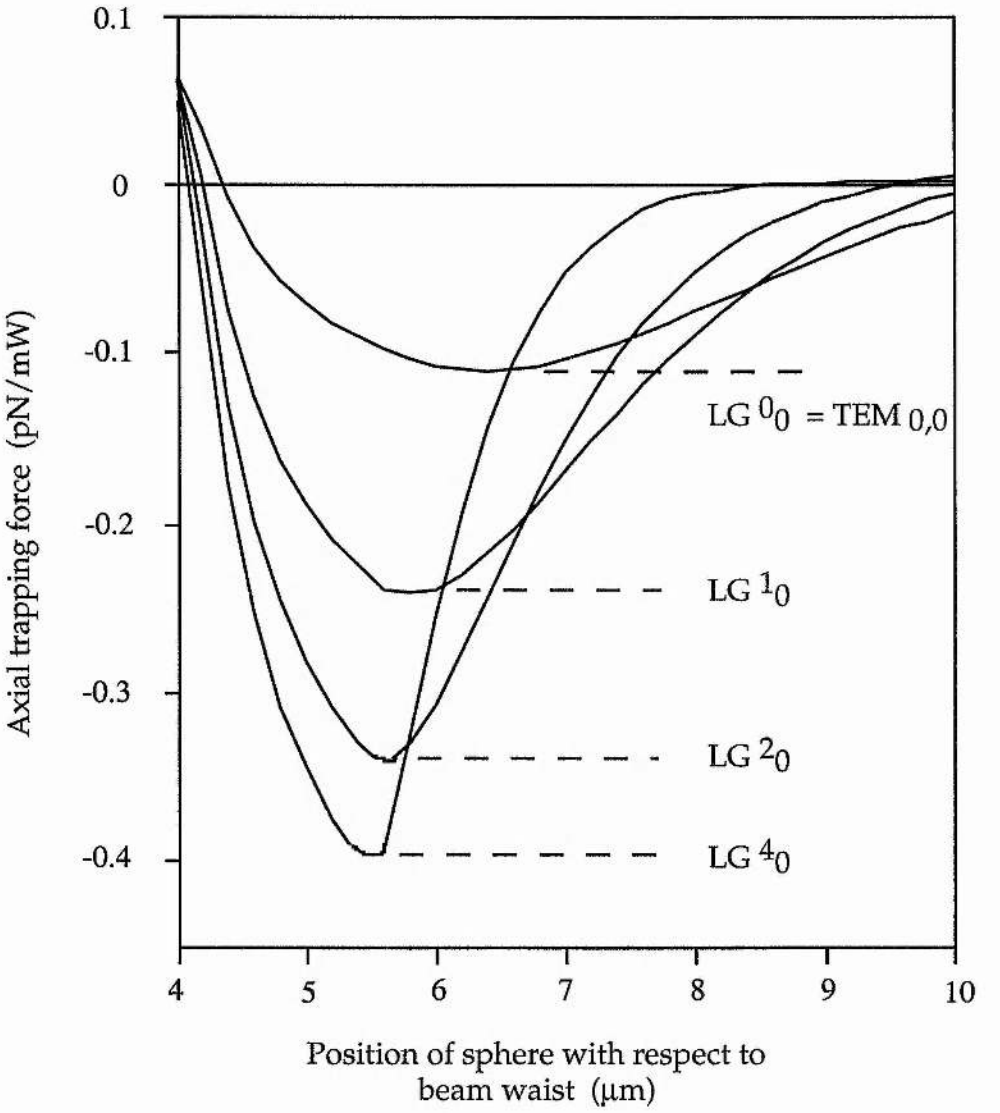

Figure VI.e Plot of the axial trapping force for an 8 μm sphere in water as a function of position, for LG modes of $p = 0$ and $\ell = 0, 1, 2$, and 4

If gravity is now also taken into account, the advantage of the LG modes becomes more apparent. To achieve a true optical trap, the negative axial trapping force must also balance the gravitational forces to obtain the equilibrium situation. For an 8 μm diameter silica sphere, the force of gravity acting on the sphere is 2.6 pN. The forces calculated in figure VI.e are obtained per mW of laser power, so 2.6 pN of negative axial trapping is required to cancel the gravitational effects. For the $TEM_{0,0}$ mode, the equilibrium situation can be reached by trapping with 26 mW of laser power

whereas the LG^4_0 mode only requires 7 mW. The high order LG modes can achieve the same optical trapping overcoming gravity, using considerably less laser power than a $TEM_{0,0}$ mode would do, due to their greater axial trapping force per unit power.

A different analysis of the improved z-trapping was also undertaken. By keeping the laser power constant, the NA of the objective lens was altered to change the net trapping force (figure VI.f). Using a laser wavelength of 532 nm and an 8 μm silica sphere, the same magnitude of negative z-trapping could be obtained by using a $TEM_{0,0}$ mode with a 1.3 NA or a LG^2_0 mode with an objective lens of NA 0.8.

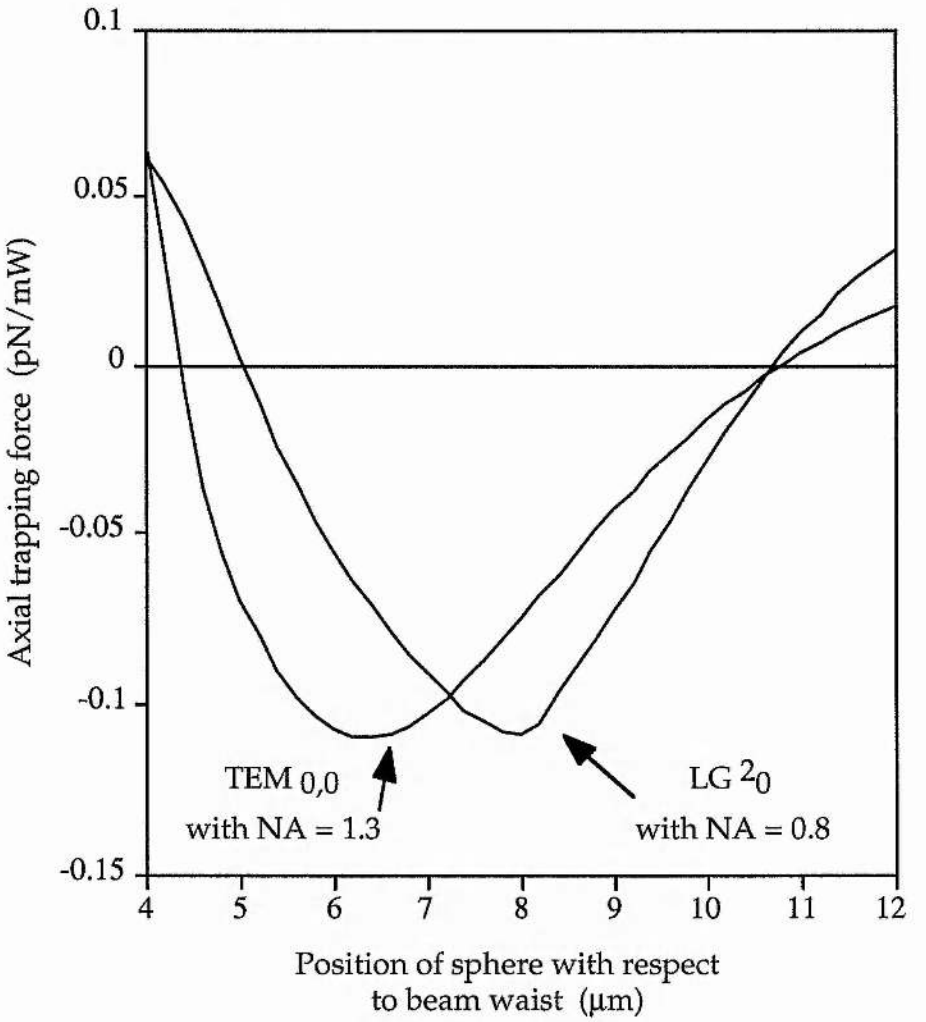

Figure VI.f Plot demonstrating the same axial trapping force by using different modes and numerical apertures

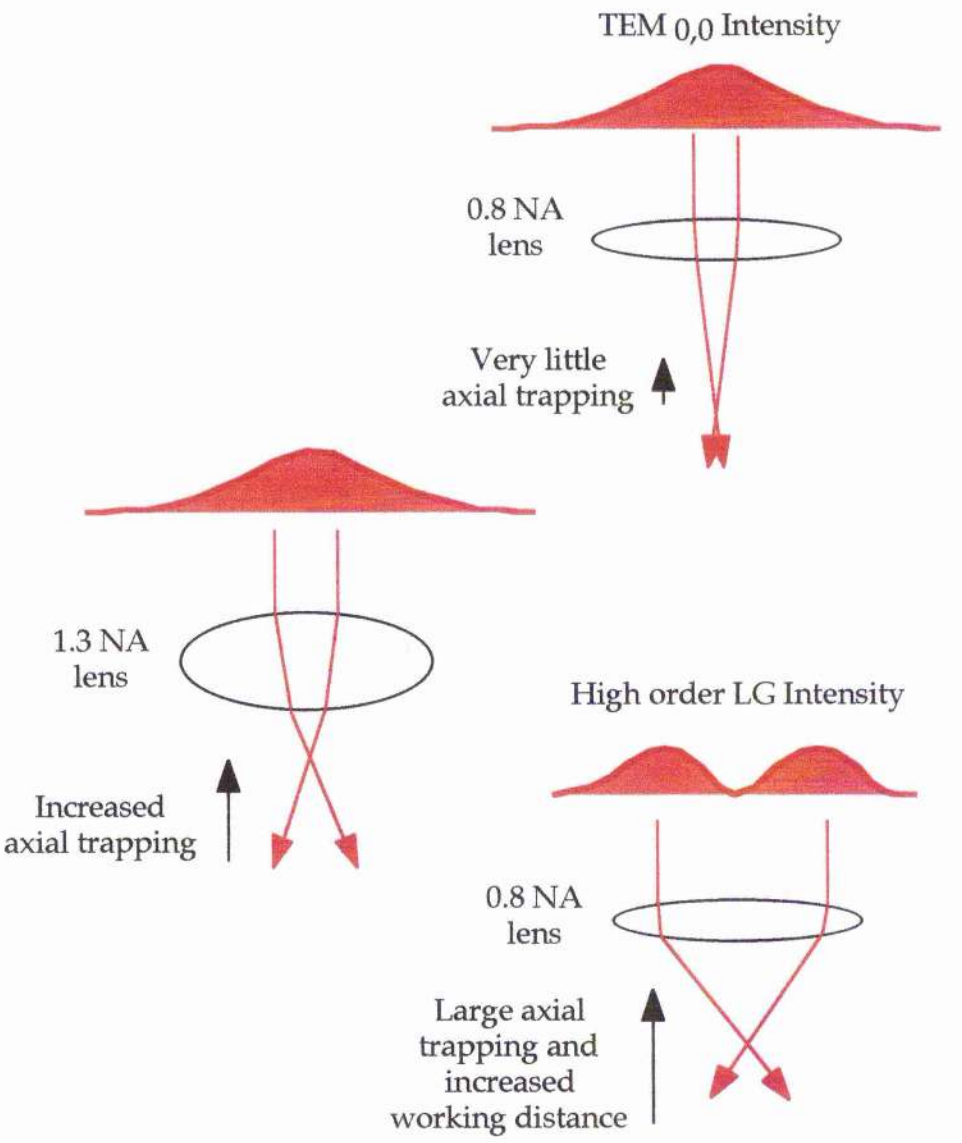

Figure VI.g Angles of incident high intensity rays with different modes and numerical apertures to achieve comparable axial trapping

This is because of the relative incident angles of the high intensity rays (figure VI.g). The high order LG mode does not require a large NA objective lens for good axial trapping as the high intensity rays of the LG ring mode are already incident at a shallow angle. By using a lower NA microscope objective, the cost of the lens can be reduced and the working distance of the

lens can be increased. This distance being the depth of the trapped particle below the beam focus, the larger this is, the more accessible the trapping region is.

The same trends in the increased axial trapping force per unit laser power have also been obtained by modelling the axial trapping of spheres of various radii and differing values of the numerical aperture of the microscope objective lens. In all scenarios, the high order LG modes always produced a net axial trapping force three or four times larger than those when using a $TEM_{0,0}$ mode.

VI. 2. 4 Inaccuracies in the modelling

There is, as always, some inaccuracy associated with these modelling predictions. There are two considerations which must be taken into account when investigating the axial trapping forces. Firstly, the paraxial description of the Gaussian modes is only approximate when the beam is very tightly focussed. This has already been studied and Barton and Alexander showed that for the experimental circumstances that we've investigated, the average error in the calculated field intensities is 5% [6]. Therefore, a similar error is expected in the modelling that we have performed of the axial trapping forces within the optical tweezers.

Secondly, the method of using the refracting rays to calculate the momenta change of the beam is subject to the geometrical optics approach. For the experimental parameters that have been used in the modelling, the ratio of the sphere's diameter to the wavelength in water is approximately 20 : 1 and this is close to the limit for geometrical optics to be valid. Although these experimental conditions are almost a borderline case as regards their validity, Gussgard in his work [5] considered similar situations and found a strong agreement between his experimental results and the ray model. This substantiates our case for using geometrical optics in our modelling.

VI. 3 Experimental set-up

The laser system itself was constructed as described in Chapter V. The laser could be operated in various HG modes with laser power levels up to a few 100's mW. The output mode was directed into the cylindrical lens mode converter using an input lens to set the beam's Rayleigh range, as described in section V. 3. 2.

By rotating the mode converter at 45° to the input HG mode, the corresponding LG mode was produced with almost 100% efficiency. The only HG mode that was propagated and used within the tweezers was a $TEM_{0,0}$ mode, which is the same as a LG^0_0 mode. This meant that the mode converter could be aligned for LG mode conversion at all times.

A 160 mm lens was inserted after the cylindrical lens mode converter to produce a collimated beam. The laser mode was then directed into the beam expanding telescope. This consisted of two lenses which were changeable so as to alter the size of the beam entering the back aperture of the microscope objective lens. All of the lenses and optics were aligned using Spindler & Hoyer (S&H) mounts for ease of aligning and centring the components.

Two beam steering mirrors were incorporated into the arrangement. These altered the angle of the beam into the back aperture of the objective lens, which enabled the focussed beam spot to be translated around the sample cell, without the need to move the cell itself. A second beam telescope was inserted between the mirrors and the beam splitter to focus the beam into the microscope objective.

The beam was reflected by a beam splitter down into the microscope objective. This was an oil immersion Plan-Neofluar objective lens from Zeiss, of 100x magnification with a numerical aperture (NA) of 1.3. It was fixed to a collar so that the objective lens could be lowered to the sample cell by rotating the collar. As the lens was an oil immersion one, index matching fluid was used on top of the cover slip of the sample cell to allow correct matching of the indices of the lens and the coverslip.

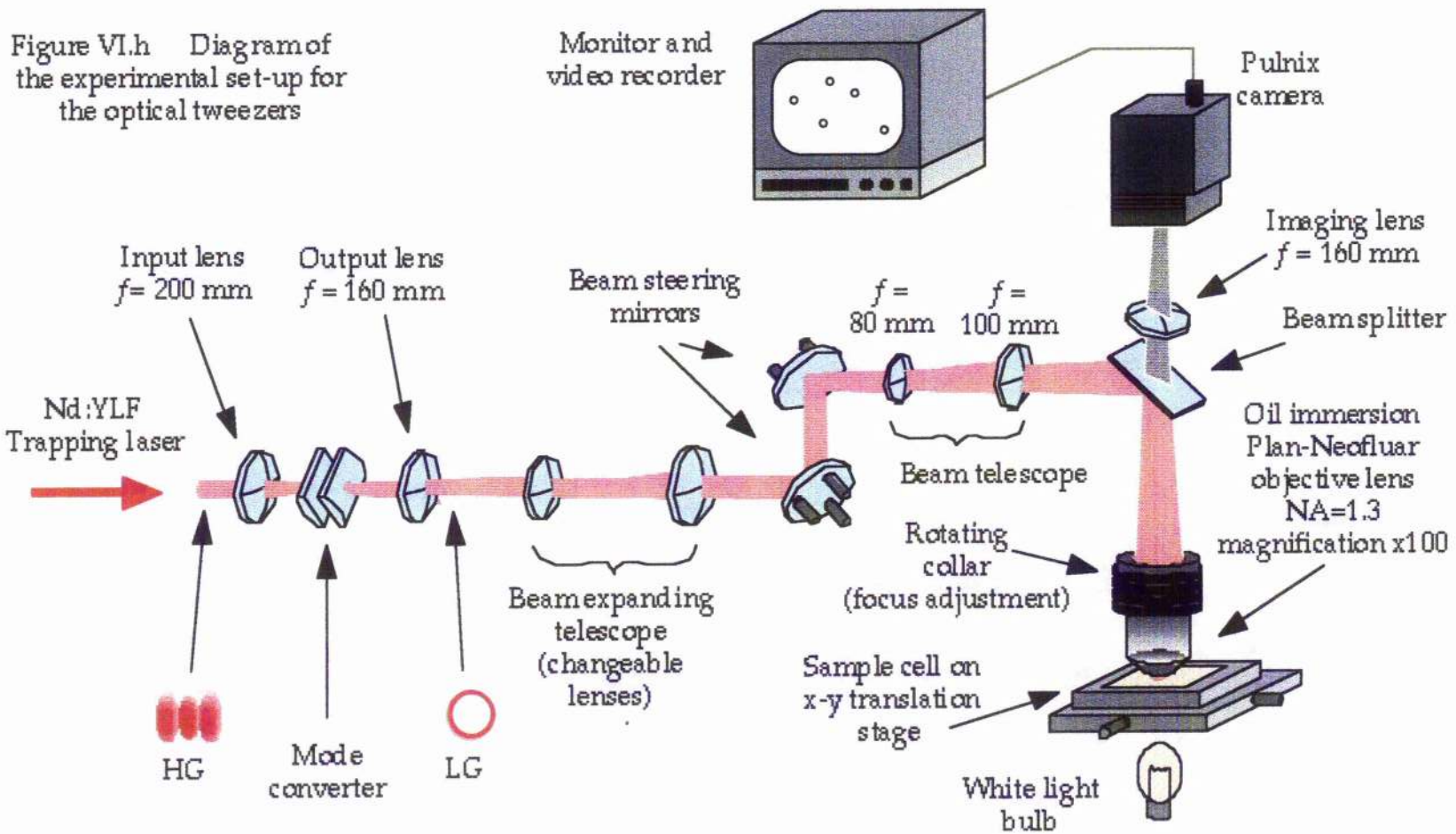

Figure VI.h Diagram of the experimental set-up for the optical tweezers

The sample cell used in our experiments was constructed from a microscope slide of thickness 1.0 mm, with a vinyl mask of thickness 100 μm stuck on top to form a well of that depth for the sample in solution to be placed. The specimens in solution were deposited into the well of the cell by means of a small pipette or syringe. A cover slip approximately 20 μm thick formed the 'lid' of this cell to seal it.

The sample cell was illuminated from underneath by a small 6 volt white light bulb. The same microscope objective lens was used to observe the tweezing of the specimens. Above the beam splitter (transparent for visible wavelengths) a 160 mm tube lens was placed to image the specimens in the sample cell down to a plane for viewing. A Pulnix camera was positioned at this point, which was connected to a video recorder and a monochrome monitor. In this way, the tweezing of particles could be investigated, observed and recorded very easily.

An additional small array camera was able to be placed in the path of the laser modes, along with suitable neutral density filters, to observe the mode intensity distribution. A calibrated power meter was used to measure the laser power levels of the modes being used. Usually, the detector was used with its attenuator attached, to measure up to 2 W, but for very low power measurements the attenuator was removed to give a full-scale reading of 2 mW.

VI. 4 Optical tweezers typical operating parameters

This section will give an overview of the experimental parameters involved within the optical tweezers. The laser mode that entered the back aperture of the microscope objective lens (which is usually of 1.3 NA), was typically a few mm in diameter with a power of a few mW. This resulted in a beam waist, within the sample cell, of about 1 μm in diameter.

The sample cell should have a depth of 50 - 100 μm with the suspended particles in the cell being a few microns in size. The largest particle that it

was possible to manipulate was about 15 μm in size, while the smallest was about 1 μm in size due to the comparable size of the focussed beam spot. The size of the force exerted on the particle by the trapping laser (the optical tweezers) was typically of the order of a picoNewton (10^{-12} N). In the experiments that we performed, the particles were all intermediate particles (i.e. having their diameter of the order of the wavelength of the laser light used) and had a refractive index higher than that of the surrounding suspending media (for example $n_{glass} \approx 1.5$ and $n_{water} \approx 1.3$).

Using the optical tweezers it was relatively easy to manipulate the particles around the sample cell. It was possible to z-trap up through the sample cell, but by far the strongest trap (by a factor of 10 or so) was the x-y trap, the horizontal trapping. The trapped particle could be dragged, or translated, through the sample cell with speeds of 10's μm/second, but this depended on the size of the particle, the viscosity of the supporting media and the relative refractive indices of the particle and supporting media.

VI. 5 Experimental threshold laser power levels for z-trapping

Once the tweezers were up and running satisfactorily, the modelling results presented in the previous section of this Chapter were experimentally verified. The exact experimental conditions could not be replicated as the silica spheres actually used were 5 μm in diameter, suspended in water and trapped in a laser beam of wavelength 1047 nm. However, similar results were expected as the spheres were intermediate particles, on the borderline of being Mie particles.

VI. 5. 1 Q factor for trapping efficiency

To compare the trapping efficiencies of different laser modes within optical tweezers, it was necessary to define a quantity that could be calculated for each set of results for each mode. One such parameter had been used before [1, 7] and this was adopted in our experimental results. A factor Q_{axial} has

been defined to relate the incident laser power P and the resulting trapping force F as follows,

$$Q_{axial} = \frac{F \cdot c}{P \cdot n_s} \tag{6.2}$$

where n_s is the refractive index of the medium suspending the sphere. The term $P\ n_s/c$ is the total linear momentum content present in the laser beam. The value of Q_{axial} then lies between 0 and 1.

For Mie particles, Q_{axial} is predicted to be independent of particle size and the laser power to achieve z-trapping (i.e. to overcome the forces due to gravity) is proportional to the cube of the diameter of the trapped particle [7]. For particles where their diameter is comparable to the wavelength, this relationship does not apply. For the much smaller Rayleigh particles, the size of the particle again affects the value of Q_{axial} and the trapping of these particles tends to be very unstable due to their Brownian motion being large enough to knock the particles out of the trapping laser beam [1]. Consequently, larger laser powers tend to be required to hold Rayleigh particles in the tweezers.

Q_{axial} is usually determined experimentally rather than calculated, due to imperfections present in the experimental arrangement. These can take the form of varying depths of sample cells and microscope objective lenses not operating at their correct wavelength, which causes focussing imperfections. Experimental Q_{axial} values have been reported for a 5 μm particle trapped close to the microscope objective lens, and the maximum value obtained has been 0.18 [1].

VI. 5. 2 Reducing the on-axis rays

As discussed earlier in section VI. 4 it is advantageous to reduce the on-axis rays of the beam as these are detrimental to the axial trapping of the particle. Various methods have been suggested and used, to reduce these on-axis rays within optical tweezers.

To combat this problem, the hybrid mode $TEM^{*}_{0,1}$, or "doughnut" mode, has been used to trap particles, as this mode has a "hole in the middle" thus eliminating the on-axis ray problem. Ashkin proposed using this mode in the tweezers arrangement [7] and the experimental observation of their use has been published by Sato et al [8], which demonstrated a 20% increase in Q_{axial}.

Other methods include using a centre field stop to create the zero on-axis intensity structure, which gave a similar improvement in Q_{axial} [5]. One particularly unique method was performed by Friese et al [9] who measured the temporal fluctuations in the back-scattered light from the trapped particle. This enabled the force per unit displacement from the trap centre to be inferred, which showed that a doughnut mode with a topological charge m = 3, produced an optical trap that was twice as strong as that using a fundamental $TEM_{0,0}$ mode.

In work that was carried out recently, here at St. Andrews, the axial trapping efficiencies of the optical tweezers were investigated experimentally by considering trapping with a standard fundamental mode and also a LG^{3}_{0} mode. As our modelling showed, the high order LG mode should be a more efficient trap (using less laser power) than previously achieved with a fundamental $TEM_{0,0}$ mode.

VI. 5. 3 The experimental arrangement

The experimental set-up was simply the standard tweezers set-up as in figure VI.h, incorporating a x100, 1.3 NA, Plan-Neofluar oil immersion microscope objective lens from Zeiss. The sample cell formed a well depth of approximately 70 μm which was filled with a suspension of water and micron-sized silica spheres. These were a mixture of spheres with 1, 2 and 5 μm diameters.

The beam telescope lenses were easily changeable to allow different beam sizes into the back aperture of the objective lens (figure VI.i). This aperture was 5 mm in diameter and had to be filled in order to achieve optimal optical trapping in the tweezers. When using the $TEM_{0,0}$ mode, overfilling

the back aperture was an advantage as the high intensity rays would be nearer the extreme sides of the lens resulting in stronger axial trapping. However, the LG^3_0 mode could not be too large for the aperture as the intensity ring would not pass through the lens and there would be a cut-off of optical trapping completely.

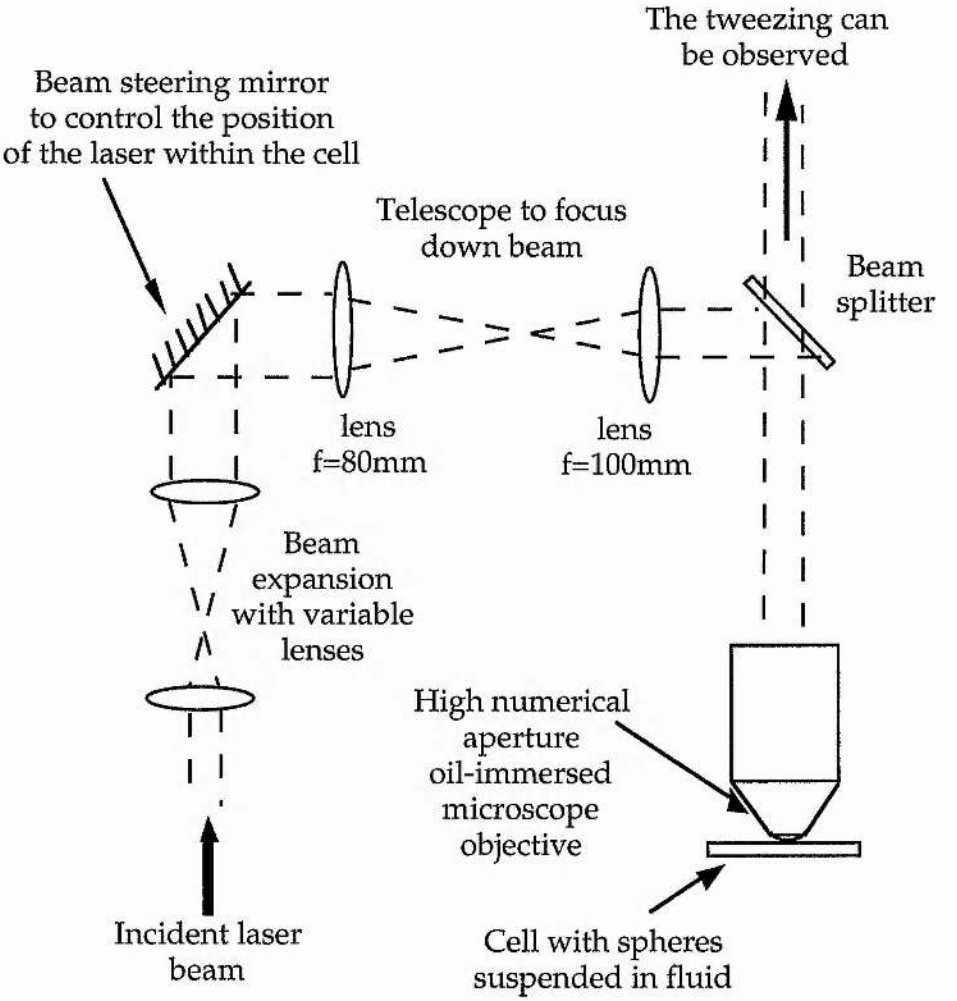

Figure VI.i Experimental arrangement incorporating the changeable lenses in the beam telescope

VI. 5. 4 Criteria for the comparison of axial trapping efficiencies for different laser modes

For each of the two laser modes under consideration, it was necessary to perform the z-trapping under the same conditions and circumstances in order to apply a direct comparison in trapping efficiency. Both modes, the $TEM_{0,0}$ and LG^3_0 modes, were produced with the diode-pumped Nd:YLF laser and the same objective lens was used for the trapping.

It was usually impossible to trap the same particle with the two modes as it took time to change the mode and check the alignment of the beam through the optics. However, there was the utmost confidence that the manufactured silica spheres were all identical for each of the 3 sizes of sphere [10]. This removed the problem of a lack of consistency in particle size.

For each of the trapping cases, a successful axial trap was defined as, in our experimental work, the ability to lift one of the silica spheres from the base of the sample cell to a distance 25 μm above the bottom. This represented a realistic working situation for the trapping and raising of particles. Once the trapped particle had been raised this distance, it was relatively easy to continue the lifting of the particle right up to the top of the cell, a distance of 70 μm, as the trapping efficiency of the tweezers increased as the trap neared the top of the cell as reported by Felgner [1]. Consequently, the hardest trapping situation is the lifting of a particle off the very bottom of the sample cell. It is for intended applications of this nature that we investigated improving the axial trapping efficiency of the optical tweezers.

The direct comparison of the axial trapping efficiencies for the two laser modes used and different size spheres, required Q_{axial} to be calculated in each instance. The force F required to lift a particle of diameter d and density ρ_p against gravity g whilst in a surrounding medium of density ρ_s, is given by [1],

$$F = \frac{\pi}{6}(\rho_p - \rho_s)d^3 g + \frac{2kT}{d} \tag{6.3}$$

where T is the temperature of the surroundings with the kT term being the force required to overcome the thermal motion of the particle in the medium. The trapping laser power was slowly reduced until a minimum power level was found that still allowed the lifting of the silica sphere from the bottom of the sample cell to a height of 25 μm. This experimentally measured threshold trapping laser power was then used with the calculated trapping force from equation 6.3, to obtain a value for Q_{axial} by using the expression given in equation 6.2.

For each combination of laser mode and size of sphere, the lenses in the beam telescope were changed to set the beam size to optimise the trapping efficiency.

VI. 5. 5 Experimental results

As the beam radius at the back aperture of the objective lens was increased by changing the beam telescope lenses, the threshold laser powers for axial trapping decreased. This is expected due to the high intensity rays becoming nearer to the extreme of the lens resulting in larger axial trapping forces. When the beam becomes too large for the 5 mm diameter aperture of the objective lens, the trapping forces are dramatically reduced and are not large enough to overcome gravity and thermal effects, and trapping is unsuccessful.

The laser power levels of the two modes under consideration were measured non-directly. For each of the magnification systems of the beam telescope, a transmission efficiency for the microscope objective was measured. This efficiency value was different for each laser mode in each magnification system, but was typically between 10% and 30% i.e. only a fraction of the laser power measured after the fixed beam telescope was actually transmitted through the microscope objective. By measuring the transmission efficiency it was possible to infer the value of the laser power at the beam focus in the sample cell.

Beam Diameter (mm) at back aperture of 5 mm	Transmission Efficiency (%)	
	$TEM_{0,0}$ mode	LG^3_0 mode
3	42	33
4	33	13
5	28	7
6	26	-
7	22	-
10	19	-

Figure VI.j Table of transmission efficiencies for the laser modes through the objective lens, with differing beam sizes at the back aperture

As stated earlier, to directly compare the performance of the two laser modes it was necessary to convert the laser trapping powers into the efficiency factor Q_{axial}. For each of the experimental set of parameters, the trapping force was calculated using equation 6.3 and the experimental efficiency factor then deduced from equation 6.2. Before directly comparing the efficiencies of the two laser modes within the optical tweezers, it was necessary to confirm that our results with the fundamental $TEM_{0,0}$ mode complemented those of Felgner [1], thus confirming the correct operation of our experimental system. This could be done in two ways by comparing Q_{axial} at the top and at the bottom of the sample cell.

Felgner's measurements of Q_{axial} were made at the top of the sample cell at a height of 85 μm above the base of the cell. However, he also made measurements of Q_{axial} at varying depths throughout the sample cell and he showed that the axial trapping efficiency decreased by a factor of approximately 10 over a depth of 70 or 80 μm. Consequently, by reducing his measured values of Q_{axial} by a factor 10, our results at the bottom of the cell could also be assessed. The minimum power measurement at the top of the sample cell was defined to be the power at which the sphere fell out of the trap whilst being held just below the coverslip at a height of 70 μm above the base.

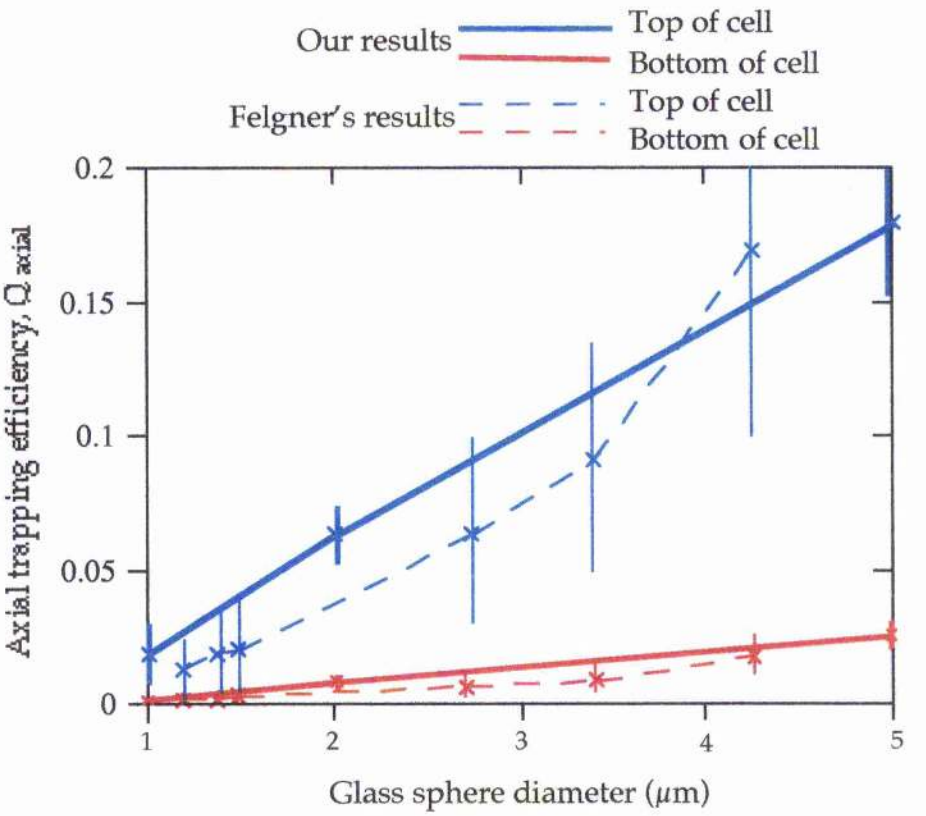

Figure VI.k Comparative plots of axial trapping efficiency with increasing sphere size at the bottom and top of a 70 μm deep sample cell using a fundamental $TEM_{0,0}$ mode

As expected, the trapping efficiency increases with increasing sphere size, due to the larger interaction area of the beam with the trapped sphere resulting in larger axial trapping forces. Our measured values of Q_{axial} at the top and at the bottom of the sample cell are in very good agreement with those of Felgner when comparing the axial trapping efficiency of a fundamental $TEM_{0,0}$ mode. It has been suggested that the decrease in trapping efficiency at the base of the cell is due to imaging aberrations caused by the increased depth of fluid, reducing the gradient forces near the focus and decreasing the trapping force. This agreement in results meant that the trapping efficiency of the LG^3_0 mode could be made with confidence and that the optical tweezers were operating correctly.

Position in the sample cell	Diameter of silica sphere (μm)	Calculated axial trapping force (pN)	Fundamental TEM $_{0,0}$		LG $^{3}_{0}$ mode	
			Minimum power (mW)	Q *axial*	Minimum power (mW)	Q *axial*
Bottom	1.0	0.014	2.62	0.001 ± 0.0001	No	trapping
	2.0	0.054	1.55	0.008 ± 0.0004	2.94	0.004 ± 0.001
	5.0	0.774	6.77	0.026 ± 0.004	4.33	0.040 ± 0.003
Top	1.0	0.014	0.16	0.020 ± 0.011	0.08	0.043 ± 0.037
	2.0	0.054	0.18	0.066 ± 0.010	0.12	0.098 ± 0.033
	5.0	0.774	0.97	0.180 ± 0.023	0.57	0.305 ± 0.068

Figure VI.1 Table of experimental results for the minimum laser powers and Q_{axial} for trapping at the base and top of the sample cell

The results for the 5 μm spheres, which are considerably larger than the focussed beam spot, show that the LG mode improves the axial trapping efficiency by approximately a factor of two. This applies to the trapping of the sphere at both the top and bottom of the sample cell. This is consistent with the doubling of the spring constant per unit power observed by Friese et al [9] when using a mode with an intensity ring. We observed little or no improvement in the trapping efficiency by increasing the order of the LG mode further (increasing the ℓ index). This is because all the modes have similar intensity distributions when optimally magnified into the objective lens.

The axial trapping of the 1 and 2 μm spheres is more complicated. At the top of the sample cell, the LG mode again gives a doubling of the axial trapping

efficiency for both sizes of sphere. However, at the base of the cell, the spheres experienced a decrease in axial trapping efficiency or a cessation of axial trapping completely. This is perhaps to be expected, as the diameter of these spheres is comparable to the focussed beam spot and more importantly, to the area of zero intensity in the middle of the LG mode. Also, the depth of the cell may introduce aberrations in the mode which would result in the mode structure not being properly maintained to trap the 1 μm spheres.

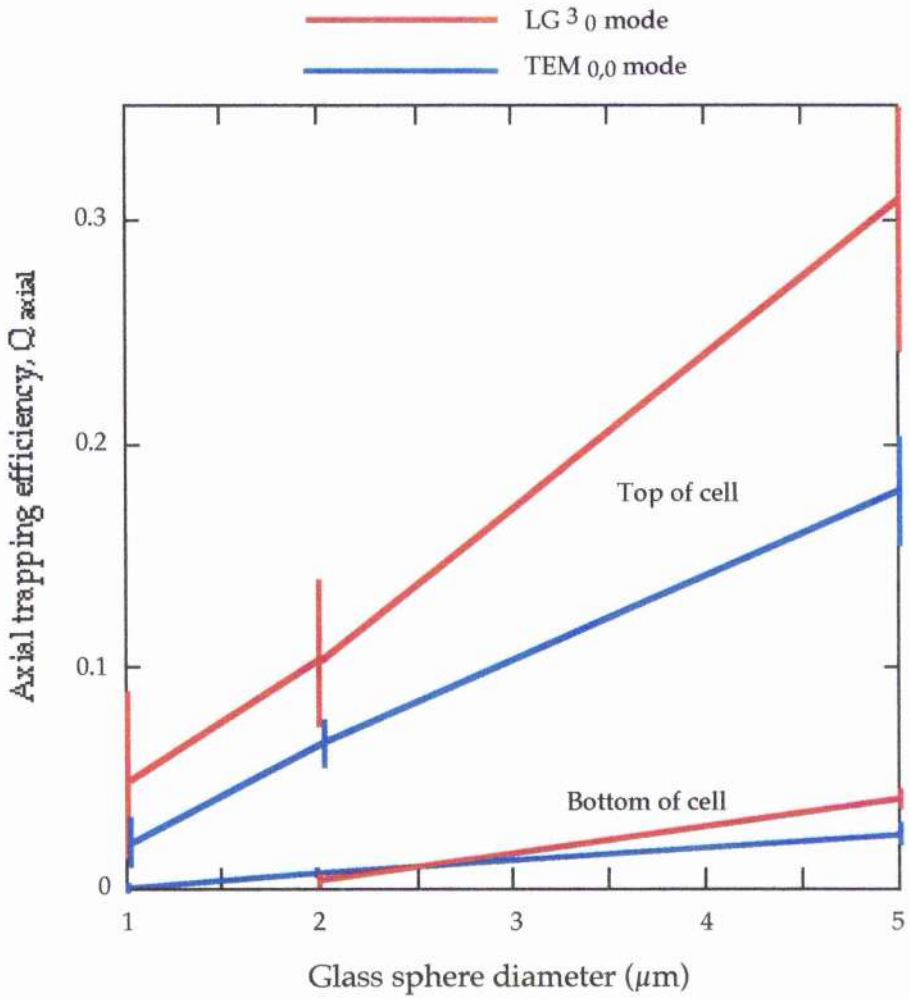

Figure VI.m The comparison of the axial trapping efficiencies using the two modes under consideration, both at the top and the bottom of the cell

In addition to the significant improvement in the axial trapping efficiency of the optical tweezers for larger particles, there was also the benefit of trapping with lower laser power levels. The 5 μm sphere could be trapped with almost half the laser power at the top and bottom of the sample cell when using the LG mode. At the top of the cell, the smaller spheres could also be trapped with a similar reduction in laser power. However, the smaller spheres at the base of the cell did not show this improvement as demonstrated by the axial trapping efficiency. The decrease in trapping laser power for particles a few micron in size, will be a welcome benefit, particularly for the fields of biology and medicine where delicate samples could be damaged by excessive laser intensity.

The quality of the microscope objective lens governs the absolute laser power levels needed due to the transmission efficiency so similar experiments were performed with a different objective lens. An Achroplan, x100 magnification, 1.25 NA oil immersion microscope objective lens from Zeiss was used, and similar improvements in the axial trapping efficiency and decreasing of the laser powers were observed.

VI. 6 Conclusions

This Chapter presented details of the experimental arrangement that was constructed and used for the operation of the optical tweezers. As well as detailing the components that make up the tweezers, the Chapter also stated what can be expected to be achieved with the tweezers. This included the typical particle sizes that can be expected to be manipulated, typical laser power levels and what the typical drag speeds might be for translating a trapped particle through the suspending media.

The first part of the work on improving optical tweezers was the numerical modelling of the axial trapping forces within optical tweezers when used with LG modes. For an 8 μm diameter silica sphere suspended in water, it was found that the high order LG modes of the type $p = 0$ and $\ell \neq 0$, would produce an axial trapping force per unit laser power up to four times greater than when using a fundamental $TEM_{0,0}$ mode. By using LG modes, optical trapping is predicted to occur at much lower laser powers and also when

using lower NA objective lenses. These benefits may assist in the tweezing of delicate biological particles by reducing the risk of the optical destruction of the sample, or their opticution [11].

I wish to acknowledge the assistance and advice from Brett Patterson and Johannes Courtial with the writing of the computer programs to perform the modelling. The results of the modelling of the on-axis trapping forces within optical tweezers were presented at the *QE12* Conference in Southampton, UK [12].

The second, experimental part of the work studying the improvement of trapping forces and observing the trapping of spheres within optical tweezers was carried out by myself, with help from a summer student (David McGloin). By comparing the performance of a fundamental $TEM_{0,0}$ mode and a high order ℓ=3 LG laser mode, it was confirmed that the LG mode resulted in an improved axial trapping efficiency within the tweezers. For an ℓ=3 LG mode, the Q_{axial} trapping efficiency factor was doubled for a 5 μm silica sphere, both at the top and bottom of the sample cell. There was a similar improvement for smaller spheres at the top of the cell, but at the bottom of the cell, there was zero trapping or very poor trapping.

The fourfold improvement in the trapping efficiency predicted by the modelling work was not experimentally obtained, as the spheres used were not Mie particles. Therefore, the improvement was less marked but is expected to be seen if the experimental parameters were changed appropriately to the Mie regime.

In addition, the trapping of spheres using a high order LG mode had the consequence of creating an optical trap using lower laser powers. Typically, the LG mode required only half of the laser power usually needed when operating optical tweezers with the fundamental $TEM_{0,0}$ mode. This will be most beneficial where laser powers are an important consideration, which is most likely to be in the fields of biotechnology where the successful manipulation and control of living cells and bacteria without optical damage is crucial.

This most recent work, experimentally demonstrating the increased trapping efficiency of optical tweezers with high order LG modes was presented at *CLEO '97* in Baltimore, USA [13]. This work has also been recently accepted for publication in the *Journal of Modern Optics* [14].

References

1. Felgner, H., O. Müller, and M. Schliwa, *Calibration of light forces in optical tweezers.* Appl. Opt., 1995. **34**: p. 977-983.

2. Simpson, N.B., L. Allen, and M.J. Padgett, *Optical tweezers and optical spanners with Laguerre-Gaussian modes.* J. of Mod. Opt., 1996. **43**: p. 2485-2491.

3. Padgett, M.J. and L. Allen, *The Poynting vector in Laguerre-Gaussian laser modes.* Opt. Comm., 1995. **121**: p. 36-40.

4. Barton, J.P., D.R. Alexander, and S.A. Schaub, *Internal and near-surface electromagnetic fields for a spherical particle irradiated by a focused laser beam.* J. Appl. Phys., 1988. **64**: p. 1632-1639.

5. Gussgard, R., T. Lindmo, and I. Brevik, *Calculation of the trapping force in a strongly focused laser beam.* J. Opt. Soc. Am. B, 1992. **9**: p. 1922-1930.

6. Barton, J.P. and D.R. Alexander, *Fifth-order corrected electromagnetic field components for a fundamental Gaussian beam.* J. Appl. Phys., 1989. **66**: p. 2800-2802.

7. Ashkin, A., *Forces of a single-beam gradient laser trap on a dielectric sphere in the ray optics regime.* Biophys. J., 1992. **61**: p. 569-582.

8. Sato, S., M. Ishigure, and H. Inaba, *Optical trapping and rotational manipulation of microscopic particles and biological cells using higher-order mode Nd:YAG laser beams.* Electron. Lett., 1991. **27**: p. 1831-1832.

9. Friese, M.E.J., H. Rubinsztein-Dunlop, N.R. Heckenberg, and E.W. Dearden, *Determination of the force constant of a single-beam gradient trap by measurement of backscattered light.* Appl. Opt., 1996. **35**: p. 7112-7116.

10. Microspheres, Bangs Laboratories, Inc., 9025 Technology Drive, Fishers, IN 46038-2886.

11. Block, S.M., *Optical Tweezers: A New Tool for Biophysics,* in *Non Invasive Techniques in Cell Biology,* J.K. Foskett and S. Grinstein, Editor^Editors. 1990, A Wiley & Sons, Inc.: p. 375-402.

12. Simpson, N.B. and M.J. Padgett. *Calculation of the trapping forces in an optical tweezers using a Laguerre-Gaussian laser mode.* in *National Quantum Electronics Conference - QE12.* September 1995. poster P2-34, Southampton, UK.

13. Simpson, N.B., L. Allen, and M.J. Padgett. *Optical tweezers with increased trapping efficiency.* in *XVII Conference on Lasers and Electro-Optics - CLEO '97.* May 1997. Paper no CTuD7, Baltimore, USA.

14. Simpson, N.B., D. McGloin, K. Dholakia, L. Allen, and M.J. Padgett, *Optical tweezers with increased axial trapping efficiency.* Accepted by *J. of Mod. Opt.,* January 1998.

Chapter VII

Optical Spanners

Contents

VII. 1 Aim of the experiments

The work described in this final experimental Chapter concerns the main objective of this research project. It again combines optical tweezers technology with Laguerre-Gaussian laser modes, by transferring orbital angular momentum from the LG mode to a trapped particle in the optical tweezers, it was possible to cause a rotation of the particle whilst being held by the tweezers. This phenomenon was dubbed "optical spanners" due to the applied torque causing a rotation, as if being acted upon by a mechanical spanner or wrench.

Firstly, an explanation of the spanners' theory will be given, i.e. how they work and the principle behind their operation. This will be followed by a short description of the experimental arrangement required for the observation of optical spanners.

The experimental results and measurements associated with optical spanners can be broken down into three sections. The first was a continuation of the computer modelling carried out in Chapter VI, which initially investigated the axial trapping forces of optical tweezers. The

extension was to allow each photon to carry $\ell\hbar$ of orbital angular momentum. By modelling the absorption of photons, the angular acceleration of the trapped particle can be predicted. This manifests itself in a rotation of the particle.

The next stage was to experimentally observe this rotation of a trapped particle - the optical spanners. The details of these observations have been given here, along with the expected rotations and angular velocities for different particles and laser power levels.

Finally, an experiment was performed that used the newly developed optical spanners as a tool to investigate a beam property of the LG modes. As the spin angular momentum of light is well defined as $\pm\hbar$, this was used as a reference to compare the $\ell\hbar$ per photon of the orbital angular momentum content of a LG^1_0 mode i.e. $\hbar$ per photon. By causing the rotation of a trapped particle in the optical spanners using orbital angular momentum, a direct, mechanical cancellation of the rotational effect could be obtained by applying the correct handedness spin angular momentum. This experimental work demonstrated the mechanical equivalence of the spin and orbital angular momentum of light, using optical spanners.

Hence, by introducing Laguerre-Gaussian laser modes into optical tweezers, not only is the performance vastly improved by an increased axial trapping efficiency and lower laser power levels (Chapter VI), but they can impart orbital angular momentum to the trapped particle causing a rotation. This is the birth of a tool called the "optical spanner" which has been developed here at St. Andrews during my PhD work.

VII. 2 What are "Optical Spanners"?

The optical spanners are an amalgam of two established fields. The first is that of optical tweezers which has been described in some details in Chapter III, and secondly that of Laguerre-Gaussian laser beams which has been dealt with in Chapter II. It is the combination of these that produces the novel optical spanner.

A micron-sized particle is trapped by optical tweezers as before. In this case, the trapping beam is an LG mode, which produces the increased axial efficiency trap as studied in Chapter VI. However, these particular laser modes, of $p = 0$ and $\ell \neq 0$, have an orbital angular momentum term in addition to that associated with the polarisation state (the spin angular momentum). This extra content is well defined as $\ell\hbar$ per photon, where ℓ is the azimuthal index of the LG mode [1].

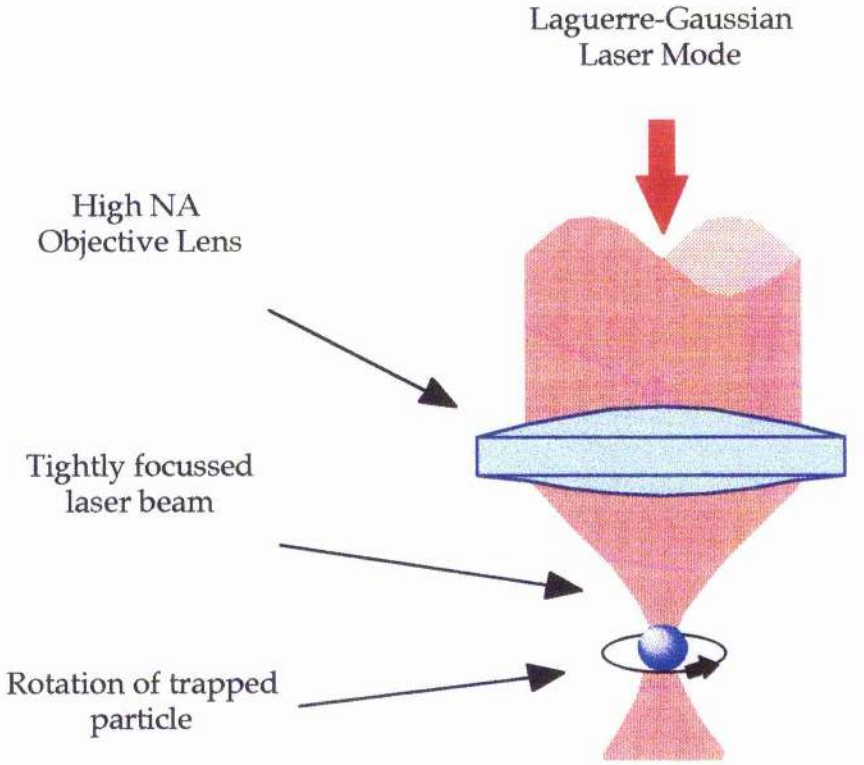

Figure VII.a The principle of optical spanners

Due to the absorption of photons by the particle, there is an angular momentum transfer from the trapping laser beam to the trapped particle. This concept was first proposed by Miles Padgett and Les Allen at a Rank Prize Symposium and reported by Amos and Gill [2]. This imparted angular momentum results in a torque on the particle and hence an angular acceleration. A terminal angular velocity, due to viscous drag, is reached which can be a few radians per second. This rotational effect on the particle converts the standard optical tweezers into an optical spanner or wrench.

The amount of orbital angular momentum available for transfer to the particle can be altered by changing the LG mode, or more specifically, changing the azimuthal index ℓ of the mode. The larger ℓ modes will result in more orbital angular momentum transfer and consequently a larger torque and angular acceleration. The final angular velocity depends critically on the particle properties (such as the absorption coefficient) and the supporting medium (for viscous forces).

Apart from demonstrating the principle of the transfer of angular momentum from a light beam to a trapped particle, the optical spanners can also be used to manipulate and rotate particles at will. In a biological application, it may be required to lift, rotate and then put down a sample cell or bacteria to accomplish some task or manoeuvre. This can be thought of as a simple jigsaw analogy: it may be necessary to move an object to a certain position but to allow it to fit it must be rotated, as you would a piece in a jigsaw. The optical spanners have the ability to be able to do just that.

VII. 3 Modelling the angular accelerations and rotations

This was an extension to the computer modelling that was described in section VI. 4 earlier in the thesis. Using the same basis of the modelling program, it was possible to assign $\ell\hbar$ of orbital angular momentum to each photon and define an absorption coefficient for the sphere being trapped. In this way, the torque acting upon the sphere due to the orbital angular momentum transfer was calculated. The angular acceleration was also deduced along with the limiting or terminal angular velocity of the sphere as it rotated. The model was thus used to predict angular accelerations and limiting angular velocities for a silica sphere suspended in water, which was acted upon by optical spanners. The results were published, along with the earlier modelling results, in the *Journal of Modern Optics* in December 1996 [3].

VII. 3. 1 Modelling the transfer of orbital angular momentum

When using a high order LG mode with $\ell \neq 0$, there must be a transfer of the angular momentum to the trapped particle due to partial absorption. If the partial absorption is small, the LG mode is transmitted through the sphere undistorted and retains its mode characteristics. The amount of orbital angular momentum transferred from the beam to the particle is simply calculated by multiplying the momentum content in the beam, $\ell\hbar$ per photon, by the number of photons that were absorbed by the particle. See Appendix III for details of the programs written for the modelling.

The resultant torque on the sphere τ, was calculated for different sphere positions along the beam axis using a laser power of 1 mW. The sphere's position along the beam axis was changed so that the region of strongest absorption, and hence rotation, was found, which was expected to be at the beam focus due to the full interaction of the beam with the particle at this point. The angular acceleration A, was simply calculated from,

$$A = \frac{\tau}{I} \tag{7.1}$$

where I is the moment of inertia of the sphere about the beam axis,

$$I = Mass \cdot \left(\frac{2}{5} \cdot r^2\right) = \left(\frac{4}{3} \cdot \pi \cdot r^3 \cdot \rho\right) \cdot \left(\frac{2}{5} \cdot r^2\right) = \frac{8}{15} \cdot \pi \cdot \rho \cdot r^5. \tag{7.2}$$

and r is the radius of the sphere and ρ is the sphere's density. It was more useful to investigate the terminal (or limiting) angular velocities per mW of laser power of the sphere in the optical spanners, rather than the angular accelerations it would experience. This limiting velocity ω_{lim} is governed by the viscosity η of the supporting medium in the sample cell [4], and was calculated from

$$\omega_{lim} = \frac{\tau}{8 \cdot \pi \cdot \eta \cdot r^3}. \tag{7.3}$$

It is important to note here the dependence of the moment of inertia and the limiting angular velocity on the radius of the sphere. If, for example, the optical spanners were used on a particle whose radius was 1 mm instead of 1 μm i.e. a factor of 1000 larger, the increase in laser power to achieve the same angular acceleration is phenomenal. The moment of inertia of the sphere would increase by a factor of 10^{15}, and to maintain the same limiting angular velocity, the laser power would have to increase from milliWatts to MegaWatts, an increase by 10^9 in laser power. This demonstrates why the optical spanners would not be able to operate successfully on particles that are much larger than a few 10's of microns in size, due to large laser powers that would be required.

VII. 3. 2 Modelling results

The same silica sphere of diameter 8 μm suspended in water, as that used in the earlier modelling in section VI. 4 was considered in this modelling extension. The trapping wavelength was 532 nm, thus the sphere could be considered as a Mie particle. The LG mode with $\ell = 0$ (fundamental $TEM_{0,0}$) possesses no orbital angular momentum and consequently cannot be used as optical spanners. An LG mode with $p = 0$ and $\ell = 4$ was used in the modelling as this was experimentally possible to reproduce and would also provide $4\hbar$ of orbital angular momentum per photon.

Two different materials for the sphere were considered. The first was simply a standard fused silica sphere which had an absorption coefficient α, of 0.2 m^{-1}. The second sphere had a larger absorption at the wavelength being considered, $\alpha = 5700$ m^{-1}, which was typical for an absorbing Schott glass (such as BG3).

As figure VII.b shows, the fused silica sphere ($\alpha = 0.2$ m^{-1}) can be expected to have a limiting angular velocity of only 7×10^{-7} rad s^{-1} mW^{-1}, which will not be observable at all. However, for the absorbing glass with $\alpha = 5700$ m^{-1}, the limiting angular velocity is predicted to have a value of around 0.02 rad s^{-1} mW^{-1}. This magnitude of rotation, which is equivalent to 3 mHz mW^{-1}, should be observable making the optical spanners a viable tool. The modelling considered the rotation of a sphere with 1 mW of laser

power, so if a laser mode was used with higher powers the expected rotation would be increased.

As expected the region that experiences the largest angular acceleration, and hence achieves the largest angular velocity, is a region along the beam axis around the focus of the same length as the sphere's diameter. When the centre of the sphere lies outside this region, the rotational effect diminishes very quickly.

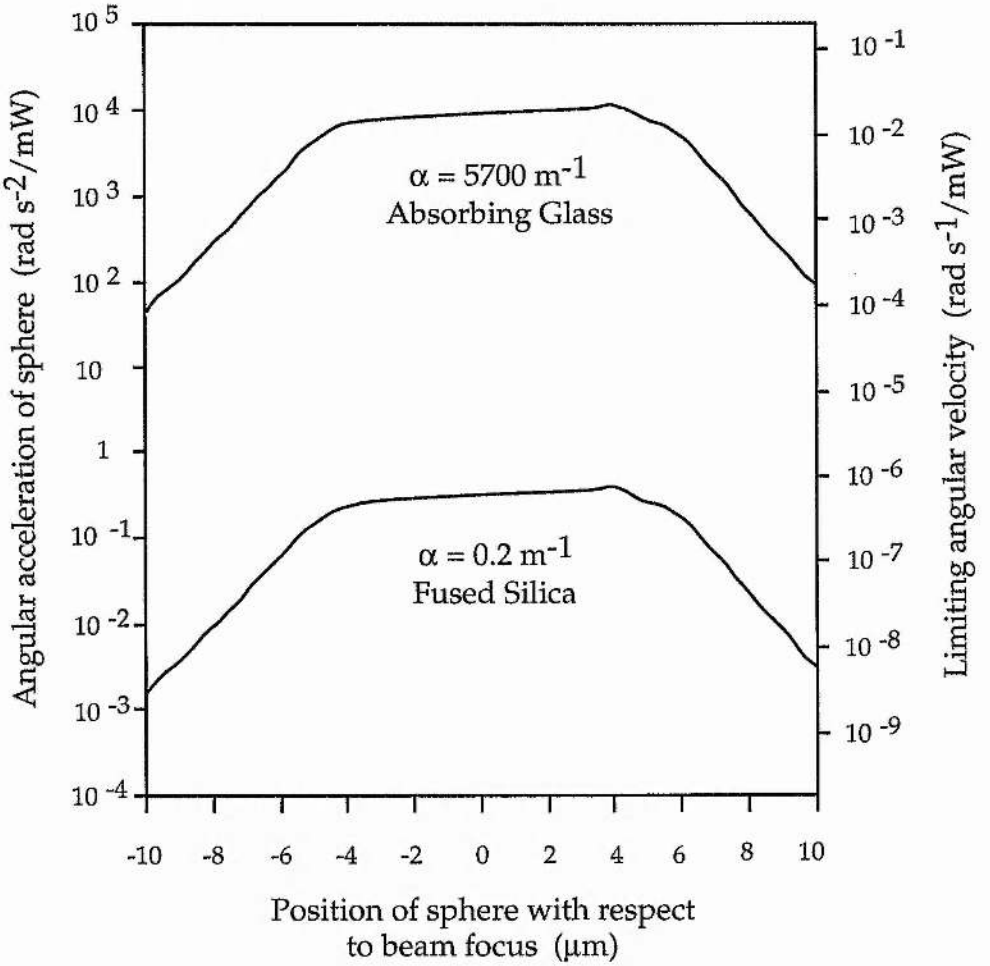

Figure VII.b The predicted angular acceleration and limiting angular velocity of an 8 μm sphere trapped with a LG $^{4}_{0}$ mode

As the torque on the sphere is proportional to the orbital angular momentum and consequently ℓ, then the resulting angular acceleration and terminal velocity are also, to a good approximation, proportional to ℓ. Therefore, the higher the mode that could be used in the optical spanners, the higher the ℓ index and consequently the larger the terminal velocity of the rotating sphere.

It is worth mentioning the absorption coefficient here. If the absorption by the sphere is too large, then the transfer of orbital angular momentum will take place but due to the lack of transmission of the rays, there will be no tweezers effect to trap the sphere. Conversely, if the absorption is very small, there will be no rotation of the sphere but the optical trap will still be improved due to the absence of the on-axis rays..

VII. 4 Experimental set-up

The details of the experimental apparatus and their arrangement do not require to be covered again as the same system was used as that described in section VI. 2 of this thesis for the operation of the improved optical tweezers. Using this set-up, an LG mode was produced and using the beam telescope, the beam size was altered so that it filled the back aperture of the microscope objective lens to give optimum axial trapping.

There was one addition to the arrangement, which was the insertion of a coloured glass filter in front of the CCD array/camera (figure VII.c). This was a piece of Schott BG38 glass which absorbed the reflected infra-red laser light, so that the image viewed on the monitor was of the trapped particle without any of the trapping laser light. This enabled the particle to be viewed without the laser light obscuring the image.

The observation of the trapping and rotation of the particle was performed by means of a monitor and video recorder as before. If the glass filter was removed, the rotation of the particle could actually be seen more easily, due to the rotation of the image of the scattered laser light.

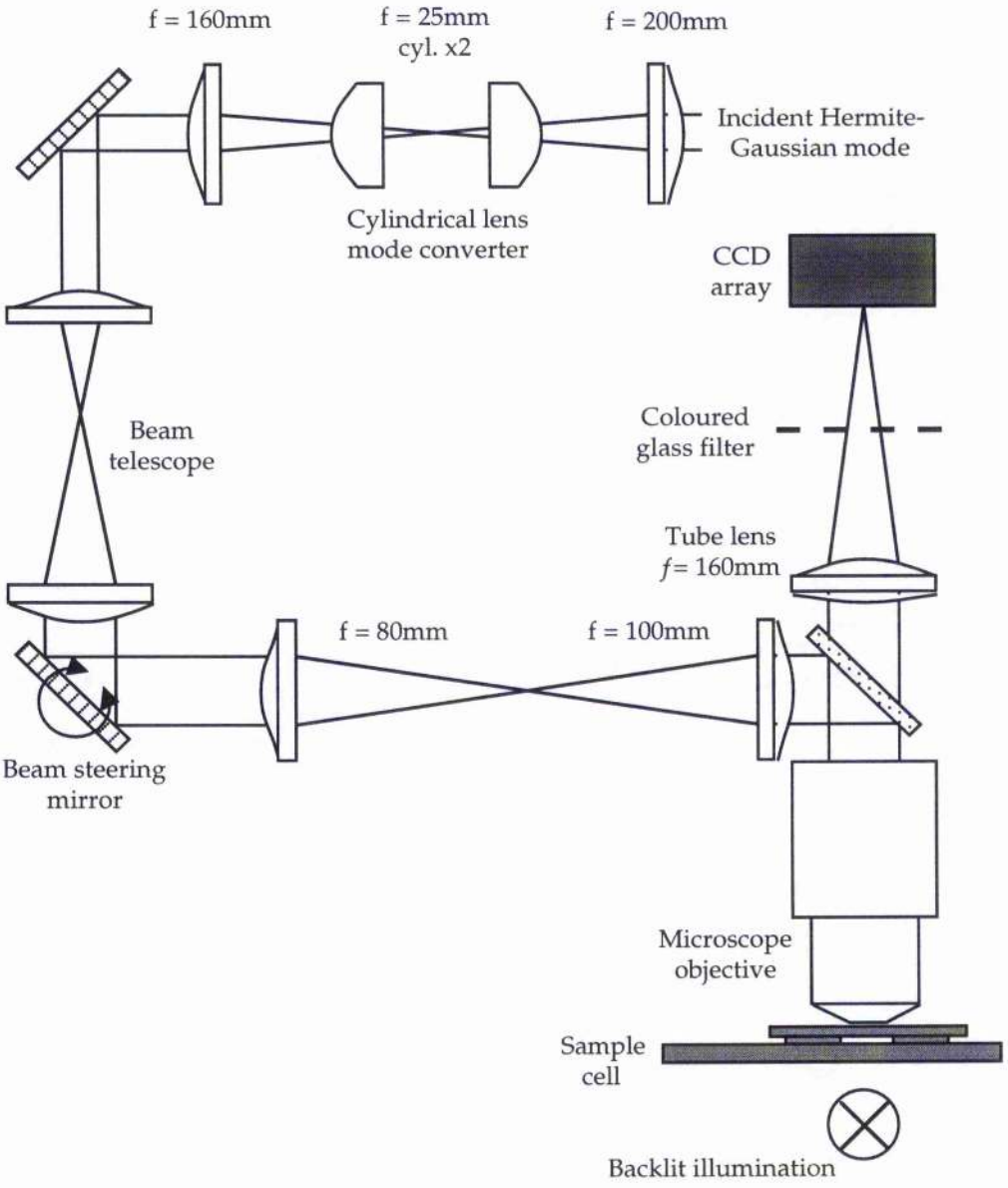

Figure VII.c Schematic diagram of the optical spanners

VII. 5 Observation of optical spanners

VII. 5. 1 Experimental observation of the rotation of particles

By using the spanners arrangement described earlier, with the trapping laser operating at a wavelength of 1047 nm and a power of approximately 15 mW the first experimental evidence of the optical spanners was obtained. The chosen mode was a LG^2_0 mode which possessed $2\hbar$ of orbital angular momentum per photon.

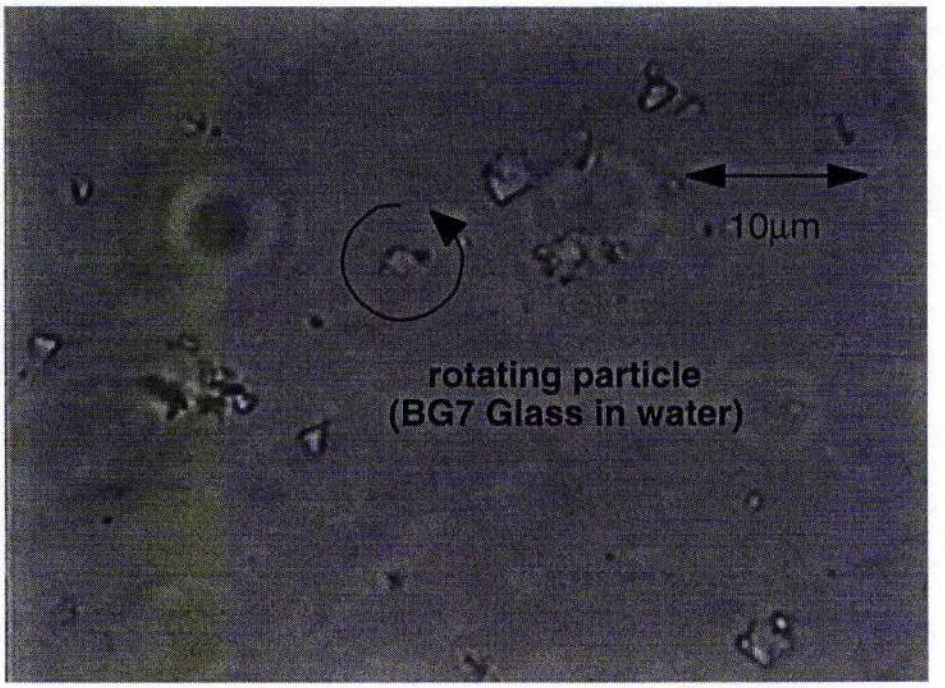

Figure VII.d Video frame showing a 4 μm fragment of glass suspended in water, which is being translated and rotated by the optical spanners, with the filter in to block the reflected trapping laser light

The first particles that were studied were fragments of glass known to be absorbing at the trapping wavelength, such as the Schott glasses BG7 and BG38. They were put in water and usually sank to the bottom of the sample

cell. By the principle of z-trapping of optical tweezers, the particles were lifted slightly off the bottom of the cell so that there were no frictional forces acting between the particle and the cell base. The principle of the optical spanners then took over and the particle began to rotate due to the transfer of the orbital angular momentum. This motion could not be related to Beth's early work of rotation with circularly polarised light, as the LG mode was linearly polarised. The effect that we observed was due entirely to the transfer of orbital angular momentum.

Rotations of up to a few Hertz were possible, but it depended on the size of the particle. The smallest particle that underwent rotation was about 2 μm in size, whilst the largest was about 15 μm in size. It is difficult to show such experimental evidence on paper, but figure VII.d shows a video frame of a glass particle 4 microns in size, that is being rotated by the spanners. A filter in front of the camera is blocking the trapping laser so that the particles can be clearly seen.

Different particles were tested later on into the work. One such material used was Teflon. Spheres of one micron in diameter were put into a solution of ethanol and they were observed to clump together in groups of up to 10 spheres. It was found that it was possible to use the optical spanners on such clumps using the same laser parameters as used for figure VII.d. As long as the clump kept the same orientation about the beam axis, the transfer of orbital angular momentum was uniform and a rotation was observed.

The video frame shown in figure VII.e demonstrates the other viewing technique for the spanners. In this case, the filter is not present in front of the imaging array and the reflected trapping laser light can easily be seen as light 'spokes' coming from the particle group, while nearly all resolution of the particles is lost. The infra-red laser light appears as white light on the monitor. As the clump rotated, the light spokes rotated and this was very clearly seen on the monitor screen. Using this technique, the rotational effects could be observed much more easily than trying to observe the actual particles rotating.

Figure VII.e Group of 10 Teflon micro-spheres in ethanol rotated by optical spanners with ℓ = 2 and 15 mW of laser power, with no filter so as to observe the reflected laser light 'spokes'

The experimentally observed angular velocities of up to a Hertz, compared very well with those predicted by the modelling. Unfortunately, direct comparison could not be made as the experimental particles were not spherical, but rotations of the correct order of magnitude were seen (up to 1 Hz) with approximately the laser power levels predicted (~ 15 mW).

The optical spanners had successfully been demonstrated and the transfer of orbital angular momentum from a high order LG mode to a trapped particle had been shown to be possible, as predicted.

VII. 5. 2 Experimental control of the rotation

There were three aspects of the rotation that had some degree of control. These could be changed experimentally, thus giving control over the rotation of the particle in the optical spanners.

- The first choice for the rotation is the direction, i.e. the handedness, either clockwise or anti-clockwise rotation of the particle. This can be chosen by altering the sign of the azimuthal index ℓ of the LG mode being used in the optical spanners. Depending on the orientation of the cylindrical lens mode converter compared to the input Hermite-Gaussian mode, either a +ve or -ve ℓ index will be produced. It is this index that will control the spiralling nature of the Poynting vector of the LG mode and hence the orbital angular momentum's handedness. Upon the transfer of this momentum, the particle experiences a rotation according to the initial handedness of the LG mode, governed by the ℓ index.

- Secondly, there is the actual magnitude of the angular velocity that can be changed. There are many factors that can change the rotation speed of the particle, as the limiting angular velocity is proportional to the applied torque (equation 7.3). To increase the torque, a higher absorption of photons by the particle could be introduced. Similarly, by increasing the ℓ index of the LG mode, more orbital angular momentum becomes available for transfer to the particle. Decreasing the viscosity of the supporting medium in the sample cell would also increase the terminal velocity.

Obviously, by increasing the laser power within the optical spanners, there would be more photons for the particle to absorb and transfer angular momentum. However, large powers are generally to be avoided, particularly in biological applications due to the risk of optical damage. If this damage was not a consideration, then higher laser powers is an obvious method of increasing the torque on the trapped particle.

- To give complete control over the rotation of the particle in the optical spanners, apart from the speed and direction of the rotation, it is

desirable to be able to start and stop the rotation at will. There are two methods of achieving this.

The first very crude method is to simply to block off the trapping laser beam. However, not only does this stop the rotation, but also the optical trap is lost and the particle is free to move of its own accord around the cell. It is not then possible to re-trap and begin rotation of the particle again, very easily. This is a convenient method of terminating the rotation and the optical trap but this is not usually a desirable situation.

The second method of controlling the start/stop behaviour of the particle is limited in some ways, but is convenient and operational. By investigating this technique, a fundamental question was also tackled, which went some way to experimentally prove that the orbital angular momentum content of the LG modes is indeed $\ell\hbar$ per photon, as predicted [1]. Not only was this line of research providing an operational benefit to the optical spanners, but also to study the interaction of spin and orbital angular momentum of light with particles. This work will be covered in the next section of this Chapter.

VII. 6 Equivalence of the spin and orbital angular momentum of light

VII. 6. 1 Transfer of angular momentum from light to matter

Angular momentum can be added to a light beam in two ways. Firstly, spin angular momentum (SAM) can be added using a birefringent optical component, such as a quarter-wave plate, which will cause the light beam to change its polarisation state and become circularly polarised or linearly polarised depending on its original polarisation. Orbital angular momentum (OAM) can also be added to a light beam, but by using an astigmatic component, one that has an azimuthal dependence of its optical thickness. An example of such a component is a cylindrical lens or a spiral phase plate, hence the orbital angular momentum present in a LG mode.

The transfer of angular momentum from a light beam to matter can be performed in the same ways. SAM is transferred using birefringence and

OAM by astigmatism. However, the transfer of angular momentum for both types can be transferred using the absorption of the material. It is this method of angular momentum transfer that was used in this particular experiment with the optical spanners, i.e. the ability to absorb both types of angular momentum in matter from a light beam.

VII. 6. 2 Is the orbital angular momentum of an LG laser mode $\ell\hbar$ per photon ?

Apart from demonstrating the operation of optical spanners, our principle motivation was also to investigate the quantised nature of the OAM. Using a linearly polarised $\ell = 1$ LG mode in the optical spanners, a rotation of a trapped particle was expected due to the transfer of OAM from the laser mode. By changing the polarisation state of the laser mode to circularly polarised, i.e. adding SAM, the laser mode then possessed $\hbar$ of OAM and $\pm\hbar$ of SAM, depending on the handedness.

The experiment set out to prove that the two angular momentum types were mechanically equivalent, in that they both combined to give a total angular momentum content per photon. For the two momentum types to interact in this way, the dominant mechanism has to be absorption as astigmatism and birefringence are selective for one type only. Depending on the handedness of the circularly polarised light, the total angular momentum per photon would be either $2\hbar$ or $0\hbar$, and experimentally, this should be visible in a doubling of the rotation speed or a stationary particle.

This doubling or complete cancellation of the angular momentum would provide some experimental evidence that the OAM content of a LG mode is indeed well defined and corresponds to $\ell\hbar$ per photon. In addition, this would create a reliable method of starting and stopping the rotation of a trapped particle as discussed in section VII. 5. 2. This method of stop/start would not destroy the optical trap and the particle would remain trapped at all times, which is a necessary requirement for future applications of optical spanners.

VII. 6. 3 Experimental details

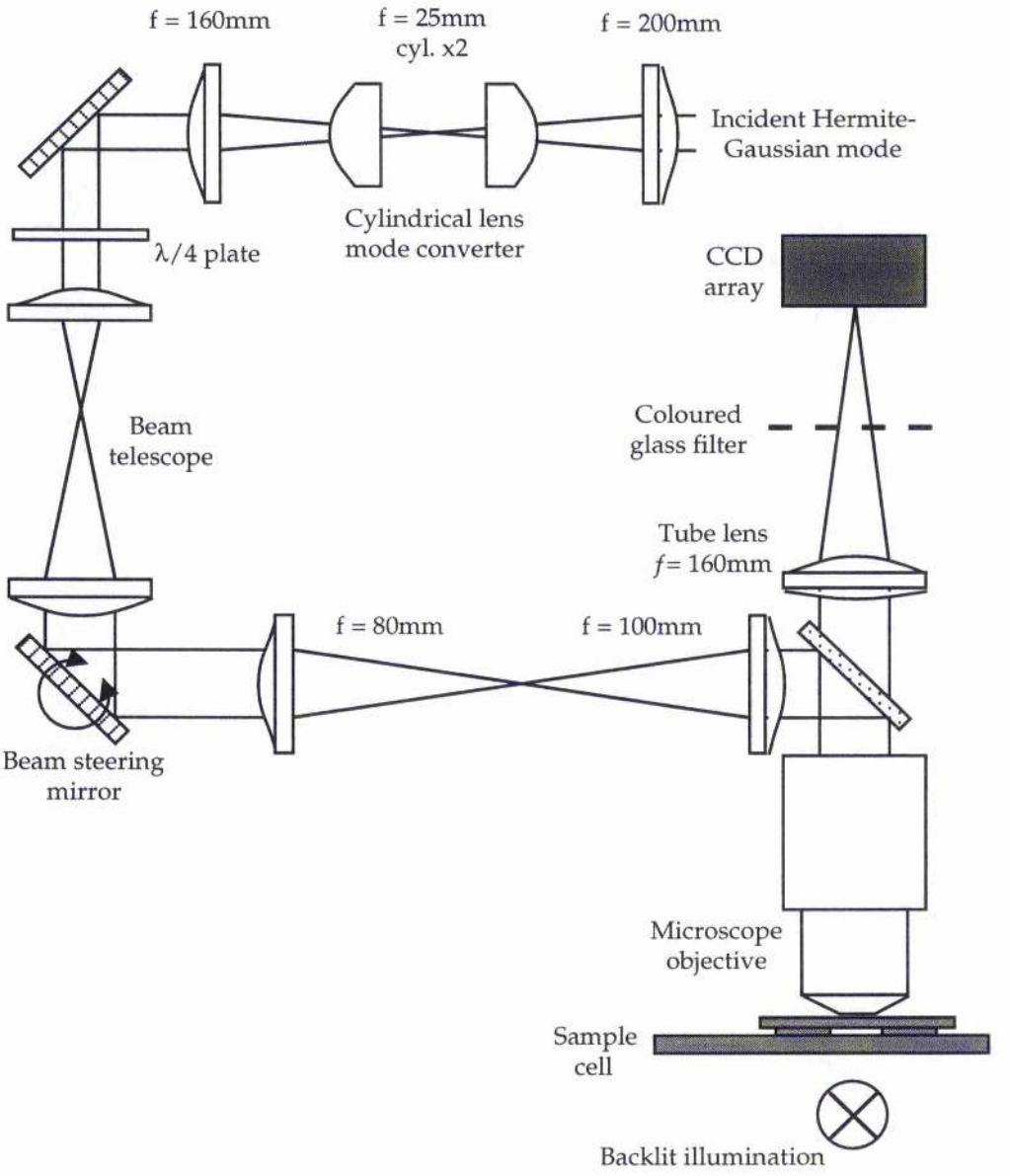

Figure VII.f Experimental configuration for observing the cancellation and doubling of the rotation of a particle trapped in the optical spanners

The experimental arrangement used to perform this work was the basic optical spanners set-up that was described in section VII. 3. There was one addition to the set-up, the inclusion of a quarter-wave plate before the beam

telescopes to control the polarisation state of the laser beam (the SAM content of the beam). The polarisation state of the beam in the plane of the trapped particle after the objective lens, was confirmed by monitoring the laser power transmitted through a linear polariser at various orientations.

The optical spanner was used to hold and rotate Teflon spheres of diameter 2 μm, with the laser operating in an $\ell = 1$ LG mode at a power of 20 mW. The spheres were suspended in a solution of ethanol, chosen for its optimum density, refractive index and viscosity. Strong z-trapping forces enabled the particles to be lifted off the bottom of the sample cell to allow the particle to rotate more freely.

By rotating the λ/4 plate, it was possible to quickly change between linearly and circularly polarised light. In this way, the SAM and OAM could add or subtract depending on their relative signs resulting in the stop/start behaviour of the rotating particle.

However, this explanation is actually a simplified version of the mechanism according to Steve Barnett [5]. The expression for the total angular momentum per photon, AM, of the LG^{ℓ}_{p} beam in the paraxial approximation, is found to be, from a rigorous solution of Maxwell's equations [5],

$$AM = \left[\ell + \sigma + \sigma \left(\frac{2 \cdot k \cdot Z_r}{2p + \ell + 1} + 1 \right)^{-1} \right] \hbar \tag{7.4}$$

where σ is equal to 0, ±1 for linearly and circularly polarised light respectively, k is the wave number and Z_r is the Rayleigh range of the light. Note that expression 7.4 is actually dependent on the Rayleigh range of the beam. It is physically unclear how the angular momentum of the beam can relate to the Rayleigh range and consequently, this explanation of the angular momentum content is not dealt with in any depth here.

For the $\ell = 1, p = 0$ LG mode in our experiments, expression 7.4 becomes

$$AM = [1 + \sigma + 0.06 \cdot \sigma] \hbar. \tag{7.5}$$

For the linear polarised $\ell = 1$ LG mode ($\sigma = 0$), the total angular momentum per photon is simply $\hbar$, which is entirely due to the OAM only. When σ is equal to +1 for one handedness of the circularly polarised light, the SAM adds to the OAM and the total angular momentum per photon is 2.06 $\hbar$. Similarly for the other handedness of circularly polarised light, the spin and orbital terms are subtractive and the total angular momentum per photon is 0.06 $\hbar$.

If we were to account for this more comprehensive mechanism in our experiment, the slight deviances from the simplistic understanding will actually be unobservable anyway, due to their small magnitude. The experimental observations were expected to be as predicted in the simple model.

VII. 6. 4 Experimental results

The $\ell = 1$ LG mode was focussed by the objective lens to a beam waist approximately 0.8 μm in diameter, which for this particular mode represents a high intensity ring 1.1 μm in diameter. Micron-sized Teflon spheres in an ethanol solution were trapped, lifted and rotated by the optical spanners. Single spheres were used, but it was found that amalgamated groups of Teflon spheres also interacted uniformly with the whole beam and rotated smoothly with a constant angular velocity. The larger the particles being rotated, the easier it was to observe the rotational changes.

For the linearly polarised $\ell = 1$ LG mode with a laser power of ~20 mW, Teflon particles were rotated with speeds of ~1 Hz. By considering equation 7.3 for the limiting angular velocity once more, the observed rotation speed implies that there is approximately 2% absorption of the laser light by the Teflon particle.

Figure VII.g shows successive video frames of a 2 μm Teflon particle held in the optical spanners with the $\ell = 1$ LG mode in the three different polarisation states. The images were taken with the glass filter in place blocking out the stray reflections of the laser light. The non-spherical shape of the particle aids the observation of the particle rotation. A line has been

drawn on the particles in the frames to assist in determining the orientation of the particle.

Once the particle was smoothly rotating in the optical spanners, more than 80% of cases would speed up or completely stop when the quarter-wave plate was rotated, changing the polarisation state of the trapping laser beam. In the remainder of the cases, the particles would speed up and slow down with the change in SAM, but would fail to stop rotating completely. This was due to the more irregular nature of these particles, which resulted in some mode transformation upon propagation through the particle. This transformation possibly gave an additional transfer of OAM resulting in an imperfect cancellation of rotation.

Similarly, when the spin and orbital components are added to double the rotation speed, only a few cases are actually observed to double in their angular velocity. This has been attributed to an experimental nonlinear relationship between the applied torque from the angular momentum transfer, the limiting angular velocity and the presence of particle asymmetry. This was experimentally confirmed by changing the laser power and keeping all other beam parameters constant. By doubling the laser power and the applied torque, it did not necessarily double the speed of rotation.

Also, by reversing the sense of the cylindrical lens mode converter, the ℓ index of the resulting LG mode can change its sign. This will cause a reversal in the rotational direction of the particle in the optical spanners when using a linearly polarised LG mode. This was observed, in good agreement with our interpretation of the mechanisms involved in the optical spanners. Similarly, by using a LG^0_0 mode (a fundamental $TEM_{0,0}$ mode), the particles could be rotated using a circularly polarised laser beam only. By changing the handedness of the circular polarisation, the particle could be rotated in either direction, which confirms the effect of the SAM alone as expected.

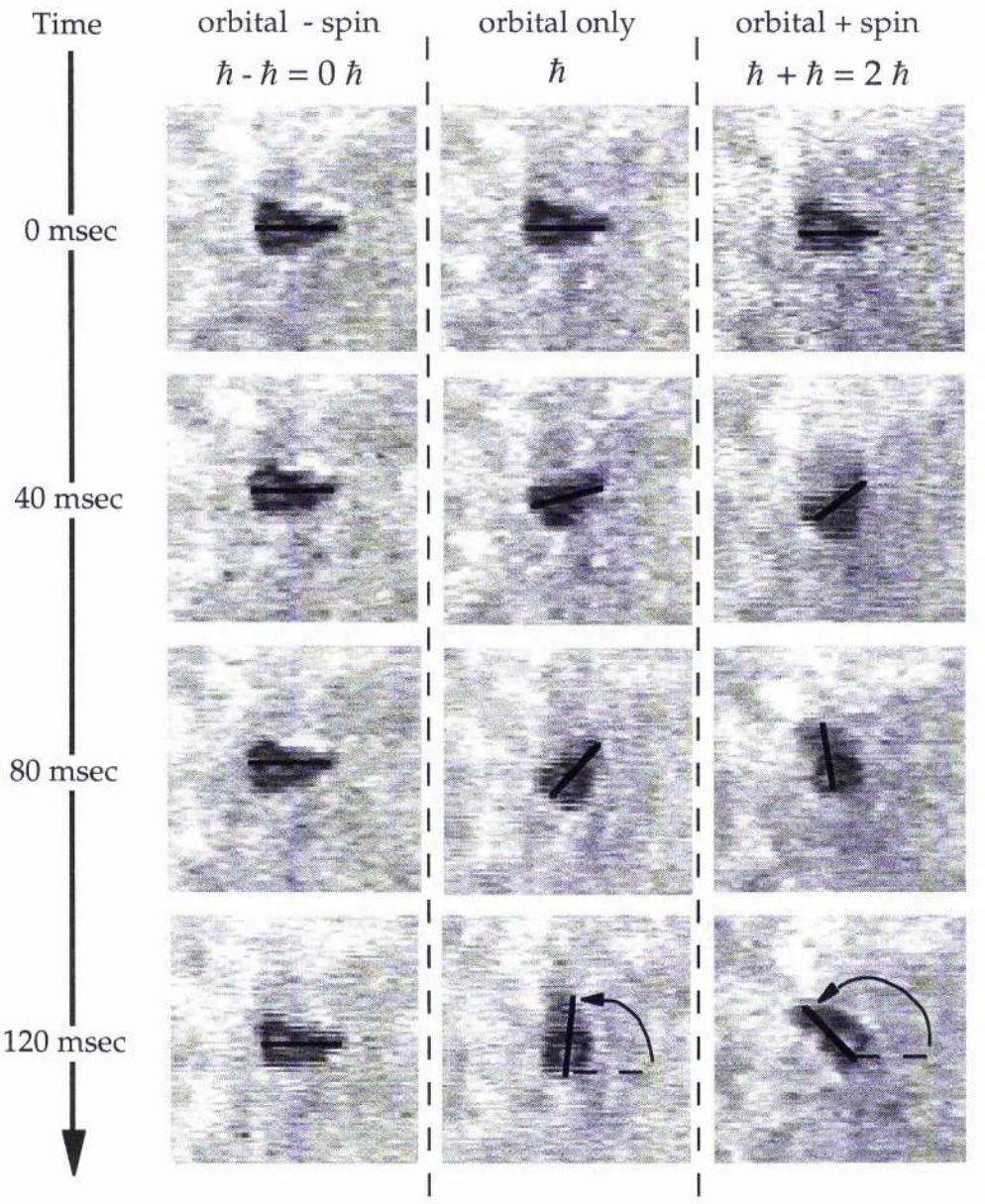

Figure VII.g Successive frames of video footage showing the stopping and speeding up of a 2 μm Teflon particle in ethanol, using optical spanners

This experimental work has not only demonstrated the operation of optical spanners, but also by controlling the polarisation state of the laser mode, a stop/start behaviour of the rotation of the trapped particle was observed. This observation of the cancellation of spin and orbital angular momentum verifies that the OAM is indeed well defined and corresponds to $\ell\hbar$ per photon, at least for $\ell = 1$. These results were published in *Optics Letters* in January 1997 [6].

VII. 7 Conclusions

This final Chapter on the experimental work summarised the research into the novel technique of Optical Spanners at St Andrews. The principles of the phenomenon were explained and the experimental arrangement was described.

An extension of the computer modelling from Chapter VI was carried out, which investigated the angular accelerations and terminal angular velocities that should be expected with the optical spanners. For an 8 μm diameter silica sphere suspended in water that was trapped by an LG^4_0 laser mode of wavelength 532 nm, it was found that the predicted rotation speed was too small to be observable (of the order of 7×10^{-7} rad s^{-1} mW^{-1}). However, by using a sphere made of an absorbing glass at 532 nm (of $\alpha = 5700$ m^{-1}), the rotation would be observable, of the order 0.2 rad s^{-1} when trapped by a laser of 10 mW power.

As for the earlier computer modelling, as well as being published as part of a paper [3], these results were also presented at the *QE12* Conference in Southampton UK [7].

The optical spanners were successfully demonstrated experimentally and these observations have been described. It has been difficult to show such rotations of the particles on paper as the data was recorded on video, but the experimental details have been described in this Chapter. The experimental technique and observation of optical spanners were presented at the *IEEE/LEOS Inaugural Meeting of the Scottish Chapter* in Glasgow, UK [8].

The optical spanners were used as a tool in the final experiment described in this Chapter. In this work, the spin angular momentum of light, $\pm\hbar$ per photon associated with the circular polarisation of light, was added to or subtracted from the orbital angular momentum to give a total angular momentum per photon. Using an $\ell = 1$ LG mode, with $\hbar$ of orbital angular momentum, a total angular momentum of 0 or $2\hbar$ per photon was predicted, depending on the handedness of the circular polarisation of the light.

This was experimentally observed by transferring the angular momentum of the light beam to a trapped micron-sized Teflon particle. With linearly polarised light, the particle rotated with an angular velocity of ~ 1 Hz. With the introduction of the circularly polarised light, the particle's rotation either stopped or got faster depending on whether the spin angular momentum was subtracting from or adding to the orbital angular momentum. This complete cancellation of the spin and orbital components shows that, as predicted, the orbital angular momentum of a LG mode is well defined as $\ell\hbar$ per photon. The details of this experimental result were presented as a Post-Deadline paper at the *IQEC '96* in Sydney, Australia [9].

As discussed in section VII. 5. 2, the stop/start behaviour of the rotation of the particles in the optical spanners is likely to be an important issue in the further development of the spanners. By using an ℓ=1 LG mode and controlling its polarisation state, the full rotational control over the trapped particle can be accomplished.

VII. 7. 1 Discussion

When the research began in St. Andrews into the transfer of orbital angular momentum from a Laguerre-Gaussian laser beam to a trapped micron-sized particle and the technique of Optical Spanners, it was believed that we were the only group studying this. We later found out that another research group lead by Halina Rubinsztein-Dunlop, at the University of Queensland in Brisbane, Australia also began research in this area at the same time as ourselves. However, the two research groups have performed different experiments and the results have complimented each others findings.

The transfer of OAM from a light beam to a particle held in optical tweezers was demonstrated in principle by He et al [4]. They transferred OAM from an $\ell = 3$ LG mode to micron-sized ceramic and metal-oxide particles using optical tweezers. They were also able to slow down, or speed up, the rotation of the particle by using the LG mode in a circularly polarised state [10]. Depending on the relative sign of the SAM (due to the circularly polarised light), the SAM and OAM either combined or subtracted from each other, to give an overall total angular momentum.

The Australian group used a radiation pressure trap, forcing the particle (which was totally absorbing and almost black) against the bottom of the sample cell and into the dark region on the beam axis. This has very limited appeal as the particles cannot be lifted off the bottom of the cell.

The work that we performed in this area differed from those mentioned above, in the type of trap used and the particle type used. Our particles were weakly absorbing, semi-transparent particles, which were trapped at the beam focus above the cell bottom, in a true x-y-z optical trap. Unlike the Australian group, we required no mechanical restraint to keep the particles in the tweezers, which is a great advantage for the complete manipulation of particles.

They did see a change in rotation speed of their particles when transferring SAM and OAM, but it could not be quantified precisely. This work by the Australian group complements our results for an $\ell = 1$ LG mode, as they obtained their observations for an $\ell = 3$ LG mode. LG modes (or optical vortices) have also been combined with optical tweezers to trap hollow glass spheres, but due to their transparency (or zero absorption) no rotating behaviour was observed [11].

Whilst in Australia for the *IQEC '96* in Sydney, I was able to meet this research group in Brisbane. We were able to compare experimental techniques, discuss mutual problems and exchange ideas on Optical Tweezers and Optical Spanners which we found most useful and beneficial.

References

1. Allen, L., M.W. Beijersbergen, R.J.C. Spreeuw, and J.P. Woerdman, *Orbital angular momentum of light and the transformation of Laguerre-Gaussian laser modes.* Phys. Rev. A, 1992. **45**: p. 8185-8189.

2. Amos, B. and P. Gill, *Optical tweezers.* Meas. Sci. Technol., 1995. **6**: p. 248.

3. Simpson, N.B., L. Allen, and M.J. Padgett, *Optical tweezers and optical spanners with Laguerre-Gaussian modes.* J. of Mod. Opt., 1996. **43**: p. 2485-2491.

4. He, H., M.E.J. Friese, N.R. Heckenberg, and H. Rubinsztein-Dunlop, *Direct observation of transfer of angular momentum to absorptive particles from a laser beam with a phase singularity.* Phys. Rev. Lett., 1995. **75**(5): p. 826-829.

5. Barnett, S.M. and L. Allen, *Orbital angular momentum and nonparaxial light beams.* Opt. Comm., 1994. **110**: p. 670-678.

6. Simpson, N.B., K. Dholakia, L. Allen, and M.J. Padgett, *Mechanical equivalence of spin and orbital angular momentum of light: an optical spanner.* Opt. Lett., 1997. **22**: p. 52-54.

7. Simpson, N.B. and M.J. Padgett. *Calculation of the trapping forces in an optical tweezers using a Laguerre-Gaussian laser mode.* in *National Quantum Electronics Conference - QE12.* September 1995. poster P2-34, Southampton, UK.

8. Simpson, N.B., K. Dholakia, L. Allen, and M.J. Padgett. *Experimental observation of optical spanners.* in *IEEE/LEOS Inaugural Meeting of Scottish Chapter.* April 1996. Glasgow, UK.

9. Simpson, N.B., K. Dholakia, L. Allen, and M.J. Padgett. *The mechanical equivalence of the spin and orbital angular momentum of light: optical spanners.* in *XX International Quantum Electronics Conference - IQEC '96.* July 1996. POSTDEADLINE PAPER no ThP3, Sydney, Australia.

10. Friese, M.E.J., J. Enger, H. Rubinsztein-Dunlop, and N.R. Heckenberg, Phys. Rev. A, 1996. **54**: p. 1593.

11. Gahagan, K.T. and G.A. Swartzlander-Jr, *Optical vortex trapping of particles.* Opt. Lett., 1996. **21**: p. 827-829.

Chapter VIII

Conclusions

Contents

VIII. 1 Summary of the thesis

In this thesis, the combination of optical tweezers with Laguerre-Gaussian laser modes has been investigated, with the resulting technique being dubbed "Optical Spanners". Each of the two research fields have been individually reviewed before the experimental work was described.

There has been much interest in Laguerre-Gaussian laser modes in recent years, due to the orbital angular momentum present in these modes [1]. It is now well established that the spin angular momentum of $\pm\hbar$ corresponds to the polarisation state of the light [2], but the LG modes have an additional component which is associated with the orbital angular momentum of light. Each mode has an azimuthal phase index ℓ, and the orbital angular momentum is well defined in terms of this parameter, to be $\ell\hbar$ per photon [1]. It was this property of the laser modes that interested us and the main thrust of the PhD was to experimentally transfer the orbital angular momentum of the beam to a particle.

The first experimental work investigated the phase and intensity structure of these LG modes. By interfering the LG mode with a plane reference wave, the resulting interference fringes typically formed spirals which demonstrated the presence of the azimuthal phase present in the modes [3].

To transfer the angular momentum to a particle, it was necessary to hold the particle to allow the interaction between the light and matter to take place.

This was achieved by using a technique known as "Optical Tweezers", which uses a tightly focussed laser beam (typically using a 1.3 NA microscope objective lens) to optically trap a particle on the beam axis just below the beam focus using gradient forces [4]. In this way, the particle is held in a complete 3-dimensional trap and can be manipulated around the sample cell at will.

By introducing a $\ell \neq 0$ LG mode into the optical tweezers arrangement, it was possible to transfer the orbital angular momentum from the beam to the trapped particle. This was experimentally observed with the resulting rotation of the particle being of the order of a Hertz. The technique has been called "Optical Spanners" [5]. However, once this had been successfully demonstrated, it was decided to experimentally confirm the well defined orbital angular momentum content in the LG mode.

By choosing a $p = 0$, $\ell = 1$ LG mode, the orbital angular momentum content in the beam was $\hbar$ per photon. This was directly compared to the known spin angular momentum of the beam which was $\pm\hbar$ for the two handednesses of circularly polarised light. By controlling the polarisation state of the laser, the two angular momentum components either added or subtracted to give a total angular momentum per photon of the beam. This manifested itself in a complete cancellation of the rotation of the particle held in the Optical Spanners or a doubling of the rotational speed. This demonstrated a mechanical equivalence of the spin and orbital angular momentum in the LG laser beam [6]. It also experimentally confirmed that the predicted orbital angular momentum in a LG mode is indeed $\ell\hbar$ per photon.

Another benefit of using LG modes within Optical Tweezers was also investigated. Due to the absence of on-axis rays for LG modes with $p = 0$, $\ell \neq 0$, the z-trapping forces are greater in Optical Tweezers compared to those when using a fundamental $TEM_{0,0}$ laser mode [7]. There was experimentally found to be a doubling in the axial trapping efficiency on 5 μm silica spheres. This also meant that the trapping of particles could be performed with less laser power than previously used, which is of great benefit for the trapping of biological samples.

This thesis has described the research carried out with Laguerre-Gaussian laser modes and how they can improve the performance of optical tweezers. This work has also produced a novel technique for manipulating and rotating micron-sized particles with the development of Optical Spanners.

VIII. 2 The future of optical spanners

If the Optical Spanners were to be marketed as a viable, operational tool, there are improvements that would need to be made to the present set-up. The work performed during the last three years has demonstrated the feasibility of the spanners but it would have to be a much more precise experimental arrangement if accurate rotational speeds were required. Ideally, it would be preferable to be able to control, and stop/start the rotation of a trapped particle by a 'dial on a black box'. This obviously requires some further development to reach this degree of control, but I believe that this would be necessary to be able to consider the Optical Spanners as a feasible, optical tool for the manipulation and rotation of particles.

There is also the other benefit of Laguerre-Gaussian modes within Optical Tweezers, which is the increased axial trapping efficiency. This is perhaps just as important a development, as the present product could be quite easily adapted to incorporate the LG mode, thus allowing the reduction of the laser power required for trapping or possibly reducing the required NA for the objective lens. Both of these measures would reduce costs and enhance the trapping efficiency of the Optical Tweezers.

There are three main areas that are likely to benefit from the existence of Optical Spanners and the improved Optical Tweezers. These will be briefly discussed in the remainder of this section.

VIII. 2. 1 Biological/medical applications

Optical Tweezers are already widely used in the fields of micro-biology and cell and bacteria manipulation as discussed in section III. 7. 1. However, the LG modes would enable lower laser powers to be used reducing the risk of

optical damage to the biological sample. This is a large advantage over traditional tweezers' systems and one that could be utilised quite readily.

The improved tweezers have been used in a biological application here in St. Andrews. Using a LG mode in our tweezers arrangement, we have successfully been able to lift cryptosporidium oocysts (water parasites), translate them and then lower them to a particular location in the sample cell. The aim is to use the improved Optical Tweezers to selectively group the oocysts in the cell. This is the beginning of some collaborative work between the University of St. Andrews and the Scottish Parasite Diagnostic Laboratory in Glasgow.

The Optical Spanners also add the element of rotation so that a biological particle or sample can be rotated at a constant speed, or for a part rotation in order to place a sample in a particular orientation at a particular site. The spanners give that extra control that may be needed for the manipulation of samples.

VIII. 2. 2 Applications in nanotechnology

The research field of nanotechnology and micro-machines opens up another exciting application for the tweezers and spanners. Optical Tweezers can be used to hold and manipulate small pieces of machinery for the building of micron-sized machines, providing the components are semi-transparent to allow the tweezers to function. Their precision could prove invaluable in the positioning of components within the new world of the micro-machines.

The Optical Spanners again will provide the additional benefit of being able to rotate the pieces of machinery, providing there is sufficient absorption of the photons. Not only will the spanners aid in the positioning of components by their ability to rotationally orientate the component, but also with the turning of cogs in machinery. At present, there is difficulty in turning such small cogs as very large electro-static devices are required. To be able to use a small, direct laser source to drive these cogs would be a great

step forwards to making these micro-machines fully self-sufficient with engines driven from a small, portable laser source.

VIII. 2. 3 Applications in micro-magnetics

The third area where Optical Spanners may prove useful is in the optical manipulation and probing of magnetic micro-samples. A collaboration has begun between Dr Ken Mackay of the Laboratoire Louis-Néel of the CNRS, Grenoble and the University of St. Andrews to investigate the manipulation and placement of magnetic micro-particles within micro-coils or micro-squids (superconducting quantum interference devices) using Optical Tweezers and Spanners.

The tweezers/spanners arrangement would be used to position the magnetic particles within the micro-coils or micro-squids, so that the behaviour of the particles could be studied within the coils. Materials could be investigated in intense magnetic fields on a nanosecond scale if probed by ultrashort optical pulses, in the search for new magnetic recording media.

The Optical Tweezers/Spanners in this application would be used as a micro-positioner, which is likely to be the most useful application. By using the micro-squids, which use quantum effects in semiconductors to measure extremely small currents, voltages and magnetic fields, a greater understanding of magnetic systems on the microscopic scale should be possible.

VIII. 3 Concluding remarks

Optical Tweezers and Optical Spanners not only have a positive future as optical tools, but the idea of their operation and what may be achievable with them is also very accessible to the general public. The issues are easy to understand and grasp and consequently there has been much interest and publicity in the work over the last few years.

Apart from the interest shown in the topic in an academic arena, at national and international conferences, there has also been a great deal of interest in

the development of Optical Spanners in the media world. This is very good for the portrayal of science to the general public as it helps them to be aware of current developments and encourages them to take a keen interest in science.

Following a presentation by myself at the *Inaugural Meeting of the Scottish Chapter of the IEEE/LEOS* at Glasgow in April 1996 [5], there has been a lot of publicity regarding the development of the Optical Spanners. An article was written in the *'Science'* magazine as a direct consequence of the conference presentation [8], which was then followed in 1997 by further articles and pieces about our research.

The first was an interview on the *BBC Radio 4 programme 'Science Now'*, with my supervisor Miles Padgett and myself, about Optical Tweezers and Spanners [9] which gave exposure to the work. This was quickly followed by general interest articles about tweezers and spanners in *'The Big Issue - Scotland'* [10], *'The Financial Times'* [11] and most recently in the *'Physics World'* magazine of the Institute of Physics [12] and the *'New Scientist'* magazine [13].

The applications and future of Optical Tweezers and Optical Spanners certainly look rosy and there may well be further developments in the near future. Perhaps the laser tools of science-fiction films and writing are not as absurd as once thought!

References

1. Allen, L., M.W. Beijersbergen, R.J.C. Spreeuw, and J.P. Woerdman, *Orbital angular momentum of light and the transformation of Laguerre-Gaussian laser modes.* Phys. Rev. A, 1992. **45**: p. 8185-8189.

2. Beth, R.A., *Mechanical detection and measurement of the angular momentum of light.* Phys. Rev., 1936. **50**: p. 115-125.

3. Padgett, M., J. Arlt, N. Simpson, and L. Allen, *An experiment to observe the intensity and phase structure of Laguerre-Gaussian laser modes.* Am. J. of Phys., 1996. **64**: p. 77-82.

4. Ashkin, A., J.M. Dziedzic, J.E. Bjorkholm, and S. Chu, *Observation of a single-beam gradient force optical trap for dielectric particles.* Opt. Lett., 1986. **11**(5): p. 288-290.

5. Simpson, N.B., K. Dholakia, L. Allen, and M.J. Padgett. *Experimental observation of optical spanners.* in *IEEE/LEOS Inaugural Meeting of Scottish Chapter.* April 1996. Glasgow, UK.

6. Simpson, N.B., K. Dholakia, L. Allen, and M.J. Padgett, *Mechanical equivalence of spin and orbital angular momentum of light: an optical spanner.* Opt. Lett., 1997. **22**: p. 52-54.

7. Simpson, N.B., L. Allen, and M.J. Padgett, *Optical tweezers and optical spanners with Laguerre-Gaussian modes.* J. of Mod. Opt., 1996. **43**: p. 2485-2491.

8. Bains, S., *Helical beams give particles a whirl,* in *Science* 5 July 1996, p. 36.

9. *Optical Spanners,* in *BBC Radio 4 - 'Science Now'* 11 January 1997,

10. Carrington, D., *Space-age spanner,* in *The Big Issue - Scotland* 6 March 1997, p. 39.

11. Derrington, A., *Microscopic tools of the trade,* in *Financial Times* 21 June 1997, p. 2, Weekend.

12. Padgett, M.J. and L. Allen, *Optical tweezers and spanners,* in *Physics World* September 1997, p. 35-38.

13. Brooks, M., *Spin doctors,* in *New Scientist* 14 February 1998, p. 34-37.

Appendices

Contents

Appendix I List of Publications and Conference Papers

I. 1 General Exposure

1. Report in "Helical beams give particles a whirl", S Bains, *'Science' magazine,* **273**, No 5271, p36, 5 July 1996

2. Short interview on *BBC Radio 4 programme 'Science Now'* about my research on "Optical Spanners", 11 January 1997

3. Report in "Space-age spanner", D Carrington, *'The Big Issue - Scotland' magazine,* **109**, p39, 6 March 1997

4. Report in "Microscopic tools of the trade", A Derrington, *'Financial Times - Weekend',* pII, 21 June 1997

5. Report in "Optical tweezers and spanners", M J Padgett and L Allen, *'Physics World' magazine,* **10**, No 9, p35-38, September 1997

6. Report in "Spin doctors", M Brooks, *'New Scientist' magazine,* **157**, No 2121, p34-37, 14 February 1998

I. 2 Journal Publications

1. "An experiment to observe the intensity and phase structure of Laguerre-Gaussian laser modes", M Padgett, J Arlt, N Simpson and L Allen, ***Am. J. Phys.*, 64**, No 1, 77-82, January 1996

2. "Second harmonic generation and the orbital angular momentum of light", K Dholakia, N B Simpson, L Allen and M J Padgett, ***Phys. Rev. A.*, 54**, No 5, R3742-R3745, November 1996

3. "Optical tweezers and optical spanners with Laguerre-Gaussian modes", N B Simpson, L Allen and M J Padgett, ***J. Mod. Opt.*, 43**, No 12, 2485-2491, December 1996

4. "Mechanical equivalence of spin and orbital angular momentum of light: an optical spanner", N B Simpson, K Dholakia, L Allen and M J Padgett, ***Opt. Lett.*, 22**, No 1, 52-54, January 1997

5. "Transfer of orbital angular momentum from a stressed fibre-optic waveguide to a light beam", D McGloin, N B Simpson and M J Padgett, ***Appl. Opt.*** **37**, No 3, 469-472, January 1998

6. "Optical tweezers with increased trapping efficiency", N B Simpson, L Allen and M J Padgett, accepted by ***J. of Mod. Opt.***, January 1998

I. 3 Conference Papers

1. "Calculation of the trapping forces in optical tweezers using a Laguerre-Gaussian laser mode", N B Simpson and M J Padgett, ***National Quantum Electronics Conference - QE12*** *(Southampton, UK),* poster P2-34, September 1995

- Awarded the ***'Alan Gibson Prize 1995'*** for best poster presentation at the *National Quantum Electronics Conference - QE12 (Southampton, UK)*

2. "Experimental observation of optical spanners", N B Simpson, K Dholakia, L Allen and M J Padgett, ***IEEE/LEOS Inaugural Meeting of Scottish Chapter*** *(Glasgow, UK),* April 1996

3. "Second harmonic generation and the orbital angular momentum of light", K Dholakia, N B Simpson, M J Padgett and L Allen, ***VI Quantum Electronics and Laser Science Conference - QELS '96*** *(Anaheim, USA),* ***Postdeadline paper,*** no.QPD6, June 1996

4. "The mechanical equivalence of the spin and orbital angular momentum of light : optical spanners", N B Simpson, K Dholakia, L Allen and M J Padgett, ***XX International Quantum Electronics Conference - IQEC '96*** *(Sydney, Australia),* ***Postdeadline paper,*** no.ThP3, July 1996

- Received ***IQEC '96 Travel Grant*** as contribution towards the trip to the XX *International Quantum Electronics Conference - IQEC '96 (Sydney, Australia)*

- Received ***award from C R Barber Trust*** (The Institute of Physics) as contribution towards the trip to the XX *International Quantum Electronics Conference - IQEC'96 (Sydney, Australia)*

5. "Non-linear optics with Laguerre-Gaussian beams", K Dholakia, N B Simpson, L Allen and M J Padgett, ***IEEE/LEOS Meeting of Scottish Chapter*** *(Heriot-Watt, UK)*, poster presentation, September 1996

6. "Optical tweezers with increased trapping efficiency", N B Simpson, L Allen and M J Padgett, ***XVII Conference on Lasers and Electro-Optics - CLEO '97*** *(Baltimore, USA)*, paper no. CTuD7, May 1997

- Received ***CLEO '97 New Focus Travel Grant*** as contribution towards the trip to the *XVII Conference on Lasers and Electro-Optics - CLEO '97 (Baltimore, USA)*

- Received ***award from C R Barber Trust*** (The Institute of Physics) as contribution towards the trip to the *XVII Conference on Lasers and Electro-Optics - CLEO '97 (Baltimore, USA)*

7. "Optical spanners", N B Simpson, K Dholakia, L Allen and M J Padgett, ***IEEE/LEOS Meeting of Scottish Chapter*** *(Glasgow, UK)*, poster presentation, September 1997

8. "The transfer of orbital angular momentum to a light beam using a stressed fibre optic waveguide", D McGloin, N B Simpson and M J Padgett, accepted at ***National Quantum Electronics Conference - QE13*** *(Cardiff, UK)*, Poster P6-2, September 1997

Appendix II - Designs for laser components

The following pages are examples of some of the designs that were drawn up for various components that were required for the construction of the new laser system. These were then machined in the workshop here in the Department of Physics and Astronomy.

Four designs are included in this thesis of the laser components that were made here. These are:

- Mount for the two aspheric lenses
- Water distribution box for supplying and disposing of cooling water
- Water-cooled mount for the Nd:YLF crystal
- Water-cooled base block for the laser diode

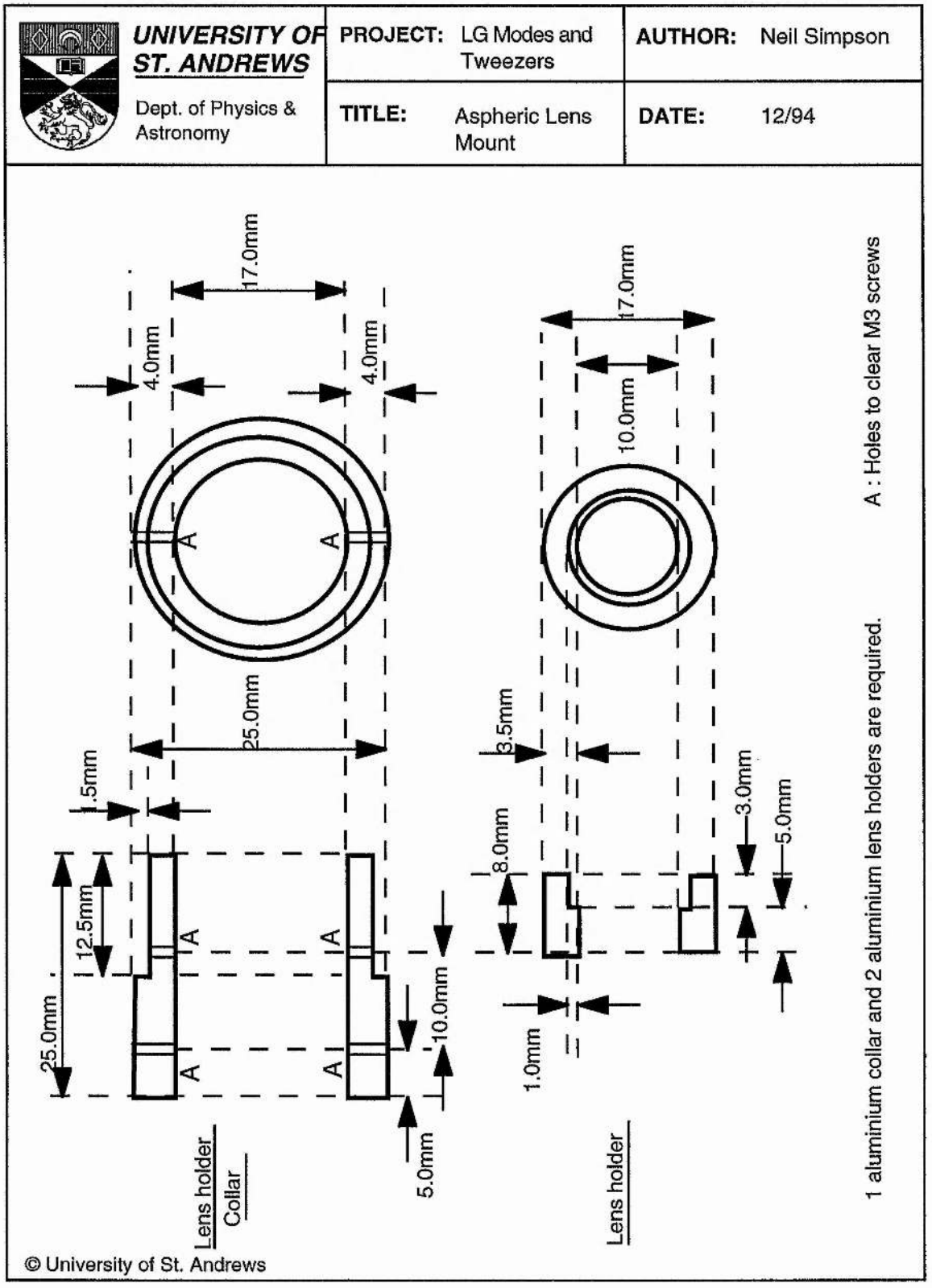
UNIVERSITY OF ST. ANDREWS
Dept. of Physics & Astronomy
PROJECT: LG Modes and Tweezers
AUTHOR: Neil Simpson
TITLE: Aspheric Lens Mount
DATE: 12/94
17.0mm
4.0mm
4.0mm
A
A
25.0mm
1.5mm
12.5mm
25.0mm
10.0mm
5.0mm
Lens holder
Collar
17.0mm
10.0mm
3.5mm
8.0mm
1.0mm
3.0mm
5.0mm
Lens holder
A : Holes to clear M3 screws
1 aluminium collar and 2 aluminium lens holders are required.
© University of St. Andrews

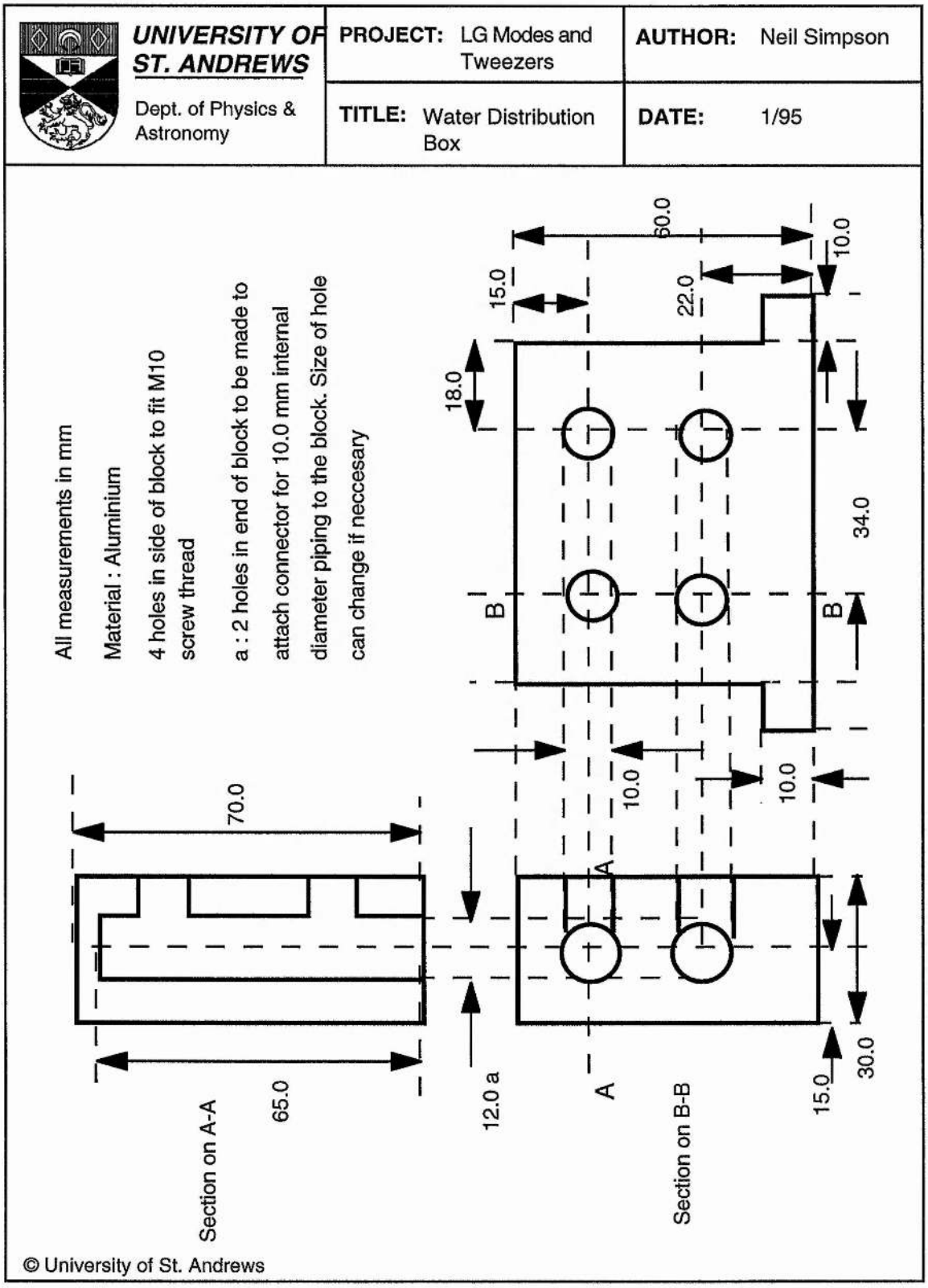
UNIVERSITY OF ST. ANDREWS
Dept. of Physics & Astronomy
PROJECT: LG Modes and Tweezers
AUTHOR: Neil Simpson
TITLE: Water Distribution Box
DATE: 1/95
All measurements in mm
Material : Aluminium
4 holes in side of block to fit M10 screw thread
a : 2 holes in end of block to be made to attach connector for 10.0 mm internal diameter piping to the block. Size of hole can change if neccesary
60.0
10.0
15.0
22.0
18.0
34.0
B
B
10.0
10.0
10.0
A
A
70.0
65.0
12.0 a
15.0
30.0
Section on A-A
Section on B-B
© University of St. Andrews

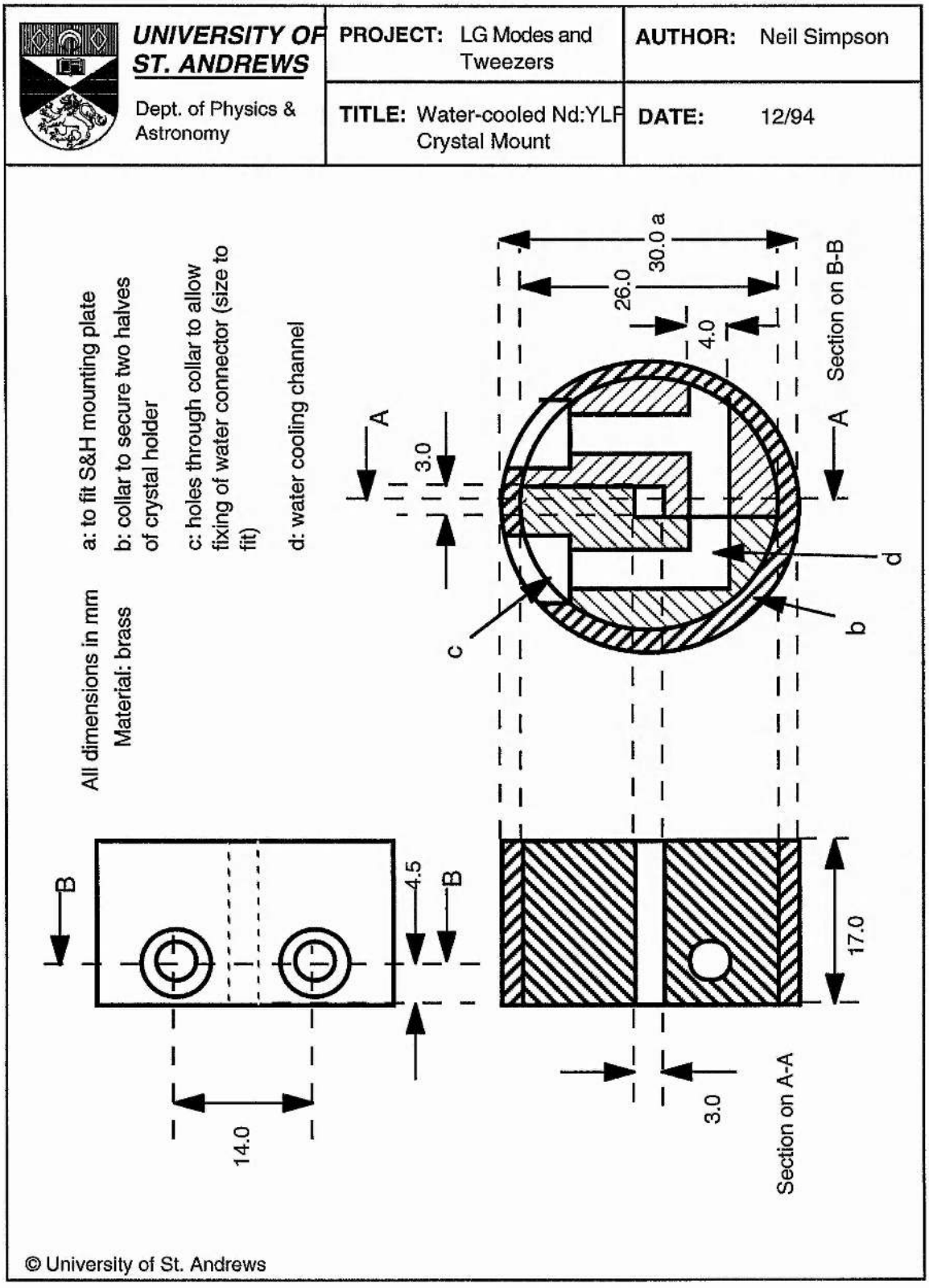
UNIVERSITY OF ST. ANDREWS
Dept. of Physics & Astronomy
PROJECT: LG Modes and Tweezers
AUTHOR: Neil Simpson
TITLE: Water-cooled Nd:YLF Crystal Mount
DATE: 12/94
All dimensions in mm
Material: brass
a: to fit S&H mounting plate
b: collar to secure two halves of crystal holder
c: holes through collar to allow fixing of water connector (size to fit)
d: water cooling channel
30.0 a
26.0
4.0
3.0
Section on B-B
A
A
d
b
c
B
B
4.5
14.0
17.0
3.0
Section on A-A
© University of St. Andrews

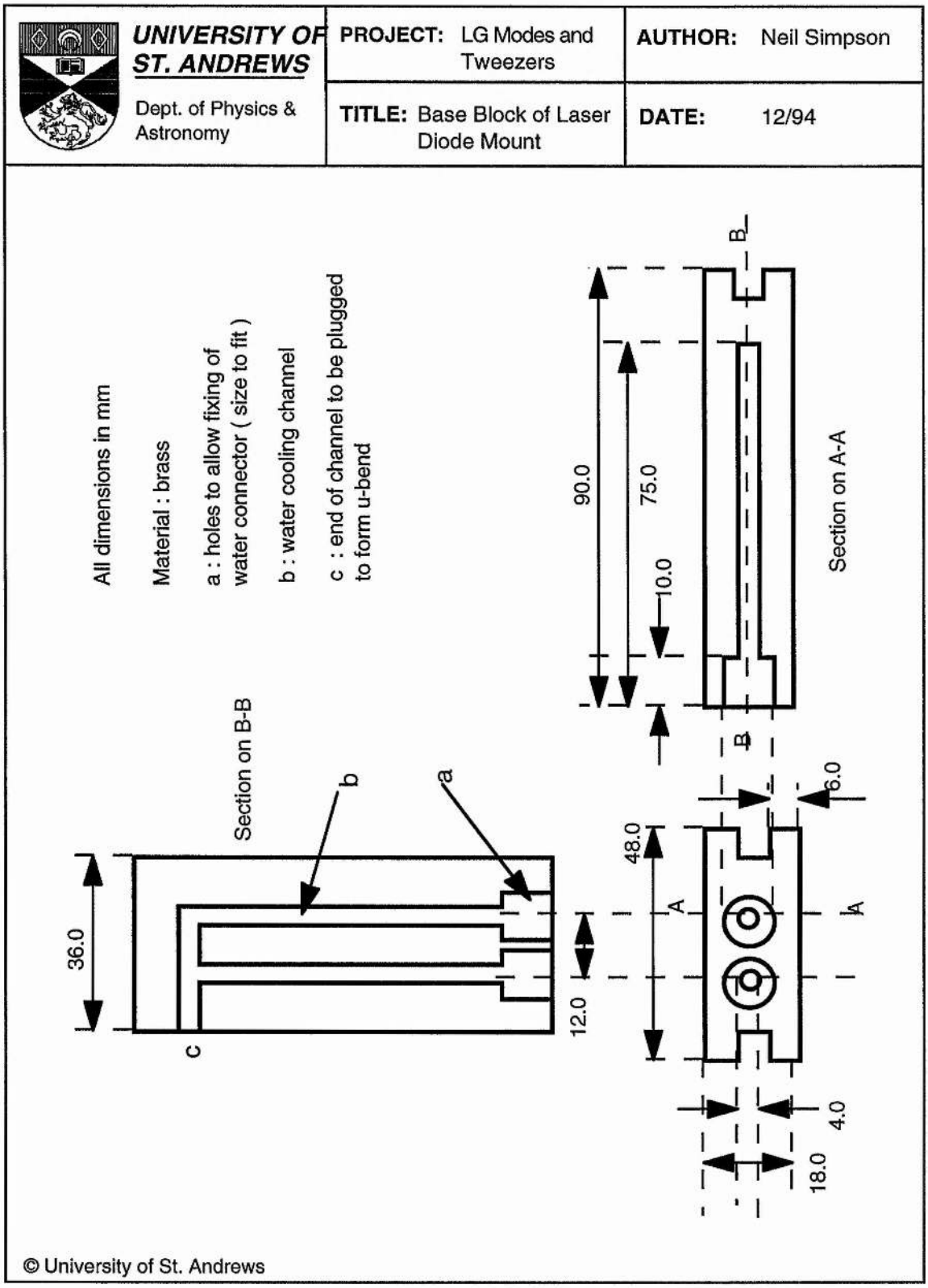
UNIVERSITY OF ST. ANDREWS
Dept. of Physics & Astronomy
PROJECT: LG Modes and Tweezers
AUTHOR: Neil Simpson
TITLE: Base Block of Laser Diode Mount
DATE: 12/94
All dimensions in mm
Material : brass
a : holes to allow fixing of water connector (size to fit)
b : water cooling channel
c : end of channel to be plugged to form u-bend
Section on B-B
Section on A-A
36.0
12.0
48.0
90.0
75.0
10.0
6.0
4.0
18.0
a
b
c
A
B
© University of St. Andrews

Appendix III - Modelling programs

The computer programs for the modelling of the axial trapping forces and the resultant angular acceleration were written in Symantec C++ on a Power Macintosh 6100/60.

III. 1 Model to calculate the axial trapping force of a beam on a sphere

```
#include <Files.h>
#include <stdio.h>
#include <stdlib.h>
#include "vectors.h"                    // Function to define vectorial operators
#include <fp.h>
#include <StandardFile.h>
#include "ModelP.h"                     // Function to calculate axial momenta change of ray
#include "outerProduct.h"               // Function to define outer product multiplication of
                                                //two vectors
#define N 500                           // total number of rays in quadrant

main()
{
        float r = 5.0;                  // radius of sphere
        float lambda = 0.000000488;     // trapping laser wavelength
        float n1 = 1.33;                // refractive index of surrounding medium
        float n2 = 1.596;               // refractive index of glass  sphere
        float ni = 1.518;               // index matching fluid
        int l = 0;                      // mode of Laguerre
        float wrel;                     // relative beam radius of Laguerre mode
        float w0 = 0.2;                 // beam waist of beam
        float theta, Thetamax, Theta, RC, z0, m1;
        float c, x1, y1, x11, y11, FractionP, w1, w2, sum1=0.0;
        int i;                          // define the ith ray
        float sum=0, Intensity[N];
        float results2[N], *momentum, momChange;

        FILE *filePointer;
        char fileName[64];

                //The following are used by the "Save As..." dialog box.
        StandardFileReply reply;

                //This initial printf statement is needed to create a console, and in
                        //the process initialises the Macintosh Toolbox, which must be done
                        //before the Save As... dialog box is used.
        printf("Multiple Ray Model");

        Thetamax = pi / 2;                      //maximum quadrant angle
        theta = Thetamax / (N-1);               // divides quadrant into equal angles

        //wrel = 1.0;                   //for l=0,  relative beam radius
        //wrel = 0.755;                 //for l=1
```

```
//wrel = 0.64;                    //for l=2
//wrel = 0.567;                   //for l=3
//wrel = 0.517;                   //for l=4
//wrel = 0.478;                   //for l=5

        //This line generates a "Save As..." dialog box.
        //The file name is returned in the "reply" structure.
StandardPutFile("\pSave data as:", "\pdata", &reply);

        //This line extracts the filename the user specified from the "reply" structure.
memcpy(fileName, reply.sfFile.name + 1, reply.sfFile.name[0]);

        // Now open the file for writing and get the file pointer.
filePointer = fopen (fileName,"w");

for (c=4.0; c<20.5; c = c+0.5)          // loop for all axial positions of sphere
{
        for (i=0; i<N; i++)             // loop for all N rays
        {
                x1 = c - (r * cos(i*theta));        // distance from waist to intercept
                RC = x1*(1+((pi*w0*w0*n1)/(lambda*1000000*x1))*((pi*w0*w0*n1)/
                        (lambda*1000000*x1)));      //radius of curvature at intercept
                y1 = sqrt((r*r)-((c-x1)*(c-x1)));       // radial position of intercept
                Theta = atan(y1/RC);            // angle of intercept point with
                                                //altered waist
                m1 = tan(Theta);                // altered gradient of incoming ray

                results2[i] = ModelP(lambda,r,n1,n2,m1,i,c,x1,y1);
                                // momenta change of ray stored as array for all rays

                z0 = (pi * w0 * w0 * n1)/(lambda*1000000);      // Rayleigh range

                w1 = sqrt(w0*w0*(1+((x1/z0)*(x1/z0))));         // beam radius at x1

                x11 = c - (r * cos((i+1)*theta));  // distance from waist to 2nd intercept
                y11 = sqrt((r*r)-((c-x11)*(c-x11)));        // radial position of intercept

                w2 = sqrt(w0*w0*(1+((x11/z0)*(x11/z0))));       // beam radius at x11

                FractionP = exp((-2*y1*y1)/(w1*w1))-exp((-2*y11*y11)/(w2*w2));
                                        // fraction of power, weighting factor

                if (FractionP<0.0) FractionP = 0.0;     // if in shadow, let = 0

                Intensity[i] = FractionP;       // fractional powers for all rays
                                                // stored as an array
        }

        momentum = outerProduct( Intensity, results2, N);
                        // product of momenta change and weighting factor
        sum1 = 0;
        for (i=0; i<N; i++)
                sum1 += momentum[i];        // momenta changes summed for the beam
```

```
            momChange = ( sum1 * lambda * 1e12 * n1) / 3e11;
                    //result in pN/mW, the 1e12 for pN, lambda to cancel from ModelP,
                    //3e11 for c and mW, h cancels from ModelP, n1 for lambda in water.

            fprintf (filePointer, "%.4f \n", momChange);   // print trapping force

        }

        fclose(filePointer);
}
```

III. 2 Function to calculate the axial momenta change of a ray through the sphere

```
#include <stdio.h>
#include <fp.h>
#include "vectors.h"
                                        // define variables within function
float ModelP(   float lambda,float r,float n1,float n2,float m1,int i,float c,float x1,float y1)
{
        float m2, m3, m4, m5, m6;                       // ray gradients
        float x2, y2, x3, y3;                           // interception points
        float IN, TR, R, R1, R2, alpha=-0.2;            // cosines and reflection coefficient
        float pin, pre, ptr, pRe, p1, Frac, X;          // photon momenta
        vector M1, M2, M3, M4, M5, M6;                  // ray unit vectors
        vector N1, N2, N3;                              // normal unit vectors

        M1.x = -cos(atan(m1)) ;         // incident unit vector
        M1.y = -sin(atan(m1)) ;         // same direction as normal N1, out from sphere
        M1.z = 0.;

        N1.x = (x1-c)/r;                // normal unit vector to 1st intercept point
        N1.y = y1/r;
        N1.z = 0.;
                                        // reflected ray unit vector
        M2 = plus(M1, (scalarProduct( 2., cross(cross(M1, N1), N1))));

        m2 = (M2.y)/(M2.x);             // reflected ray gradient

                                        // refracted ray unit vector
        M3 = minus(scalarProduct((n1/n2),(minus(scalarProduct(-1., M1),scalarProduct((dot
                (scalarProduct(-1., M1),N1)),N1)))),(scalarProduct((sqrt(1. -(vAbs(
                scalarProduct((n1/n2),(minus((scalarProduct(-1., M1)),(scalarProduct((dot
                ((scalarProduct(-1., M1)),N1)),N1)))))) *vAbs(scalarProduct((n1/n2),(minus
                ((scalarProduct(-1., M1)),(scalarProduct((dot((scalarProduct(-1., M1)),N1)),
                N1)))))))),N1)));

        m3 = (M3.y)/(M3.x);             // refracted ray gradient

                                        // 2nd intercept with sphere
        x2 = (1./(2.*(1.+(m3*m3))))*((2.*c)-(2.*m3*y1)+(2.*m3*m3*x1)+(2.*sqrt(((-2.)*c*m3*
                y1)+(2.*c*m3*m3*x1)-(y1*y1)+(2.*y1*m3*x1)-(m3*m3*x1*x1)+(r*r)-(m3*m3*
                c*c)+(m3*m3*r*r))));
        y2 = (m3*x2)+y1-(m3*x1);

        N2.x = (x2-c)/r;                // normal unit vector to 2nd intercept point
        N2.y = y2/r;
        N2.z = 0.;
                                        // distance over which photons are absorbed
        X = ((sqrt ((pow((x1-x2),2)) + (pow((y1-y2),2))))) * cos(atan(m3)) * 0.000001;

        if (isnan(X)) X = 0.0;          // if no distance let it be zero

        Frac = exp( alpha * X);         // fraction of photons absorbed over distance X
```

```
                                        // internally reflected ray unit vector
M4 = plus(scalarProduct(-1.,M3),(scalarProduct(2.,(cross(cross((scalarProduct
        (-1.,M3)),(scalarProduct(-1.,N2))),(scalarProduct(-1.,N2)))))));

m4 = (M4.y)/(M4.x);                     //internally reflected ray gradient

                                        // 3rd intercept with sphere
x3 = (1./(2.*(1.+(m4*m4))))*((2.*c)-(2.*m4*y2)+(2.*m4*m4*x2)+(2.*(sqrt(((-2.)*c*m4*
        y2)+(2.*c*m4*m4*x2)-(y2*y2)+(2.*y2*m4*x2)-(m4*m4*x2*x2)+(r*r)-(m4*m4*
        c*c)+(m4*m4*r*r)))*((M4.x)/(fabs(M4.x)))));
y3 = (m4*x3)+y2-(m4*x2);

N3.x = (x3-c)/r;                        // normal unit vector to 3rd intercept point
N3.y = y3/r;
N3.z = 0.;
                                        // refracted ray unit vector
M5 = minus(scalarProduct((n2/n1),(minus(M4,scalarProduct((dot(M4,(scalarProduct(-
        1.,N3)))),(scalarProduct(-1.,N3))))),(scalarProduct((sqrt(1. - (vAbs(
        scalarProduct((n2/n1),(minus(M4,(scalarProduct((dot(M4,(scalarProduct(-
        1.,N3)))),(scalarProduct(1.,N3)))))))*vAbs(scalarProduct((n2/n1),(minus
        (M4,(scalarProduct((dot(M4,(scalarProduct(-1.,N3)))),(scalarProduct(-
        1.,N3))))))))))),(scalarProduct(-1.,N3)))));

m5 = (M5.y)/(M5.x);                     // refracted ray gradient

                                        // emerging refracted ray unit vector
M6 = minus(scalarProduct((n2/n1),(minus(M3,scalarProduct((dot(M3,scalarProduct
        (-1.,N2))),scalarProduct(-1.,N2))))),(scalarProduct((sqrt(1. - (vAbs
        (scalarProduct((n2/n1),(minus(M3,(scalarProduct((dot(M3,scalarProduct(-
        1.,N2))),scalarProduct(-1.,N2)))))) * vAbs(scalarProduct((n2/n1),(minus(M3,
        (scalarProduct((dot(M3,scalarProduct(-1.,N2))),scalarProduct(-
        1.,N2))))))))))),scalarProduct(-1.,N2))));

m6 = (M6.y)/(M6.x);                     //emerging refracted ray gradient

            // Now the momentum changes must be calculated

IN = fabs(dot(M1, N1));                 // cos of angle between incident and normal
TR = fabs(dot((scalarProduct(-1.,N1)), M3));    //cos of angle between refracted and
                                                    normal

                                        // Perpendicular Fresnel coefficient
R1 = (((n1*IN)-(n2*TR))/((n1*IN)+(n2*TR)))*(((n1*IN)(n2*TR))/
        ((n1*IN)+(n2*TR)));
                                        // Parallel Fresnel coefficient
R2 = (((n2*IN)-(n1*TR))/((n2*IN)+(n1*TR)))*(((n2*IN)(n1*TR))/
        ((n2*IN)+(n1*TR)));

R = ( R1 + R2 ) / 2.0;                  // average Fresnel taken
```

```
                                    // momentum change of single photon
        pin = ((cos(atan(m1)))/(lambda))*(-(M1.x))/(fabs(M1.x));
        pre = (cos(atan(m2))/lambda)*(M2.x)*R/(fabs(M2.x));
        ptr = (cos(atan(m6))/lambda)*(M6.x)*((1-R-(R*(1-R)))/(fabs(M6.x)))*Frac;
        pRe = (cos(atan(m5))/lambda)*(M5.x)*(((1.-R)*R)/(fabs(M5.x)))*Frac;

        p1 = pin - pre - ptr - pRe;        // final momentum change for photon in x direction

        if (isnan(p1)) p1 = 0.0;           // let = 0 if imaginary

        return (p1);                       // return the momenta change of ray

}
```

III. 3 Model to calculate the angular acceleration on a sphere by a Laguerre beam

```
#include <Files.h>
#include <stdio.h>
#include <stdlib.h>
#include "vectors.h"                    // Function to define vectorial operators
#include <fp.h>
#include <StandardFile.h>
#include "outerProduct.h"               // Function to define outer product multiplication of
                                                //two vectors
#include "Absorb.h"                     // Function to calculate the fraction of intensity
                                                //absorbed  by sphere for each ray

#define N 500                           // total number of rays in quadrant

main()
{
        float r = 4.0;                  // radius of sphere
        float lambda = 0.000000532;     // trapping laser wavelength
        float n1 = 1.33;                // refractive index of surroundings
        float n2 = 1.5;                 // refractive index of glass
        float ni = 1.518;               // index matching
        float wrel;                     // relative beam radius of Laguerre mode
        float NA = 1.3;                 // numerical aperture
        float W0 = (1.8 * lambda * 1000000) / (pi * NA);        // Hermite beam waist
        float w0;                                               // Laguerre beam waist
        float theta, Thetamax, Theta, RC, z0, m1, ymax ;
        float c, x1, y1, x11, y11, FractionP, w1, w2, sum1=0.0;
        int i;                          // define the ith ray
        int l=4;                        // Define order of Laguerre mode
        float sum=0, Intensity[N],results2[N];
        float IntAbs[N], TotIntAbs, torque, Inertia, AngAcc;

        FILE *filePointer;
        char fileName[64];

                //The following are used by the "Save As..." dialog box.
        StandardFileReply reply;

                //This initial printf statement is needed to create a console, and in the process
                        //initialises the Macintosh Toolbox, which must be done before the
                        //Save As... dialog box is used.
        printf("Multiple Ray Model");

        Thetamax = pi / 2;              //maximum quadrant angle
        theta = Thetamax / (N-1);       //divides quadrant into equal angles

        //wrel = 1.0;                   //for l=0
        //wrel = 0.755;                 //for l=1, relative beam radius
        //wrel = 0.64;                  //for l=2
        //wrel = 0.567;                 //for l=3
        wrel = 0.517;                   //for l=4
        //wrel = 0.478;                 //for l=5
```

```
w0 = W0 / wrel;                    // calculate Laguerre beam radius

        //This line generates a "Save As..." dialog box.
        //The file name is returned in the "reply" structure.
StandardPutFile("\pSave data as:", "\pdata", &reply);

        //This line extracts the file name the user specified from the "reply"structure.
memcpy(fileName, reply.sfFile.name + 1, reply.sfFile.name[0]);

        // Now open the file for writing and get the file pointer.
filePointer = fopen (fileName,"w");

for (c=-12.0; c<12.; c = c+0.5)          // loop for all axial positions of sphere
{
        for (i=0; i<N; i++)              // loop for all N rays

        {
                x1 = c - (r * cos(i*theta));        // distance from waist to intercept
                RC = x1*(1+((pi*w0*w0*n1)/(lambda*1000000*x1))*((pi*w0*w0*n1)/
                        (lambda*1000000*x1)));      // radius of curvature at intercept
                y1 = sqrt((r*r)-((c-x1)*(c-x1)));       // radial position of intercept
                Theta = atan(y1/RC);            // angle of intercept point with
                                                //altered waist
                m1 = tan(Theta);                // altered gradient of incoming ray

                results2[i] = Absorb (r,n1,n2,m1,c,x1,y1);
                                // distance within sphere stored as array for all rays

                z0 = (pi * w0 * w0 * n1)/(lambda*1000000);      // Rayleigh range

                w1 = (sqrt(w0*w0*(1+((x1/z0)*(x1/z0)))));       // beam radius at x1

                x11 = c - (r * cos((i+1)*theta)); // distance from waist to 2nd intercept
                y11 = sqrt((r*r)-((c-x11)*(c-x11)));        // radial position of intercept

                w2 = (sqrt(w0*w0*(1+((x11/z0)*(x11/z0)))));   // beam radius at x11

                        // max radius to consider allowing for past 1/e point
                ymax = (1.8 * w1) / wrel;

                //Weighting factor for l=0
                //FractionP = exp((-2*y1*y1)/(w1*w1))-exp((-2*y11*y11)/(w2*w2));

                //l=1
                //FractionP = (((2*y1*y1)+(w1*w1))/(w1*w1))*(exp((2*y1*y1)/
                        (w1*w1)))-(((2*y11*y11)+(w2*w2))/(w2*w2))*(exp((-2*y11*
                        y11)/(w2*w2)));
                //l=2
                //FractionP =(((2*pow(y1,4))+(2*w1*w1*y1*y1)+(pow(w1,4)))/
                        (pow(w1,4)))*(exp((-2*y1*y1)/(w1*w1)))-(((2*pow(y11,4))+
                        (2*w2*w2*y11*y11)+(pow(w2,4)))/(pow(w2,4)))*(exp((-
                        2*y11*y11)/(w2*w2)));
```

```
                //l=3
                //FractionP =(((6*pow(y1,2)*pow(w1,4))+(3*pow(w1,6))+(6*pow
                        (w1,2)*pow(y1,6))+(4*pow(y1,6)))/(3*pow(w1,6)))*(exp((-
                        2*y1*y1)/(w1*w1)))-(((6*pow(y11,2)*pow(w2,4))+(3*
                        pow(w2,6))+(6*pow(w2,2)*pow(y11,6))+(4*pow(y11,6)))/(3*
                        pow(w2,6)))*(exp((-2*y11*y11)/(w2*w2)));

                l=4
                FractionP = ((((3*pow(w1,8))+(6*pow(w1,6)*pow(y1,2))+(6*pow
                        (w1,4)*pow(y1,4))+(4*pow(w1,2)*pow(y1,6))+(2*pow
                        ((((3*pow(w2,8))+(6*pow(w2,6)*pow(y11,2))+(6*pow(w2,4)*
                        pow(y11,4))+(4*pow(w2,2)*pow(y11,6))+(2*pow(y11,8)))
                        /(3*pow(w2,8)))*(exp((-2*y11*y11)/(w2*w2))));

                // l=5
                //FractionP =((((15*pow(w1,10))+(30*pow(w1,6)*pow(y1,4))+
                        (30*pow(w1,8)*pow(y1,2))+(10*pow(w1,2)*pow(y1,8))+
                        (4*pow(y1,10))+(20*pow(w1,4)*pow(y1,6)))/(15*pow
                        (w1,10)))*(exp((-2*y1*y1)/(w1*w1))))-((((15*pow(w2,10))+
                        (30*pow(w2,6)*pow(y11,4))+(30*pow(w2,8)*pow(y11,2))+
                        (10*pow(w2,2)*pow(y11,8))+(4*pow(y11,10))+(20*pow
                        (w2,4)*pow(y11,6)))/(15*pow(w2,10)))*(exp((-2*y11*y11)/
                        (w2*w2))));

                if (y1 > ymax) FractionP = 0.0;          //aperturing, if ring larger
                                                         //than new1/e radius
                if (FractionP<0.0) FractionP = 0.0;      // if ring in shadow, let = 0

                Intensity[i] = FractionP;          // fractional powers for all rays
                                                         // stored as an array
                IntAbs[i] = Intensity[i] * results2[i];  //Fraction intensity absorbed
        }

        sum1 = 0.;
        for (i=0; i<N; i++)
                sum1 += IntAbs[i];       // fractional intensity summed for the beam

        TotIntAbs = sum1;                          // total intensity absorbed

        torque = (lambda * TotIntAbs * 1 ) / (3e8 * 2.0 * pi * 1000.0);      // on sphere

        Inertia = (8.0 * pi * 2000.0 * pow((r * 1e-6),5.0)) / 15.0;           // of sphere

        AngAcc = torque / Inertia;                 // experienced by sphere

        fprintf (filePointer, "%.4f \n", AngAcc);        // print angular acceleration

    }
    fclose(filePointer);
}
```

III. 4 Function to calculate the fraction of intensity absorbed by sphere for each ray

```
#include <stdio.h>
#include <fp.h>
#include "vectors.h"
                                        // Defines variables within function
float Absorb (float r,float n1,float n2,float m1,float c,float x1,float y1)
{
        float m2, m3;
        float x2, y2;
        //float alpha=-4600.0;          // absorption coefficient for BG12
        float alpha=-0.2;               // absorption coefficient for BG3
        float X, fraction;
        vector M1, M2, M3;
        vector N1;

                M1.x = -cos(atan(m1));          //incident unit vector
                M1.y = -sin(atan(m1));
                M1.z = 0.;

                N1.x = (x1-c)/r;                // normal unit vector to 1st intercept point
                N1.y = y1/r;
                N1.z = 0.;
                                                // reflected ray unit vector
                M2 = plus(M1, (scalarProduct( 2., cross(cross(M1, N1), N1))));

                m2 = (M2.y)/(M2.x);              / reflected ray gradient

                                                / refracted ray unit vector
                M3 = minus(scalarProduct((n1/n2),(minus(scalarProduct(-1.,M1),scalarProduct
                        ((dot(scalarProduct(-1., M1),N1)),N1)))),(scalarProduct((sqrt(1. -
                        (vAbs(scalarProduct((n1/n2),(minus((scalarProduct(-1., M1)),
                        (scalarProduct((dot((scalarProduct(-1., M1)),N1)),N1)))))) *
                        vAbs(scalarProduct((n1/n2),(minus((scalarProduct(-1., M1)),
                        (scalarProduct((dot((scalarProduct(-1., M1)),N1)),N1)))))))),N1)));

                m3 = (M3.y)/(M3.x);             // refracted ray gradient

                                                // 2nd intercept with sphere
                x2 = (1./(2.*(1.+(m3*m3))))*((2.*c)-(2.*m3*y1)+(2.*m3*m3*x1)+(2.*sqrt(((-
                        2.)*c*m3*y1)+(2.*c*m3*m3*x1)-(y1*y1)+(2.*y1*m3*x1)-
                        (m3*m3*x1*x1)+(r*r)-(m3*m3*c*c)+(m3*m3*r*r))));
                y2 = (m3*x2)+y1-(m3*x1);
                                                // distance of ray path inside sphere
                X = ((sqrt ((pow((x1-x2),2)) + (pow((y1-y2),2))))) * cos(atan(m3)) * 0.000001;

                if (isnan(X)) X = 0.0;          // if no ray path, absorption is zero

                fraction = 1-exp(alpha * X);    // fraction intensity of ray absorbed by sphere

                return (fraction);
}
```

III. 5 Definition of vectorial operators

```
#include <stdio.h>
#include <fp.h>
#include "vectors.h"

float dot( vector a, vector b )                    // dot product of two vectors
{
        return( a.x * b.x + a.y * b.y + a.z * b.z );
}

vector cross( vector a, vector b )                 // cross product of two vectors
{
        vector c;
                c.x = a.y * b.z - b.y * a.z;
                c.y = a.z * b.x - b.z * a.x;
                c.z = a.x * b.y - b.x * a.y;
        return( c );
}

float vAbs( vector a )                             // magnitude of vector
{
        return( sqrt( dot(a, a) ) );
}

vector plus( vector a, vector b )                  // addition of two vectors
{
        vector c;
                c.x = a.x + b.x;
                c.y = a.y + b.y;
                c.z = a.z + b.z;
        return( c );
}

vector minus( vector a, vector b )                 // subtraction of two vectors
{
        vector c;
                c.x = a.x - b.x;
                c.y = a.y - b.y;
                c.z = a.z - b.z;
        return( c );
}
```

```
vector scalarProduct( float a, vector b )          // product of scalar and vector
{
        vector c;
                c.x = a * b.x;
                c.y = a * b.y;
                c.z = a * b.z;
        return( c );
}


void vPrint( vector a )                            // print a vector's components
{
        printf("{%f, %f, %f}", a.x, a.y, a.z);
}


float *outerProduct ( float *a, float *b, int n )  // product of elements of two vectors
{
        int i;
        float *c;
                c = (float*) malloc(n * sizeof(float));

        for (i = 0; i < n; i++)
                c[i] = a[i] * b[i];
        return c;
}
```